Amplification of Brain Aggregated-Amyloid Beta by developing an Amyloid Beta Conformational Seeding Assay

Von der Fakultät für Lebenswissenschaften

der Technischen Universität Carolo-Wilhelmina

zu Braunschweig

zur Erlangung des Grades

eines Doktors der Naturwissenschaften

(Dr. rer. nat.)

genehmigte

D i s s e r t a t i o n

von Shyamkumar Krishnan

aus Gandhidham / Indien

1. Referentin:	Dr. Christiane Ritter
2. Referentin:	Professorin. Dr. Susanne Engelmann
3. Referent:	Professor. Dr. Stefan Dübel

eingereicht am: 20.04.2015
mündliche Prüfung (Disputation) am: 23.07.2015
Druckjahr 2015

Vorveröffentlichungen der Dissertation

Teilergebnisse aus dieser Arbeit wurden mit Genehmigung der Fakultät für Lebenswissenschaften, vertreten durch die Mentorin der Arbeit, in folgenden Beiträgen vorab veröffentlicht:

Posterbeiträge

1) Shyamkumar Krishnan and Thorsten Lührs. “Structural Investigation into Experimental Alzheimer Transmissibility” 4th International PhD Symposium Helmholtz International Graduate School for Infection Research on 17th December 2010.

2) Shyamkumar Krishnan and Thorsten Lührs. “NMR Structural Investigation of Alzheimer Transmissibility”. 3rd International PhD Symposium Helmholtz International Graduate School for Infection Research on 16th December 2009.

What we have learnt
is like a handful of earth;
What we have yet to learn
Is like the whole world

- Auvaiyar, Tamil poet, India.

Table of Contents

Abbreviations

AA	Amyloid Protein A
ACH	Amyloid Cascade Hypothesis
AD	Alzheimer's Disease
ADDL's	Aβ- Derived Diffusible Ligands
ALS	Amyotrophic Lateral Sclerosis
Amp	Ampicillin
AP	Amyloid Plaques
apoC-II	Apolipoprotein C-II
ApoE	Apolipoprotein E
APP	Amyloid Precursor Protein
Aβ	Amyloid Beta
Aβ-PMCA	Amyloid Beta Protein Misfolding Cyclic Amplification
BACE-1	β- Secretase Cleavage Enzyme
BH	Brain Homogenate
CAA	Cerebral Amyloid Angiopathy
CMC	Critical Micellar Concentration
CSA	Conformational Seeding Assay
CTAC	Cetyltrimethylammonium Chloride
CTF	Carboxy Terminal Fragment
CV	Column Volume
CVA	Cerebral Vascular Amyloid
DARR	Dipolar Assisted Rotational Resonance
DHPC	1,2-dihexanoyl-sn-glycero-3-phosphocholine
DM	Muscular Dystrophy
DS	Down Syndrome
EF-TEM	Energy Filtered-Transmission Electron Microscope
EM	Electron Microscopy
Em	Emission
Ex	Excitation
FAD	Familial Alzheimer Disease
FTLD	Fronto-temporal Lobar Degeneration

HD	Huntington Disease
HFIP	Hexafluoroisopropanol
HuAPP	Human Amyloid Precursor Protein
IMAC	Immobilized Metal-ion Affinity Chromatography
LB	Lewy Bodies
LB	Lysogeny Broth
LCPs	Luminescent Conjugated Polyelectrolyte Probes
LN's	Lewy Neuritis
mm	Millimeters
mM	Millimolar
Mox	Methionine Sulfoxide
MS	Mass Spectrometer / Mass Spectrometry
NFT	Neurofibrillary Tangles
nM	Nanomolar
nm	Nanometer
NMR	Nuclear Magnetic Resonance
OD^{600}	Optical Density at 600nm wavelength
PBS	Phosphate Buffer Saline
PC	Polycarbonate
PCR	Polymerase Chain Reaction
PD	Parkinson's Disease
PHF	Paired Helical Filament
PI	Protease Inhibitor
PiB	Pittsburgh compound B
PK	Proteinase-K
pM	Picomolar
PMCA	Protein Misfolding Cyclic Amplification
PP	Polypropylene
PP	Polypropylene
PrP^{C}	Prion Protein Cellular
PrP^{Sc}	Prion Protein Scrapie
PS	Polystyrene
Psen1	Presenilin-1

Psen2	Presenilin-2
RT	Room Temperature
RPM	Rounds Per Minute
sAPP	Soluble Amyloid Precursor Protein
sAPPα	Soluble Amyloid Precursor Protein Alpha
sAPPβ	Soluble Amyloid Precursor Protein Beta
SD	Supplementary Data
SDS	Sodium Dodecyl Sulfate
SG	Savitzky-Golay
ssNMR	Solid State Nuclear Magnetic Resonance
TDP-43	TAR DNA Binding Domain
TEM	Transmission Electron Microscope
TFE	Trifluoroethanol
TG	Transgenic
Thio-T	Thioflavin-T
TM	Trans-Membrane
UV	Ultra Violet
WT	Wild-type
μM	Micromolar
μm	Micrometer

Abstract

The “Amyloid Hypothesis” deliberates that Amyloid Beta (Aβ) peptides (Aβ40 & Aβ42) aggregation and accumulation in the brain primarily influences and progresses Alzheimer Disease (AD) pathogenesis. Several recent findings in AD have shown that Aβ and tau aggregates can transmit disease pathogenesis in a prion-like manner by transferring their conformational properties to normally folded units. In addition, there is a growing body of evidence accumulating that Aβ too can seed and act in a prion-like manner. Recently a link was reported between distinct brain-Aβ42 conformations and rapid clinical decline, defining Aβ42 structural conformation to be a new variable in AD pathogenesis (Cohen et al. 2015). The critical question of how Aβ42 structural conformations (strains) correlate to AD specific pathology in the brain remains to be a poorly understood phenomenon.

The development of thioflavin-T fluorescence based *in-vitro* seeding assays have enabled fibril amplification of Aβ conformations from brains, however these assays have been largely limited to utilizing soluble Aβ40 as the substrate. Additionally it is also established in seeding studies that Aβ42 fibrils cannot seed the monomeric Aβ40 substrate. Due to this, the bioactive Aβ42 AD specific toxic 3D conformation in brain remains elusive and continues to be a major bottleneck in AD research.

Our research confronts this challenge by developing an *in-vitro* based Aβ Conformational Seeding Assay (Aβ-CSA) that utilizes recombinant Aβ(1-42)M35L peptide as the substrate. At the start, suitable assay conditions were established to detect *de-novo* aggregated Aβ seeding in the assay. Later, when brain material was seeded it resulted in prolongation of Aβ substrate aggregation in the assay. This delay was overcome by PK digestion, but still the brain aggregated- Aβ material in the brain homogenate did not seed in the assay. Mimicking the brain membranous milieu in the assay using a phospholipid DHPC model, lead to seeding of brain aggregated-Aβ material in the assay. The seeding of the brain aggregated-Aβ seed was possible as the 4mM DHPC micellar condition markedly suppressed the substrate Aβ spontaneous primary nucleation. This suppression enabled the brain

aggregated-Aβ seeding mechanism to dominate over the spontaneous nucleation of the substrate Aβ and enabled brain aggregated-Aβ amplification in the assay.

Brain homogenates from 6-month transgenic mice [APP/PS1 (TG/WT)] and BL6 mice were used as brain-Aβ seeds in the assay. The TG mice contain brain aggregated-Aβ seeds; WT and BL6 were used as negative controls. The brain aggregated-Aβ seeded fibril growth kinetics was distinctly detected in the assay with a higher fluorescence and a shorter lagtime. Brain aggregated-Aβ seed amplification was later confirmed by two methods: (i) TEM investigation & (ii) A novel biophysical fibril fragmentation method Acoustic-SSA (Selective Shear Amplification) developed in our lab for prion amplification. This technique exploits the fibril mechanistic property to fragment and form seeds when sonication shear force is applied. The sonicated APP/PS1(TG) brain seeded aggregates did not seed in the developed assay compared to the robust seeding observed in sonicated APP/PS1(WT) and BL6 seeded fibrils. This indicates difference in specific mechanical fragmentability between the APP/PS1(TG) seeded and APP/PS1(WT) or BL6 brain homogenate seeded fibrils hinting conformational difference.

The developed Aβ-CSA with Aβ(1-42)M35L as the substrate is the first assay to amplify brain aggregated-Aβ and show distinct differences by seeding kinetics, TEM and Acoustic-SSA. The developed Aβ-CSA platform is an early step towards amplifying the brain aggregated-Aβ involved in Alzheimer's disease.

1 Introduction

1.1 Introduction to Alzheimer's disease

1.1.1 Alzheimer's disease Highlights

Alzheimer's Disease (AD) is a devastating neurodegenerative disease characterized by dementia, cognitive impairment and behavioral disorders that affect normal living in humans. It is the most frequent form of dementia affecting an estimated 25-50% of people aged above 85 in the developed world (Hong-Qi et al. 2012). AD is one of the killer diseases, for which there are no cures, drugs and therapies to slowdown or halt the disease progression. The cost of caregiving imposes a huge economic burden on the nation and families. There are more than 1.2 Million AD patients living in Germany alone and approximately more than 28-36 million people are known to be affected worldwide (www.deutsche-alzheimer.de). AD is known to strike 1 in 20 person between the ages 65-69 years and 1 in 3 persons between the ages 80-90. These are the statistics of the dementia cases, of which approximately 70% end-up being diagnosed with AD later is very alarming. AD running through families has been known to strike at age even less than 50 years. By the year 2050, the prevalence of AD has been forecasted to quadruple up to 1 in 85 persons worldwide unless effective measures of prevention and treatment are discovered (Brookmeyer et al. 2007).

1.1.2 History of Alzheimer's disease

It has been more than a century since German neuropathologist Dr. Alois Alzheimer (1864-1915) first described AD condition in the year 1906. Since then, there has been an explosive growth in the number of people affected by this disease. The first case of AD was documented in 51-year-old women from Frankfurt by the name Auguste Deter aged 51 years. She displayed a range of strange behavior, including personality changes and severe loss of short-term memory and finally succumbed to

the disease in Frankfurt in the year 1906. Autopsy results showed uniformly atrophic brain with no intrinsic macroscopic abnormalities (Fig.- 1.1). On histopathological examination, there were plaques, neurofibrillary tangles and arteriosclerotic differences.

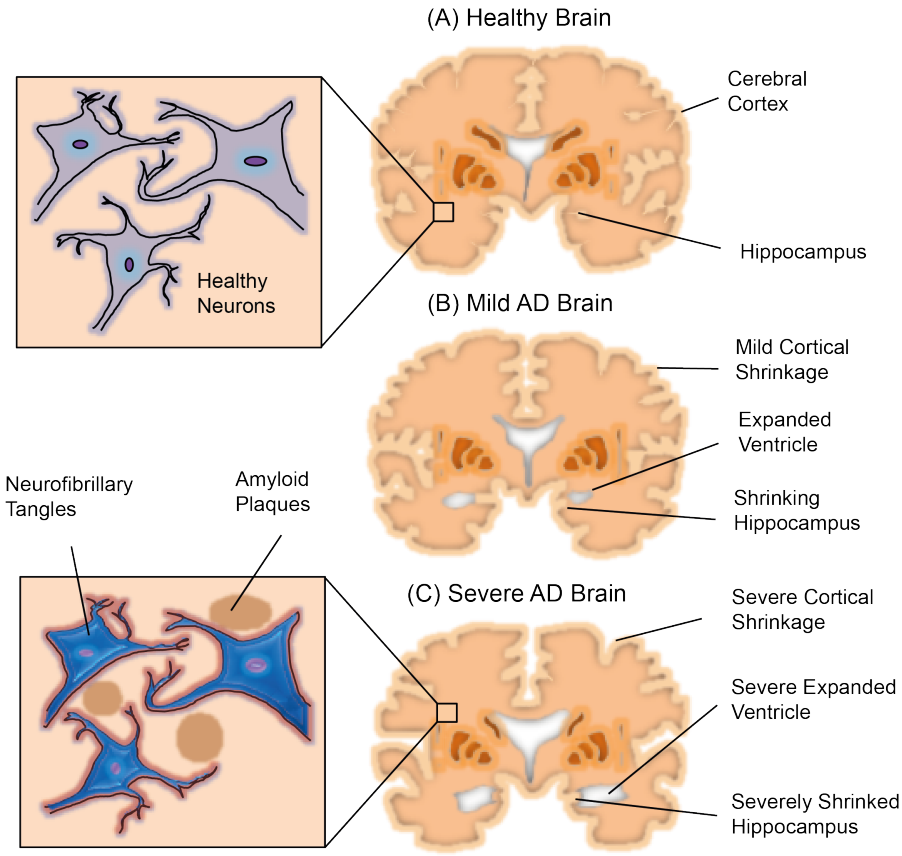

Fig.- 1.1: Neuropathological and Anatomical features in Normal vs. AD brain. (**A**) Healthy brain displaying healthy neurons in the inset. (**B**) Brain affected by Mild AD showing differences compared to the healthy brain. (**C**) Severe affected AD brain showing overall atrophy followed by amyloid plaques and neurofibrillary tangles in the inset.

Brain tissue preparations by Bielschowsky's silver method showed distinct changes in neurofibrils when compared to the controls. With the progress in research, it was concluded that arteriosclerosis was no more essentially the hallmark of the disease. Rather, presence of neuritic plaques and neurofibrillary tangles were confirmed in all AD cases, representing as the hallmark of the disease (Fig.- 1.1). Emil Kraeplin, who was director of the Royal psychiatric clinic in Munich, separated this disease condition from senile dementia and termed it as Alzheimer in the textbook of psychiatry in year 1910. Molecular characterization of neuritic plaques and fibrillary

tangles was performed in 1960's with development of EM (Electro Microscopy). Isolation of two fibrillar proteins (Amyloid Beta and Tau) in plaques and neurofibrillary tangles (Fig.- 1.1) was one of the major challenges solved in understanding the neurobiology of the disease (Selkoe et al. 2012).

1.1.3 Discovery of Amyloid Beta (Aβ) and Tau

Isolation of fibrillar proteins from the plaque was a major challenge, and was being pursued by researchers in the 1960's. George Glenner developed the isolation methods for protein purification from the plaque (Glenner & Bladen 1966). Later X-Ray diffractions were performed from the purified protein fibrils for biophysical studies, which indicated to the presence of high beta sheet content in the protein isolate (Eanes & Glenner 1968). He was majorly interested in purifying the majorly occurring amyloid protein found in the cerebral blood vessels called it the cerebral vascular amyloid. His team developed a biochemical protocol in the 1980's, which exploited the non-solubilizing character of the amyloid protein. Using strong chaotrophic denaturants, the protein was purified and could be solubilized, characterized on the SDS-PAGE and HPLC and found to be in the range of 3KDa in size (George G. Glenner & Wong 1984). This evidently indicated that the protein present in the neurofibrillary tangles is different in amino acid composition as compared to the amyloid protein found in the brains (Masters et al. 1985; G G Glenner & Wong 1984; Wong et al. 1985). They chose to call this protein as Amyloid Beta (Aβ) protein.

1.1.4 Amyloid Beta Biogenesis

With the Partial amino acid sequence available from (George G. Glenner & Wong 1984), the cDNA encoding part of amyloid beta precursor was cloned (Goldgaber et al. 1987) (Tanzi et al. 1987). They predicted from the full-length cDNA to be a 695 amino acid type-I transmembrane protein, which contained 17-residue signal peptide, a single membrane-spanning region and a short cytoplasmic tail. This was called as Amyloid Precursor Protein (APP). The amyloid beta region was predicted to begin at 28 residues amino terminal to the transmembrane domain extending 11-15 residues

further into the domain. Major isoforms of APP were later discovered resulting from alternative splicing in the APP gene. The widely abundant APP in humans was found to contain 751 amino acids encoding exon 7 (Ponte et al. 1988). Cultured Neurons and various transfected cell lines that over-expressed APP released a large soluble ectodomain called as soluble APP (sAPP) in the medium (Schubert et al. 1989; Sisodia et al. 1990). The cleavage left behind a 10kDa Carboxy Terminal Fragment (CTF) within the cell (Palmert et al. 1988).

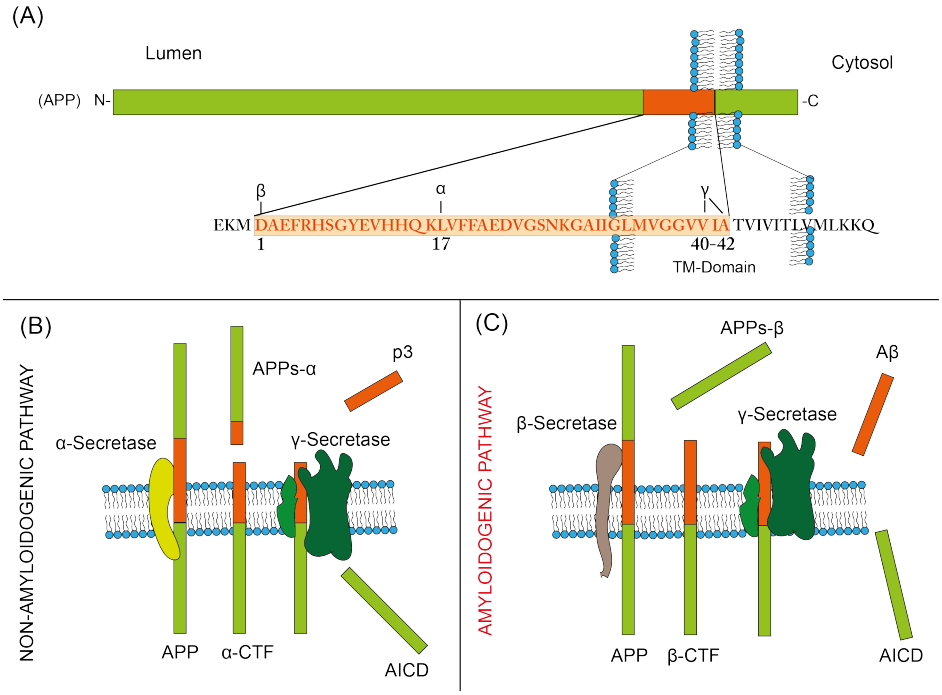

Fig.- 1.2: APP cleavage and formation of Amyloid Beta. Sequential cleavage of the amyloid precursor protein (APP) occurs by two pathways. (**A**). The Aβ-peptide starts within the ectodomain and continues into the transmembrane region (orange). (**B**) Non- amyloidogenic processing of APP involving α-secretase followed by γ-secretase is shown. (**C**) Amyloidogenic processing of APP involving BACE1 followed by γ-secretase is shown. The above figure adapted and modified from (O'Brien & Wong 2011)**.**

The cleavage site was later determined by protein sequencing of the CTF (Esch et al. 1990). The sAPP form ended with Gln15 and the CTF amino terminus was Leu17, suggesting that Lys16 was cleaved by an ecto-peptidase in either of the fragments. The unknown endo-peptidase involved in APP secretion was henceforth called as α-secretase and the soluble APP was called as sAPPα. Later, the APP processing by α-secretase was understood to occur both intracellularly (De Strooper et al. 1993)

and on the cell surface (Sisodia 1992). The action of APPs cleavage by α-secretase was proved to be amino acid sequence dependent (Zhong et al. 1994). As α-secretase action involves cleavage within the Aβ region (non-amyloidogenic), it was concluded that pathogenic amyloid protein must be formed by a different pathological pathway (amyloidogenic). A smaller peptide was found containing a portion of Aβ, designated as p3, which started with position of 17 of Aβ, clearly suggesting that it would have been derived from 10kDa CTF present intracellularly after α-secretase cleavage of APP.

Meanwhile, studies indicated the minor amounts of all APP peptides are turned over to produce secreted Aβ (Seubert et al. 1992). Aβ was also detected in plasma and cerebrospinal fluids of humans and mammals. This finding of Aβ peptide constitutively being produced and secreted sparked major interests in the number of investigations focused on Aβ generation. Moreover, it was also shown that a new soluble APP was found, cleaved precisely at the amino terminus of Aβ designated as sAPPβ. This finding indicated that β-secretase cleavage occurred in the secretory pathway as well. The picture got clearer in the analysis of a rare APP mutation called as the Swedish Mutation, where β-secretase role was dominant and provided the first direct evidence for a role in enhanced Aβ production (Mullan et al. 1992).

As terminating soluble APP's have been identified at the β-secretase site, it was clear that there was one more peptide involved in the cleavage that generated the C-Terminus of Aβ and p3 fragment. It was designated as γ-Secretase. γ-Secretase activity was henceforth proven to occur after α-secretase and β-secretase activity on APP and the γ-Secretase acted on the CTF fragments later. The sequence specificity of γ-Secretase was described (Tischer & Cordell 1996) and was shown that substitution of negatively charged residues at 40-46 position, precluded the formation of Aβ and APP maturation with the membrane boundary at position 46/47. Sequential cleavage of the amyloid precursor protein (APP) occurs by two pathways as follows. (i) Non-amyloidogenic processing of APP involves α-secretase followed by γ-secretase yielding p3 (Fig.- 1.2B). (ii) Amyloidogenic processing of APP involves BACE1 cleavage followed by γ-secretase yielding Aβ's (Refer Fig.- 1.2C). Both the

processes generate soluble ectodomains (sAPPα and sAPPβ) and identical intracellular C-terminal fragments (AICD) (Fig.- 1.2B&C).

1.2 Current Understanding of Alzheimer's disease

Currently, among few of the AD Pathology Hypotheses, Amyloid cascade hypothesis (ACH) has been widely accepted with certain modifications in the field. Recently, an experimental validation of the amyloid hypothesis has been provided where accumulation of Aβ has been shown to drive tauopathy (Choi et al. 2014). This has added further credence to this hypothesis. The original Amyloid cascade hypothesis posited that AD progression is due to deposition of protein Amyloid Beta (Aβ). Aβ, which form fibrils and later these fibrils accumulate and pack tightly to form amyloid plaques is known to be the commencing point in AD (Hardy 2006). In the progress and quest to understand how these fibrils form and lead to neurotoxicity, it was found that, there was lack of correlation between the deposited Aβ in the amyloid plaques in terms of the amount, location and cognitive impairment or neurodegeneration (Benilova et al. 2012).

1.2.1 Amyloid Hypothesis

Amyloid cascade hypothesis (ACH) postulates that, Aβ deposition is the primary event in the disease, which leads to astrocytosis, microglial reactivity and the development of NFT's (Hardy & Higgins 1992; Hardy & Selkoe 2002) (Fig.- 1.3). Points supporting Amyloid Cascade Hypothesis are as follows:

i. The APP gene is found on chromosome 21 & AD-like neuropathology is invariably seen in Down's syndrome.
ii. Inherited mutations in the APP gene that flank or occur within the Aβ region alter the amount or aggregation properties of Aβ and precipitate early-onset AD.
iii. Inherited mutations within the Presenilin 1 and 2 genes increase the Aβ42/Aβ40 ratio throughout life and cause very early and aggressive forms of

AD.

iv. ApoE e4 allele is a major risk factor for developing late-onset AD, whereas the e2 allele appears to be protective. Apo E regulates degradation of Aβ.
v. Mice transgenic for human APP show a time-dependent deposition of Aβ and develop certain AD-like neuropathological and behavioral changes.
vi. Injection of synthetic Aβ or co-expression of mutant APP with mutant tau accelerates tau hyperphosphorylation and leads to tangle AD-like formation.
vii. *Ex-vivo,* Aβ exhibits disease-relevant toxic activity.
viii. The levels of formic acid extracted Aβ peptides correlate with disease severity.
ix. Synthetic Aβ peptides are toxic to hippocampal and cortical neurons, both in culture and *in-vivo*.

Despite the evidence provided by AD causing mutations in Aβ, there are certain lacunas with the amyloid cascade hypothesis, as 99% of AD cases are known to be sporadic in nature for which there is no explanation in the hypothesis. The hypothesis fails to explain amyloid beta in what conformation or form causes neuronal death? Due to this riddle, there were several extensions proposed to the existing hypothesis. Several researches suggest that there is a negative correlation between extracellular fibrillar amyloid burden and cognitive impairment or dementia (Price et al. 2009) . To accommodate these recent findings, the amyloid cascade hypothesis has been modified to propose that non-fibrillar, soluble Aβ-oligomers, rather than insoluble Aβ accumulates present in plaques, are responsible for initiating AD pathology (Glabe 2006; Shankar et al. 2007). In support of this Aβ-Oligomer model, levels of soluble Aβ correlated better with the degree of dementia in humans than amyloid deposits in the brain (Lesné et al. 2006). The Aβ-Oligomer hypothesis is currently dominating in the field, positing that Aβ-oligomers are more neurotoxic than the fibrils plaques themselves as drivers of neurodegeneration in the brain. However, the limitations of Aβ-Oligomer hypothesis has been that, the term “Oligomer” has been poorly defined and characterized in literature. And there are discrepancies in methods used in oligomer preparations from Aβ peptides and brain extraction techniques used to derive native Aβ-oligomers from the brain employed across the labs (Benilova et al. 2012), which adds to further complexity in defining the oligomer.

The basic definitive proof of Amyloid hypothesis and cascade has been lacking. However, by far, this hypothesis has been the most accommodating hypothesis accounting for AD progression. Until an infectious Aβ conformation can be generated with only the Aβ peptide, the amyloid protein based hypotheses of AD will continue to remain unproven and debated in the field.

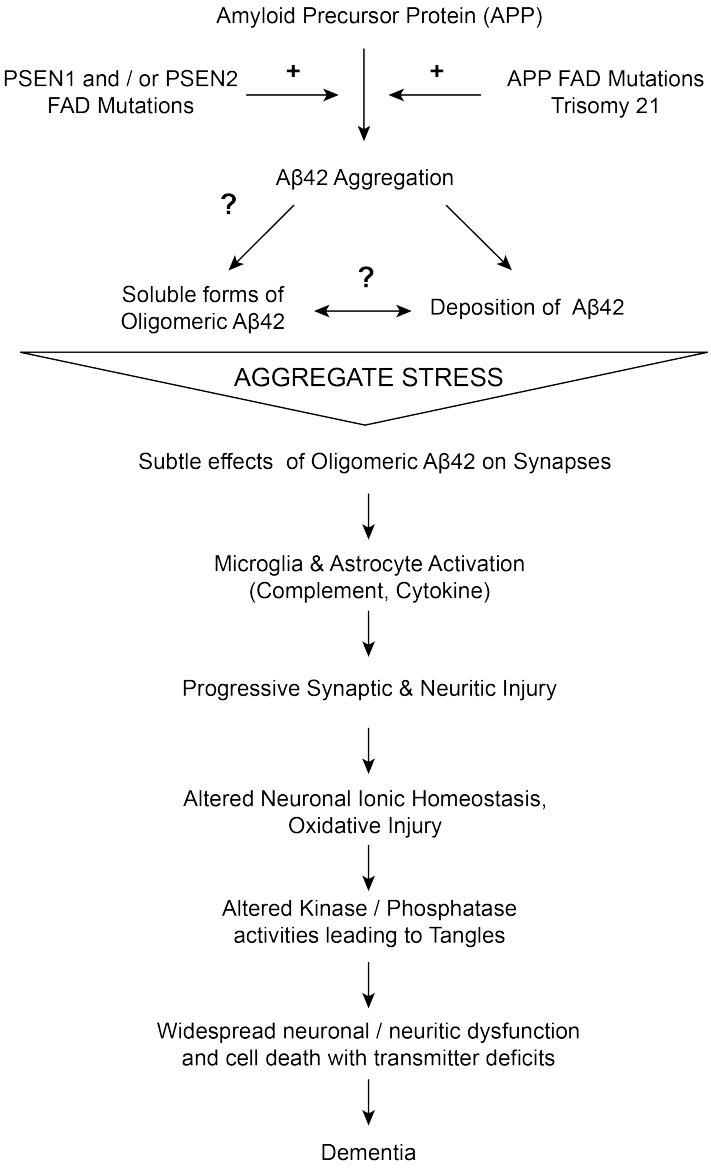

Fig.- 1.3: Modified amyloid cascade hypothesis. Question marks indicate less understood critical processes being investigated in AD. Adapted and modified from (Karran et al. 2011).

1.3 Amyloid Protein Chemistry and Biophysics

German scientist Rudolph Virchow first introduced “Amyloid” term in the year 1854. It was used to denote a macroscopic tissue abnormality that exhibited positive iodine staining. Amyloid proteins demonstrate inherent birefringence when stained with Congo red dye. At that point of time, the amyloid substance was considered composed of starch by Virchow. Later in the year 1859, it was Friedreich and Kekule, who demonstrated the presence of mass of protein in the amyloid deposit based on its high nitrogen content. Initially investigation into amyloid started as protein and later on any protein that had the inherent propensity to change conformation and aggregate to form fibrils were included in the amyloid class of protein (Sipe & Cohen 2000). The characteristics of amyloid protein when compared to other proteins, is their ability to form higher aggregates, oligomers and later into fibrillar structures. These fibril structures are highly resistant to protein turnover mechanisms and non degradable by the proteosomal machinery. This phenomena leads to accumulation of the amyloid protein, which later causes diseased condition due to amyloid protein accumulation and hence called as “Amyloidosis” (Hardy et al. 1986).

1.3.1 Amyloid Beta Biophysics

Amyloid formation process shares similarities to crystallization process, and may be therefore considered as an analogous phenomenon to understand. At the start a nucleus is formed, which then grows and gives rise to soluble intermediates, later with time, these finally aggregate to insoluble fibrils. X-ray diffraction studies have revealed cross-β model as a generic model for amyloid fibrils (Eanes & Glenner 1968). X-ray diffraction of amyloids shows characteristic meridional and equatorial reflections. Diffraction studies on Aβ fibrils have revealed a cross–β pattern (Kirschner et al. 1986). Diffraction pattern identified that β-strands were perpendicular to the main fibril axis and β-sheet was parallel to the same axis. The characteristic two diffraction sets observed values were 4.7 Å - 4.8 Å (Meridional) and 10Å - 11Å (Equatorial) corresponded to inter-strand and stacking distances respectively (Marshall & Serpell 2009) (Fig.- 1.4). Parallel β-strand organization was the most

commonly found in most of the amyloid fibrils (Balbach et al. 2002) and the β-strands are coordinated either in in-register or in a β-solenoid arrangement.

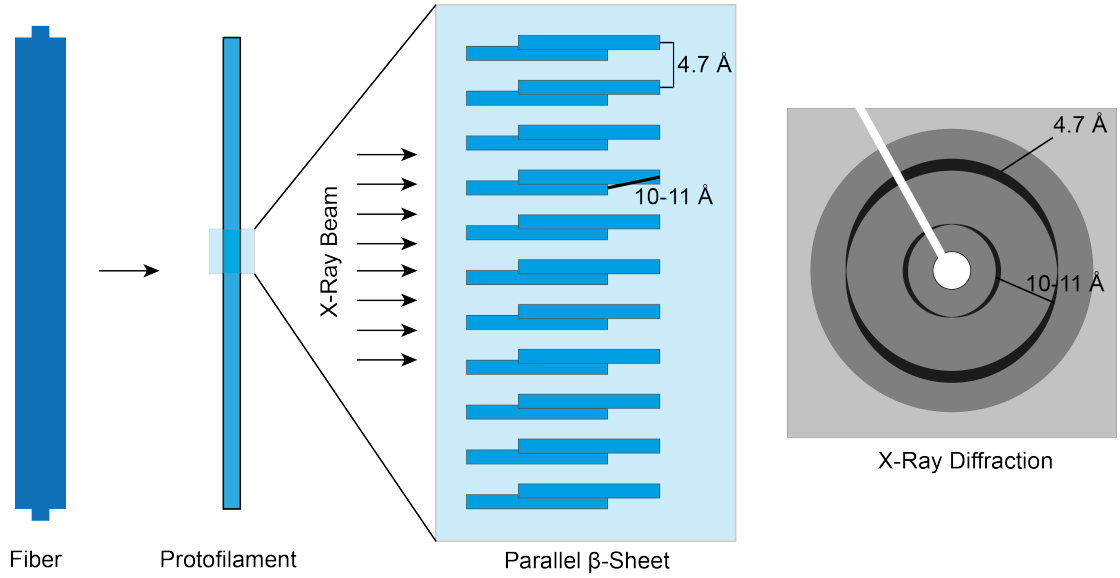

Fig.- 1.4: X-Ray diffraction of Amyloid Fibril. A schematic of a Parallel β-sheet arranged in cross beta arrangement, diffracted by an X-Ray to obtain an diffraction pattern showing the 4.7 Å -4.8 Å (Meridional) and 10 Å-11 Å (Equatorial) reflections that define cross-beta structure (Marshall & Serpell 2009).

The first evidence that Aβ could contain parallel β-sheets and anti-parallel β-sheets in arrangement has been observed in few Aβ peptide fragments (Petkova et al. 2004).

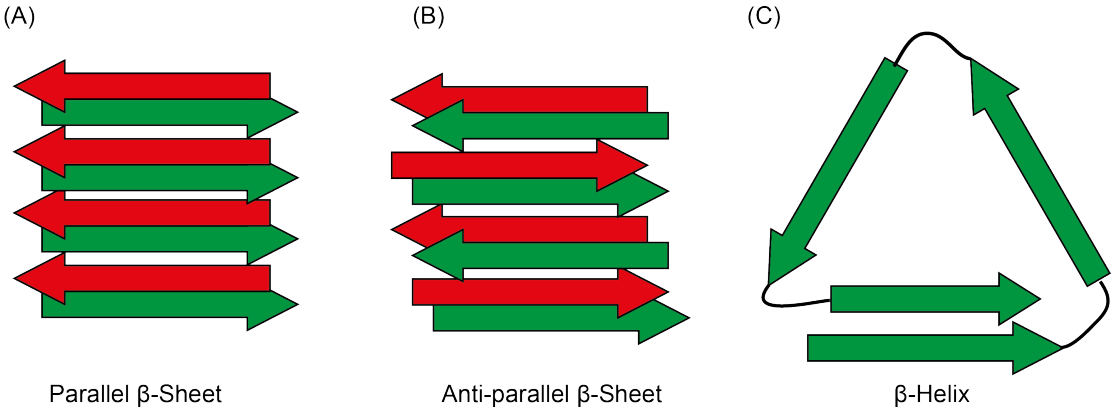

Fig.- 1.5: Schematic representations of cross β-sheet structures that amyloid proteins can adopt. (**A**) Parallel β-sheet (**B**) Anti-parallel β-sheet and (**C**) Top view of β-helix. Adapted and modified from (Tycko 2011).

Shorter Aβ peptides contain only one β-strand, whereas the full length Aβ peptide

contains two or more β-strands segments. Anti-parallel β-strand arrangement was recently found in the full peptide Aβ(1-40) D23N (Iowa mutation) (Tycko et al. 2009). The cartoon representations of various possible cross-β structures are shown in Fig.-1.5. Knowledge about the amyloid fibril structures are important for a number of reasons namely (i) To design compounds that can inhibit amyloid fibril formation or (ii) bind specifically to amyloid by rational drug design approaches (Sievers et al. 2011; Sato, Kienlen-Campard, Ahmed, Liu, Li, Elliott, Aimoto, Constantinescu, J.-N. Octave, et al. 2006).

1.3.2 Primary Structure of Aβ peptide

The amyloid plaques resulting from aggregation of Aβ fibrils peptides are the hallmarks of AD. Aβ peptides evolving from sequential cleavage have been explained in Aβ biogenesis section (Refer, Section- 1.1.4). Upon cleavage by gamma secretase of APP, the Aβ peptides are released mainly as unstructured monomers. From the hydrophobicity of the primary Aβ- structure, it can be divided into four regions: two hydrophobic and two hydrophilic parts (Fig.- 1.6).

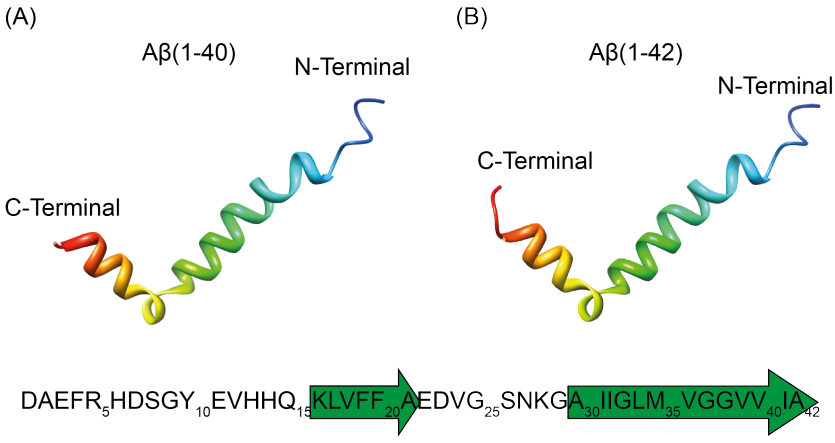

Fig.- 1.6: Random Coil Aβ peptide Sequence and swiss homology model of (**A**) Aβ40 and (**B**) Aβ42 rendered using chimera, showing C terminal and N terminal ends of the peptide(Arnold et al. 2006). The two hydrophobic regions L17-A21 part and the C-terminus A30-V40/A42 exhibit secondary structure propensity for β-structure and are highlighted as green arrows in the primary structure (Abelein et al. 2014).

The first 16 N-terminal residues constitute a hydrophilic tail that is unstructured. The two hydrophobic regions are L17-A21 part and the C-terminus A30-V40 / A42 (Fig.-1.6), that are separated by the hydrophilic central region E22-G29. The predominant Aβ forms in AD are Aβ40 and Aβ42 shown below in random coil conformation (Fig.-1.6). Amyloid fibrils are intrinsically insoluble and non-crystalline in nature making them non-amenable to high structure determination techniques such as X-ray crystallography or high-resolution solution state NMR. Based on solution state NMR, solid state NMR and electron microscopy studies it has been concluded that a hairpin-like conformation constitutes a common motif for the Aβ peptide in most of the described fibril structures. However there have been molecular heterogeneities observed, resulting from different hydrogen bonding partners in different hairpin conformations (Abelein et al. 2014). The interacting hairpins are known to be the building blocks of the fibrils and how these hairpin variations are organized in the cross-section of the fibrils, perpendicular to the fibril axis constitute the amyloid beta fibrillar heterogeneity (Paravastu et al. 2008a).

The contacts between the β strands in the hairpin motifs have been summarized in the Fig.-1.7 taking into account different proposed models for Aβ. Fig.- 1.7 shows a schematic model of Aβ42 and Aβ40 sequence, summarizing current models for how the two β-strand regions may fold into β-turn-β (hairpin conformation) with variable intermolecular residue contacts. Investigation into multiple β-turn-β units at the fibril cross-section of Aβ42 also has been reported, where Met35 has been shown to form intermolecular contact with Gly37, indicating that the cross-section is composed of two β-turn-β units with a two fold symmetry (Sato, Kienlen-Campard, Ahmed, Liu, Li, Elliott, Aimoto, Constantinescu, J. Octave, et al. 2006). Several studies have concluded that the proposed models are over-simplifications. The N and the C terminal of the peptide show significant mobility making structure hard to assign by conventional low-resolution methods, thereby preventing the development of a detailed model.

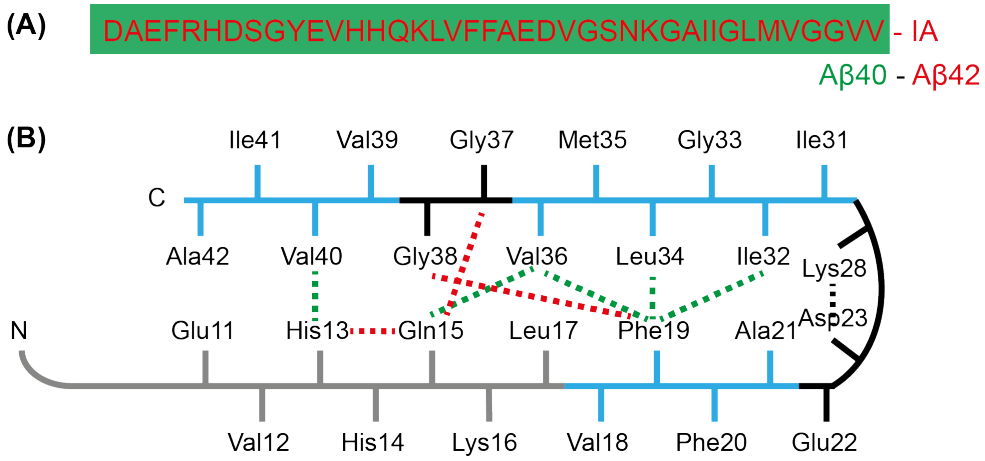

Fig.- 1.7: Sequence and structure of Aβ40 and Aβ42 fibrils with intermolecular contacts. (**A**) Primary sequence of Aβ40 and Aβ42. (**B**) Structural constraints in Aβ40 and Aβ42 fibrils. NMR investigation in Aβ40 fibrils have shown that residues 1-10 are unstructured and residues 11-40 adopt a β-turn-β fold (Paravastu et al. 2008a; Tycko 2006). Side chain packing is observed between phe19-Ile32, Leu34 and Val36 and between Gln15-Val36 as well as between His13-Val40 (green dashed lines). In both Aβ40 and Aβ42 fibrils, the hairpin conformation is stabilized by hydrophobic interactions (cyan residues) and by a salt bridge between the residues Asp23-Lys28 (black dashed line). In Aβ42 fibrils, residues 1-17 may be unstructured (in gray), with residues 18-42 forming a β-turn-β fold. Molecular contacts have been reported within the monomer unit of Aβ42 fibrils between the residues Phe19-Gly38 (red dashed line) (Thorsten et al. 2005). DARR NMR measurements of Aβ42 specifically show the sidechain-packing registry within the β-turn-β structure involving the molecular contacts between Phe19-Leu34 (green dashed) and between Gln15-Gly37 (intermolecular) and His13-Gln15, this model suggests that the N-terminal β-strand starts at-least at residue 13, showing the first 10 residues are unstructured (red dashed). In the Aβ42 fibrils, ssNMR measurements show contacts between Phe19-Leu34 and amide exchange measurements indicate solvent accessible turns at His13-Gln15, Gly25-Gly29 and Gly37-Gly38 (Black Segments) (Ahmed et al. 2010). Fig. Adapted modified from (Ahmed et al. 2010).

1.3.3 Structural model of Aβ42 Fibrillation

The starting point of fibrillation is formation of a protofilament structure, which acts as the interface for fibril formation. The protofilament structure consists of C-terminal hydrophobic sequence of Aβ folding into β-turn-β conformation; the fibrils are composed of multiple β-turn-β units that polymerize in a parallel and in-register orientation. The 3d structural $A\beta42^{35Mox}$ model of protofilament consist of two stacked, intermolecular, parallel, in register β-sheets that perpetuate along the fibril axis. The residues L17, F19 and A21 of the β1-sheet mediate the hydrophobic intermolecular contacts with the even number residues of β2-sheet (Fig.- 1.8). Fibril extension most likely occurs at the tip of the formed protofilaments. The interactions

between the Aβ42 molecules are hypothesized to occur by domain swapping-type interaction between the β-strands, implying the presence of distinct surface at the opposing ends. A hydrophobic cleft is formed by β1-strand and β2 strand of the template at the odd end of the protofilament. The incoming Aβ42 monomer could initially bind by means of the contiguous hydrophobic stretch of residues 17-21. This complex could be further stabilized by intermolecular salt-bridge (D23-K28) formation and backbone hydrogen bonds. Nevertheless, the newly added monomer could still disassociate as the β2-strand has substantially fewer interactions with the template than the β1-strand. Therefore, the last added monomer would be stabilized permanently only by the addition of next monomer. This suggests a sequence-selective, cooperative mechanism of Aβ fibril extension that follows first order kinetics. From this, it was concluded that the Aβ1-42 fibrils are stabilized by intermolecular domain swapping interactions similar to those seen in other amyloids (Thorsten et al. 2005).

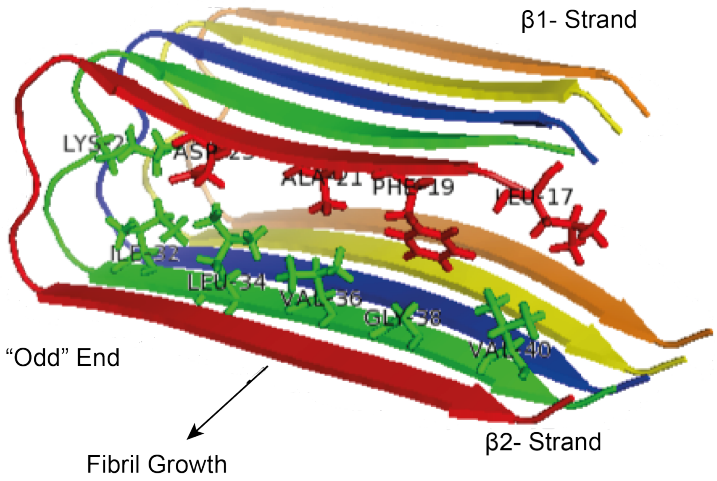

Fig.- 1.8: Aβ42^{35Mox} fibrillation model (PDB: 2BEG) (Thorsten et al. 2005). Ribbon diagram of the core structure of residues 17-42 of five Aβ molecules, each represented in a different colour, depicting the intermolecular nature of the inter-β-strand interactions. Individual molecules are labeled. Colored arrows indicate the β-strands of each Aβ molecule, the non-regular secondary structure is indicated by spline curves through the C-alpha atom coordinates of respective residues. Rendered using academically licensed PyMol.

Intrinsic sample polymorphism of fibrillar Aβ structures has been a major obstacle for ssNMR studies, as it results in samples with low structural homogeneities. Aβ fibril

studies with ssNMR and electron microscopy have finally come to an acceptance that the structure of Aβ is not uniquely determined by the amino acid sequence. Rather, the fibril structure also depends on precise buffer preparation details and subtle variations in growth conditions. Obviously, these structural variations at molecular level lead to variations in ssNMR spectra (Petkova et al. 2005; Qiang et al. 2011). Nevertheless, an emerging consensus supports the polymorphism of fibril structure morphology, possibly with multiple structures co-existing, even though all tertiary structures are based on parallel in-register β- sheet secondary structures, generally showing hairpin variants among the contacts between the β-strands. The fibril cross-sections display either twofold or three-fold symmetry for structural models determined from experimental constraints concerning the arrangement of the ordered hairpins (Paravastu et al. 2008b). In the next section, we will discuss more about structural models on Aβ polymorphisms.

1.4 Amyloid Beta Polymorphism

One of the central principles of biochemistry is that protein structures are entirely uniquely determined by primary amino acid sequences. This principle does not apply to the amyloid beta peptide. Amyloid Beta displays a plethora of aggregates and adopts heterogeneous fibrillar forms *de-novo* and *in-vivo* conditions also referred as amyloid beta polymorphisms (Walker et al. 2008; Levine et al. 2010; Arce et al. 2011; Toyama & Weissman 2011).

1.4.1 *De-novo* Aβ Polymorphisms

Aβ fibrils investigation by electron microscopy (EM) has revealed structurally polymorphic conformations of Aβ, which include protofibrils, low and high molecular mass oligomers. Later with long incubation times *in-vitro* they assembled in polymorphic fibrils (Goldsbury et al. 2005). Subtle variations in fibril growth conditions lead to significant, reproducible and self-propagating variations in molecular structure of Aβ40 fibrils. It was later shown by EM and Solid State NMR, that these different fibril morphologies have different underlying molecular structure and it was not mere

lateral protofilament association in the fibrils. These different morphologies were also demonstrated to have different neuronal toxicities. These findings in amyloid fibrils are analogues to prion strains in prion diseases (Petkova et al. 2005; Wang et al. 2011). The conformational details of the non-β-strand segments in the peptide, the contact between β-sheets and the fraction of the peptide sequence that becomes structurally ordered in the fibrils have been reported to vary (Bertini et al. 2011). The N-terminal and the C-terminal of Aβ40 have been reported to be “staggered”, meaning that the two β-strands from the given peptide molecule do no make contact with one another. The direction of the stagger itself is difficult to determine from experimental measurements and has been postulated to be a source of polymorphism (Paravastu et al. 2008a; Petkova et al. 2006). Fibrils extracted from AD brain tissue when seeded to isotopically labeled monomeric Aβ40 and investigated by NMR concluded that AD brain derived Aβ seeded fibrils were homogenous as compared heterogeneity observed in concomitantly aggregated Aβ40 (Paravastu et al. 2009).

Monoclonal antibodies were raised that could specifically recognize prefibrillar oligomers. Immunological analysis of prefibrillar oligomers revealed the existence of Aβ polymorphisms in prefibrillar oligomers that can be distinguished based on their monoclonal antibody reactivity. These polymorphic prefibrillar oligomers were also able to seed the monomeric Aβ and are capable of seeding their own replication (Kayed et al. 2010). Five distinct fibrillar aggregates of Aβ40 were reported and each of these conformational structures were shown to exhibit unique physical properties and the extensive β-sheet content in the fibrils were correlated to their greater stability (Kodali et al. 2010). Molecular models have been proposed for Aβ polymorphism lately, where eight new microcrystal structures of segments of Aβ were determined. These structures formed self-complementing β-sheet pairs, called as steric zippers. These steric zippers reveal variety of modes of Aβ self-association (Colletier et al. 2011). A second type of amyloid polymorphism was suggested called as packing polymorphism. In packing polymorphism, the same peptide sequence can form distinct steric zipper structures by virtue of different packing in the fibril spine (Wiltzius et al. 2009).

1.4.2 *In-vivo* Aβ Polymorphisms

Excessive accumulation of Aβ also occurs in the brain of cognitively normal aged people. The neuronal toxicity of Aβ was hence postulated to be dependent on its molecular composition and it was shown in the study that soluble beta-amyloid aggregates that accumulate in Alzheimer disease are different from those of normal aging with respect to the composition as well as the aggregation and toxicity properties (Piccini et al. 2005; Moore et al. 2012). Luminescent conjugated polyelectrolyte probes (LCPs) are able to distinguish Aβ42 fibril conformation formed under both quiescent and agitated conditions. LCPs are also shown to resolve conformational heterogeneity of amyloid deposits in frozen brain sections (Nilsson et al. 2007). An extensive review on diversity of Aβ in the aged brain and literature studies connecting to molecular heterogeneity is particularly useful to clarify the complex pathology of AD (Walker et al. 2008). Difference in structural rearrangement of side chains in one β-strand and presence of exposed hydrophobic surfaces in asymmetric Brain Derived Aβ and symmetric agitated *in-vitro* Aβ are attributed to higher toxicity in brain-derived fibrils (Wu et al. 2010).

Quantitative binding studies using radio-ligand ^{11}C-PiB (Pittsburgh compound B) have revealed difference in binding of the Ligand with AD brain homogenates, non-demented humans and plaque bearing transgenic mice. Transgenic mice had the lower ligand binding per mole of Aβ peptide. The binding was lowest in synthetic peptide formed fibrils of Aβ40 and Aβ42. This difference in binding affinities indicates a structural difference in *in-vivo* formed fibrils in humans and transgenic mice (Levine et al. 2010). These distinct molecular polymorphic conformations or Aβ-strains could have different toxic effects related to phenotypic diversity in amyloid diseases too. The structural origin for such polymorphisms still remains elusive (Lim 2013). In a study by Jucker, it was shown that the polymorphic Aβ lesions present in the APP/PS1 mice brain when injected into APP-23 mice induced Aβ deposition with the morphological, conformational and Aβ40:Aβ42 ratio characteristics of Aβ as observed in aged APP/PS1 mice. The result from this study suggests that β-amyloidosis in the brain, C-terminal chain length of Aβ variants might contribute to the nature of the Aβ

conformers and the morphotypes can be sustained by seeded Aβ induction (Heilbronner et al. 2013).

Recently, in a study by tycko and coworkers, the molecular structure of Aβ40 fibrils seeded from the brains of two AD patients were shown to have a single predominant fibril structure in each patient. Also these Aβ40 fibril structures were different as compared to *in-vitro* produced Aβ fibrils (Lu et al. 2013). In he next section, we shall discuss the molecular basis of Aβ polymorphism with the help of models proposed in literature.

1.4.3 Steric Zipper model of Aβ Polymorphism

The core structure of the Aβ fibril might not include the complete primary sequence, but rather diverse steric zipper interfaces. Each one of these interfaces can serve as the spine for structural fibril formation; this type of diversity in fibril spine formation is referred as Segmental Polymorphism (Refer, Fig.- 1.9B). In a second type of Amyloid polymorphism, the short Amyloid peptide segments can form distinct steric zippers by virtue of difference in packing of the fibril spine and β-sheet can arrange either parallel or anti-Parallel. (Refer, Fig.- 1.9A).

β-Sheets formed from the same Amyloid segment are referred to as homotypic interaction and from different amyloid segments are referred to as heterotypic interactions. Aβ fiber diversity and polymorphism are compatible with this notion where fibers are formed from the same or mixed pair of Aβ segments displaying different morphologies owing to the above explained polymorphic associations.

This overall suggest a combinatorial effects of all these different polymorphism mechanisms that constitute amyloid fiber diversity and polymorphs (Refer Fig. 1.9C). In, single-chain registration polymorphism, two segments of the same chain forms two steric zippers with different registrations of their side chains (Refer, Fig.- 1.9D). Combinatorial and single chain registration polymorphism are proposed models of amyloid polymorphism and yet have not been observed at an atomic level (Wiltzius et

al. 2009). Eleven short segments of 6-8 residues from the Aβ42 peptide representing thirteen diverse steric zipper interfaces have been determined at atomistic detail, each of which can serve as the spine for fiber formation.

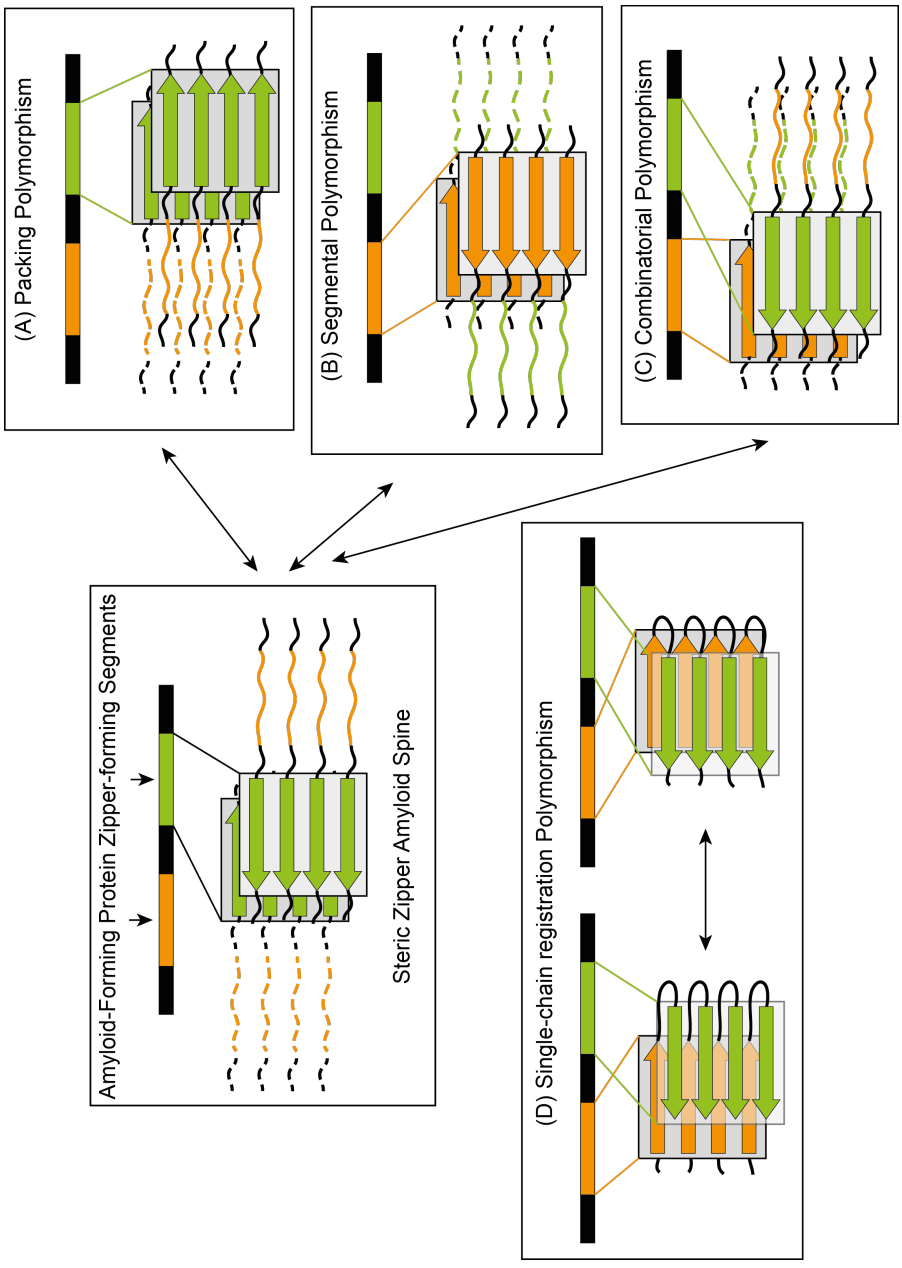

Fig.- 1.9: Steric zipper model for Polymorphisms in Amyloid proteins. (**A**) Packing, (**B**) Segmental, (**C**) Combinatorial and (**D**) Single chain registration Polymorphisms. Adapted from (Wiltzius et al. 2009).

This merely constitutes the segmental polymorphism in Aβ, considering the packing and other mechanisms of polymorphism, there are many undetermined polymorphic structures (Colletier et al. 2011).

1.5 Prion-like Alzheimer disease proteinopathy

In the 1980's, the prion disease was proved to be the disease caused by protein misfolding process (Prusiner et al. 1984). "Prion disease" is a neurodegenerative disease caused by aggregation of an amyloid protein that extracellularly aggregates within the CNS (Central Nervous System) and forms plaques in the brain, which rupture the normal tissue. This disruption leads to spongy architecture in the brain, due to vacuoles formed in the neurons (Cohen 1995). This amyloid protein causing prion disease was later called as Prion Protein (PrP), the normal endogenously folded cellular form was called as (PrP^{C}) and the misfolded pathogenic form was called as Scrapie Prion (PrP^{Sc}). Prion propagation is by transmission of the misfolded protein state. On gaining entry into healthy organism, the misfolded protein induces the existing normal protein to adopt itself into misfolded conformation. These freshly formed misfolded protein acts like an template which further can propagate the misfolded conformation by breaking down into seeds (Misfolded templates), and these seeds convert the other existing normal protein in the organism to misfolded protein state starting a prion cascade (Prusiner & Kingsbury 1985).

It was during the same time, AD was also classified as an amyloid disease, caused by the aggregation of protein called Aβ (Amyloid Beta) (George G. Glenner & Wong 1984). The aggregation and deposition of Aβ peptides are believed to be central events in the pathogenesis of AD. For more than 40 years, there exists certain similarities between prion diseases and Alzheimer's disease and has evoked a speculation suggesting that AD might be infectious in a manner similar to prionoses (Prusiner 1984). Both the proteins (Prion and Aβ) caused neurodegeneration-shared similarity with respect to high beta sheet content in the purified brain plaques (Prusiner 1984). These shared featured between the two diseases lead to investigation of AD pathology akin to prion disease, and it was estimated that incubation studies on AD transmissibility would require few more years of incubation time than the CJD (Creutzfeldt-Jakob disease) prion disease (Goudsmit 1982; Brown et al. 1982). In order to test this hypothesis, nonhuman primates were intracerebrally inoculated with brain material from AD patients, but this experiment proved to be not conclusive (Goudsmit et al. 1980). Intracerebral inoculation of buffy coat from the

blood of AD patients into hamsters was also reported to induce prion-like spongiform encephalopathy (Manuelidis et al. 1988), but a subsequent follow up of the study failed to replicate the same finding (Godec et al. 1991). Surprisingly in later it was always shown that, inoculation of brain homogenates containing Aβ aggregates into susceptible transgenic mice and wild-type marmosets accelerated Aβ amyloidosis, suggesting that Aβ aggregates in the brain homogenate are capable of self-propagation and could act like prions. *In-vitro* aggregation of Aβ and the prion is known to be a nucleation-dependent polymerization process (Refer, Introduction, section 1.7) (Fig.- 1.10). This process is potentially applicable to all amyloid proteins too (Eisenberg & Jucker 2012). In the disease state, the conformation of the protein is driven towards an aberrant 3D structure by the process of corruptive templating.

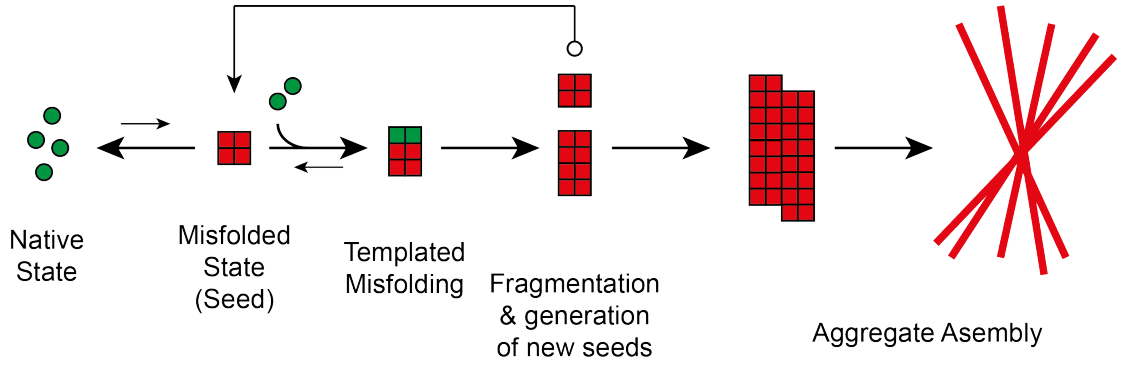

Fig.- 1.10: Model of Nucleated Polymerization (NP) mechanism. The model proposes that the native and misfolded state of the Aβ peptide are reversible. Although the native conformation is strongly preferred but below a critical concentration of the peptide no aggregation occurs and in case if it exceeds the critical concentration level the peptide can form a corruptive seed that then amplifies the template misfolding to other Aβ monomers. Seed addition can rapidly induce aggregation and eliminated the lag period in fibril formation. Fragmentation of the larger aggregates can generate new seeds, which can accelerate fibril formation. Model adapted from (Harper & Lansbury 1997)

1.5.1 Amyloid beta induction in non-human primates

Owing to longer incubation period in monkeys, the first experimental result emerged in the year 1993. In this study Marmosets (*Callithrix Jacchus*), were inoculated intracerebrally with brain tissue from an early onset AD patient. After incubation of 6-7 years, these inoculated animal brains were analyzed. Moderate number of amyloid plaques associated with argyrophilic dystrophic neuritis along with cerebral amyloid

angiopathy and no neurofibrillary tangles were found. The plaques also stained positive for the Aβ antibody. This study finally concluded that β-amyloidosis is a transmissible process (Baker et al. 1993; Baker et al. 1994). The same study was further continued to rule out the possibility of aging related Aβ plaque deposition in relation to inoculation, and it was found that animals injected in the elderly cohort showed amyloid pathology with 4 years of incubation, whereas there were only 4 out of 26 marmosets found to be amyloid positive in the elderly marmoset control group. These data, therefore proves that, β-amyloid found in middle aged marmosets injected with Alzheimer brain tissue was, therefore, not a consequence of their ageing (Maclean et al. 2000).

A very long-term comprehensive study on seeding of β-amyloidosis in primates was investigated and results were published in the year 2006. In this study, it was found that intracerebrally injected Aβ containing brain homogenates from either human AD subject or marmoset, induced β-amyloidosis in both aged and young monkeys. In the study synthetic Aβ was also inoculated in both aged and young monkeys and surprisingly, inoculation with synthetic Aβ did not induce cerebral amyloidosis. It was concluded from this study that Aβ or its associated factors could initiate or accelerate the process of cerebral amyloidosis in primates (Ridley et al. 2006). In a recently published study, AD-like pathology was shown to be induced by synthetic Aβ-Oligomers in non-human primates. In particular, the authors saw evidence of neurofibrillary tangles, a cardinal feature of AD that rodent models fail to recapitulate unless they express mutant tau (Forny-Germano et al. 2014).

1.5.2 Amyloid beta induction in transgenic mice

With the development of AD mouse models, the Aβ induction experiments were carried out in transgenic mice, offered flexibility to study in large numbers with significantly lower incubation period as compared to that in primates. The first mice model was β-APP mice model; AD brain homogenates from human were infused unilaterally into hippocampus and neocortex of 3-month-old β-APP transgenic mouse. Later were euthanized and examined after 4 weeks to find no amyloid deposition, however at the end of 5 months, profuse Aβ senile plaques and vascular

deposition was found, some of which were birefringent with Congo Red. There was considerably, less limited deposition in the age matched β-APP and non-AD brain inoculated mice controls. There was no beta-amyloidosis in mice receiving extract from a young control case too (Kane et al. 2000). The same study was continued to clarify anatomical distribution of seeded Aβ -immunoreactivity. It was noted that, transgene-derived Aβ deposits were present bilaterally in the forebrain, but plaque load was still clearly greater in the extract-injected hemisphere, providing an evidence for seeding activity (Walker et al. 2002).

Intracerebral injection of dilute Aβ containing brain extracts from AD patients or aged β-APP transgenic mice were performed in young APP/PS1 and APP23 mice and it induced cerebral β-amyloidosis in the mice in a time and concentration dependent manner. Synthetic Aβ mixtures of fresh and aged Aβ42 and Aβ40 did not induce seeding activity in the transgenic mice brain. Hence, it was concluded that, phenotype of the exogenously induced amyloidosis depended both on the source of the seeding agent and also on the host, giving rise to notion of Aβ polymorphic strains *in-vivo* similar to that in prions (Meyer-luehmann 2006).

With the APP23 mice, it was shown that amyloidosis could be achieved in many different brain areas of the mice through injection of dilute Aβ containing brain extracts. Stainless steel wires coated with minute amounts of Aβ containing extracts also induced amyloidosis despite boiling in water and only by plasma-sterilization did not induce amyloidosis. The exogenously induced amyloidogenic process determined the Aβ deposition in the brain region of the host akin to strain specific seeding in prions (Eisele et al. 2009). Later studies by the same group demonstrated that intraperitoneal inoculations with Aβ rich extracts was also induced β-amyloidosis in the β-APP transgenic mice after prolonged incubation times (Eisele et al. 2010).

The β-amyloid inducing factor in the brain extract was investigated and was found that the Aβ in the brain were more PK-resistant than the synthetic fibrillar Aβ generated *in-vitro* and this *in-vivo* PK resistance retained the amyloid inducing capacity in APP23 transgenic mice. Fragmentation of Aβ seeds by extended sonication increased the seeding capacity of the extract (Refer, Fig. 1.10 for

understanding). In this study, PK sensitive Aβ (fractionated) was shown to induce amyloidosis 30% less as compared to the normal seeding extract (unfractionated). These findings demonstrate that small and soluble Aβ seed can induce amyloidosis also raises the possibility that these seeds may mediate β-amyloidosis in the brain (Langer et al. 2011).

1.5.3 Summary of inoculation studies

From all the above studies, there is a commonality, the transgenic mice produced higher amount of Aβ and when confronted with the introduced seed, the overall process of amyloidosis accelerated and in absence of seed, the mice still had age dependent amyloidosis. In a new transgenic model designed, HuAPPwt (Human APP wild-type), these mice never acquired amyloidosis with age. With these mice, it was shown that Aβ deposition could only be induced by injection of AD brain extract into these mice. In addition, without exposure to this material the mice shall never develop alterations. This finding clearly indicated the role of injected seed as the amyloidogenic agent. (Morales et al. 2011). On the similar lines human APP21 rat model was also developed, which does not manifest endogenous deposits of Aβ within the course of its median lifespan of 30 months. These animals were injected with the AD brain extract at the age of 3 months and incubated for 9 more months. After a 9-month incubation period, these rats too developed senile plaques and cerebral amyloid angiopathy in the injected hippocampus, whereas control rats remained free of such lesions (Rosen et al. 2011). Bioluminescence imaging technique was used to monitor Aβ deposition *in-vivo* in live bigenic mice (APP23 : Gfap-luc). In this study, the bigenic mice were inoculated by purified brain-Aβ aggregates and with synthetic Aβ aggregates in separate cohorts. The synthetic inoculated cohorts exhibited lower specific biological activity compared to the brain derived Aβ aggregate inoculated cohorts (Stohr et al. 2012). Overall, there is a burgeoning evidence to indicate that aggregated Aβ in the brain extract is essential for its β-amyloid-inducing activity and that the Aβ conformation *in-vitro* can be different from the one found in the brains. This has also been discussed in Aβ polymorphism section of this thesis. In the next section we will discuss, how amyloid aggregation has been studied *in-vitro*.

1.6 Amyloid Binding Dyes

Small molecules like Congo Red and Thioflavin-T have been essential tools for characterizing Aβ aggregates, both *in-vivo* and *in-vitro*. These small molecules can also be used to monitor Aβ self-assembly *in-vitro* and confirm Aβ deposits *in-vivo*.

1.6.1 Thioflavin-T

Thioflavin-T is a benzothiazole containing fluorescent dye first observed to bind to amyloids *in-vitro* (VASSAR & CULLING 1959) and later *in-vivo* (Naiki et al. 1989) (Refer, Fig. 1.11B). Binding was also observed with synthetic Aβ fibrils (LeVine 1993). This technique of using Thioflavin-T was adopted for quantifying relative amounts of aggregated Aβ in solution and also to monitor kinetics of fibril formation (LeVine 1999). Since then, Thioflavin-t has been widely adopted for monitoring Aβ aggregation.

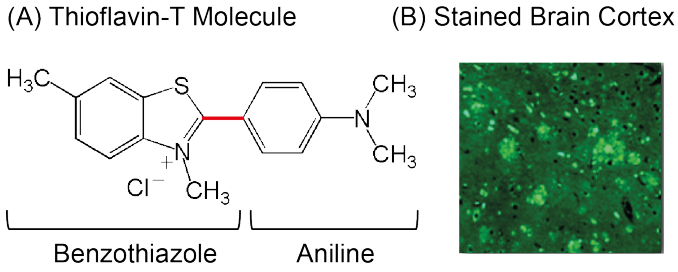

Fig.- 1.11: Thioflavin-T fluorescence (**A**) Structure of Thioflavin T (**B**) AD transgenic Mice brain cortex stained with Thioflavin-T (200x) (Shi et al. 2011)

It was observed that, abolishment of β-sheet structure completely diminished thioflavin-T binding, providing indications that thioflavin-t binds to the cross- β secondary structure. Thioflavin-T fluorescence is known to increase when it binds to Aβ fibrils, because of the rotational freedom of the carbon-carbon bond between the benzothiazole and aniline rings is restricted (red) (Fig.- 11A).

In the unbound state, the ultra fast twisting dynamics around the carbon-carbon bond are thought to effect rapid self quenching of the excited state due to rotational freedom and thereby resulting in low emission (Singh et al. 2010; Srivastava et al.

2010). So, the mechanism of action of thioflavin-T binding to the fibrils can be summarized as the increase in the population of excited state when bound, due to the carbon-carbon bond restriction and rotational freedom in the carbon-carbon bond leading to self quenching in the unbound state. Binding of thioflavin-t to fibrils has been extensively used to monitor aggregation kinetics of fibril formation in many studies. The next section shall detail amyloid aggregation models that have been proposed using thioflavin-t fluorescence.

1.7 Amyloid aggregation pathway models

Techniques using thioflavin-t fluorescence have been developed to study and characterize the kinetics behind self-assembly of Aβ proteins into fibrils. Using the data from kinetic experiments involving amyloid formation *in-vitro* hypotheses have been formulated. Aggregation kinetic experiments have often reported different results, especially during the early times in the aggregation process before the fibrils have formed. As a consequence two competing hypotheses have been proposed to explain the results: Nucleated polymerization (NP) mechanism (Jarrett & Lansbury 1993; Lomakintt et al. 1996) and nucleated conformational conversion (NCC) mechanism (Serio 2000). A simple schematic illustration of the nucleated polymerization model has been explained in the Fig.-1.10. Some of the salient features of the NP model are: (i) the lagtime exists for the seed to form, and the concentrations of oligomers smaller than the seed (critical nucleus) are assumed to be negligible and it represents the aggregate with the highest energy along the pathway. (ii) The concentration of soluble amyloid protein must exceed the critical fibril concentration for fibrils to form. (iii) The aggregation lagtime depends strongly on the initial concentration of the protein present (Powers & Powers 2006). On the contrary, several lines of evidence have shown presence of non-vanishing oligomer concentrations when monomer concentration is below the critical fibril concentration. These results led researchers to propose the NCC mechanism. In NCC mechanism, quickly formed oligomers undergo a slow conformational transition from a largely unstructured aggregate to a more organized nucleus (seed) that can grow into β-sheet dominated fibril (Lee et al. 2011). Since, there could be major structural

differences between unstructured oligomers and highly ordered fibrils, some researches have suggested that the early oligomers may resemble micelles, when the free monomers are above critical micellar concentration (Schmit et al. 2011).

There is much debate as to whether amyloid fibrils nucleate directly from protein solution or whether oligomers form first and then convert into fibrils (May be both the processes could be occurring concurrently). Since both NP and NCC mechanisms could be two extremes of underlying nucleation, a recently proposed NCC model, where it operates like a NP model (Schreck & Yuan 2013) takes a more balanced approach. i.e.- it contains the feature that the concentration of the seed (nuclei) is proportional to the monomer concentration raised to the n_c power, as hypothesized in the NP model (Fig.-1.12a). There are more complex processes that add up to the large number of possible aggregation scenarios where elongation, dissociation and fragmentation processes determine whether fibrils grow longer or whether they break into smaller aggregates and drive the overall aggregation kinetics (Fig.- 1.12 b, c & d) (Cohen, Vendruscolo, Welland, et al. 2011).

In an elaborate study on Aβ42 aggregation, researchers reported that Aβ fibrils act as nucleation centers, speeding the assembly of monomers into toxic oligomers through a fibril-catalyzed secondary nucleation reaction, rather than classical mechanism of homogenous primary nucleation. The result from this study reveals a positive feedback loop that originates from the interactions between the monomeric and fibrillar forms of Aβ42 peptide (Cohen et al. 2013) (Fig. – 1.12 e & f). This study is one of the rigorous works on Aβ42 kinetics in which Cohen and his coworkers considered three possible models for Aβ42 aggregation and tested them against experimentally measured aggregation. In the first model, the rate of Aβ42 aggregation was only dependent on monomer concentration. However, fibril stabilities are also known to influence aggregation and fibril fragmentation would be a major aggregation driver (Fig.- 1.12d), as breaking fibril produces more fibrillar ends and Aβ assemblies can primarily start growing from those ends. The second model reflects the above-mentioned scenario, with the formation of Aβ aggregates depending strictly on the fibril concentration.

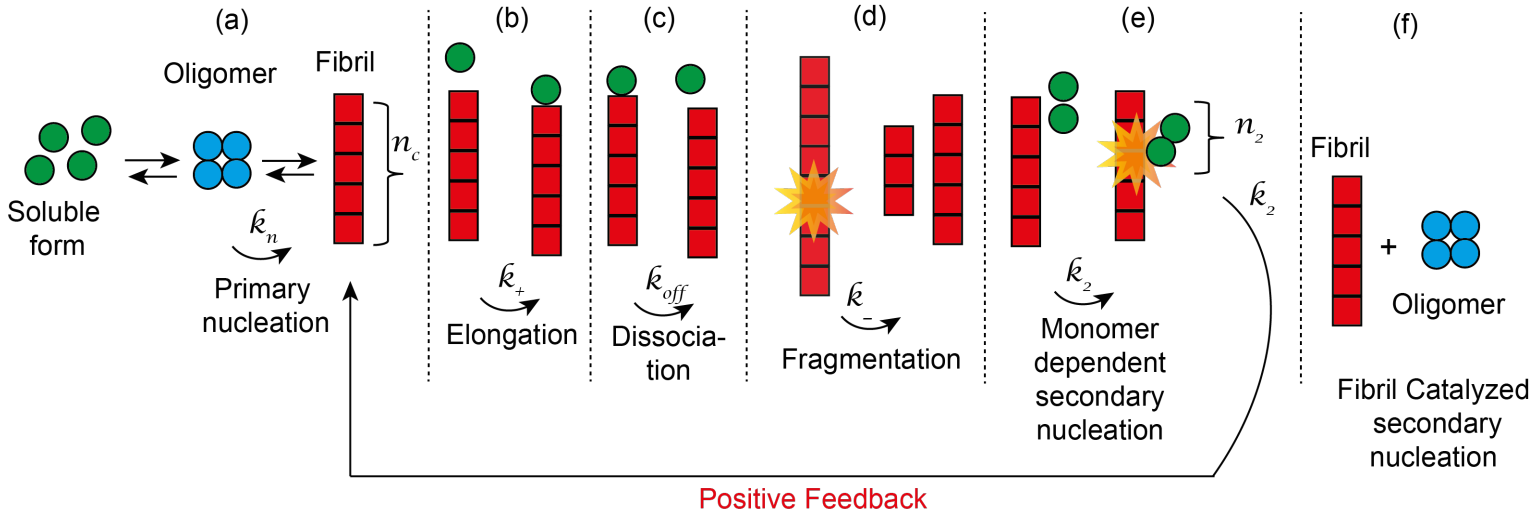

Fig.- 1.12: Schema illustrating the microscopic processes that occur during amyloid aggregation. Primary nucleation (**a**) leads to formation of a small aggregate of size n_c that could undergo a conformational change from a soluble form (green) to an oligomer (cyan) which later form fibrils (Red) with β-sheet content (Schreck & Yuan 2013). The fibrils grow linearly (**b**) from both ends (elongation) and also dissociate (**c**) by Becker-Döring type kinetics of monomer addition and subtraction pathways. The secondary pathways (**d**) fragmentation by Smoluchowski pathways and (**e**) Monomer dependent secondary nucleation lead to creation of new fibril ends from pre-existing fibrils. The secondary nucleation processes depend on the fibril concentration and monomer concentration to a power n_2. The value of n_2=2 in the above Fig. (Cohen, Vendruscolo, Dobson, et al. 2011). (**f**) Fibril catalyzed secondary nucleation where the surfaces of the fibrils act as the catalytic centers for the monomers to form oligomers (cyan). Oligomer formation promotes Aβ aggregation by a positive feedback loop indicated in the Fig. (Cohen et al. 2013).

In the third model, the possibility considered was –secondary nucleation- in which the surfaces of the fibrils catalyze the formation of entirely new aggregates at a rate that depends on the concentration of both monomers and fibrils (Fig.- 1.12f). All of these three models were tested with 10 initial monomer concentrations. The third model gave the best fit for the experimental data suggesting that once fibrils form, they catalyze formation of new oligomers (Fig.- 1.12f). At present, very little is known about the structure of the oligomers (cyan color) formed by secondary nucleation (Fig.- 1.12f). In an parallel kinetic study on nucleated polymerization and secondary nucleation indicated that secondary nucleation can occur on the surface of only specific types of Aβ fibrils indicating polymorphism specific growth kinetic processes (Jeong et al. 2013). Polymorphic fibril structure specific kinetic processes have also been reported to differ between agitated and quiescent Aβ40 fibrils in a study indicating different rate constants for aggregation (Qiang et al. 2013). Conclusively, this section summarizes, the commonly followed pathways by amyloid peptide to convert from its native state to amyloid fibrils (Fig.- 1.12) and describes the mechanisms of nucleation and the other allied processes like elongation, dissociation, fragmentation that overall contribute to fibril amyloid state.

1.7.1 Monitoring amyloid aggregation kinetics

The simplest way to represent the aggregation pathway that leads to formation of amyloid fibrils is by plotting the amyloid aggregate content in the sample versus time. This approach arises from the technique to monitor in real time the amount of amyloid material present after the induction of aggregation. The most widely used technique involves employing thioflavin-t dye, whose fluorescence increases upon binding to the amyloid material. The plot obtained from thioflavin-t fluorescence based aggregation kinetics usually resembles a sigmoidal trace. The aggregation trace can be divided into three phases as shown in the Fig.- 1.13.

At the starting of the process, the amount of amyloid material does not increase as indicated by the black curve (Fig.-1.13). This phase is usually referred to as the

lag-phase. Several molecular events that occur in this phase have been simplified and illustrated in the inset below for simpler understanding. The protein undergoes an assembly followed by increase in size as the time passes leading to formation of a multimer / oligomer that nucleate to form the seed. It is important to understand that, formation of non-amyloidogenic oligomers during the lag-phase cannot be detected by the thioflavin-t spectroscopy. The rate-limiting step aggregation is the formation of the seed to promote fibrillation. The high-energy barrier for nucleation causes an elongated lag phase in spontaneous fibril formation. The length of lag-phase is generally referred to as the lagtime. The kinetic analysis of lagtime is employed to get information about the size of the seed and the rate of fragmentation of fibrils (Knowles et al. 2009). It has been shown that fibril fragmentation rates strongly affects aggregation kinetics as fibril fragments acts as a seed to augment aggregation. In the case of adding a seed (red-curve) (Fig.- 1.13), the lag-phase can be suppressed and increasing the seed concentration can all together eliminate the lag-phase in the seeded reactions.

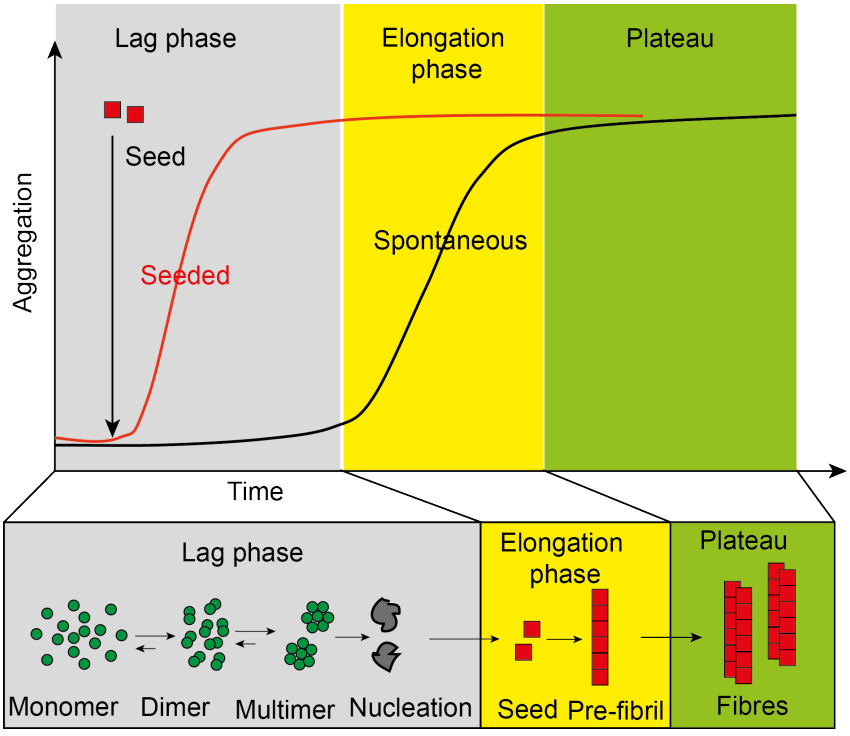

Fig.- 1.13: Spontaneous and Seeded amyloid aggregation versus time. Aggregate mass on the Y-axis and time on the X-axis. The three phases of amyloid formation and the processes involved as simplified and explained in the legend below.

At the end of lag-phase, the aggregation nuclei or the seed is formed, following the conversion of non-amyloid like oligomers into amyloid-like ones. Consequently, the fluorescence of thioflavin-t positive aggregates formed increase over time evidenced by increased fluorescence intensity recorded. This phase is called as the exponential phase or the elongation phase. In this phase, template dependent and template independent conversion of non-amyloid-like into amyloid-like oligomers, fragmentation of formed aggregates along with formation of new aggregates by monomer or oligomer binding to the aggregate ends takes place resulting in fibril elongation. At the end of exponential phase the fluorescent intensity curve reaches the plateau phase. The thioflavin-t fluorescence signal does not increase further and amyloid fibrils are found in the sample when analyzed by electron microscopy.

In conclusion, the plot of amyloid content (aggregation) versus the time (Fig.-1.13) gives fundamental kinetic information about the mechanism of protein aggregation and its processes as described in the section (Refer, Section. 1.7 & Fig.-1.12). The kinetics of the aggregation can be depend on several factors like the primary protein sequence, hydrophobic protein stability, monomeric substrate concentration, secondary structural preference, charges, agitation, physicochemical environment (Chiti et al. 2003; DuBay et al. 2004; Agopian & Guo 2012).

1.7.2 Seeded Fibril Growth

In the seeded fibril formation process, the lag phase is considerably abolished, accompanied by faster aggregate formation on addition of a preformed seed (cyan curve) (Refer Fig.- 1.14A). The added seeds are shown in cyan color as they belong to a different molecular conformation when compared to the red seeds that are formed in the *de novo* in the aggregation pathway. By addition of cyan seeds, the conformational template is available to the substrate. The added seed actively recruits soluble or oligomeric Aβ to form fibrils resembling its conformational template (Fig.1.14A). The spontaneous (black curve) aggregation (Fig.- 1.14B) occurs in the similar fashion as shown in the Fig.- 1.13. Addition of seed to the substrate results in amplification of the seed template by seeding mechanism.

Exploiting this seeding property of the Aβ fibril growth, quantification techniques have been developed to detect minute quantities of Aβ42 seeds using an *in-vitro* assays (Arosio et al. 2014). Extending the seeding property, molecular templating seed mechanism has been shown in the case of Aβ40 fibrils, where seeding propagated different fibril morphologies bearing respective underlying molecular structures. These structures were found to be self-propagating when fibril were grown from preformed seeds in the assay and they resembled the parent fibril structure (Petkova et al. 2005). In the next section, we will look at some seeding assays that have been used for both detection and characterization of Aβ material from the brains and other biological specimens.

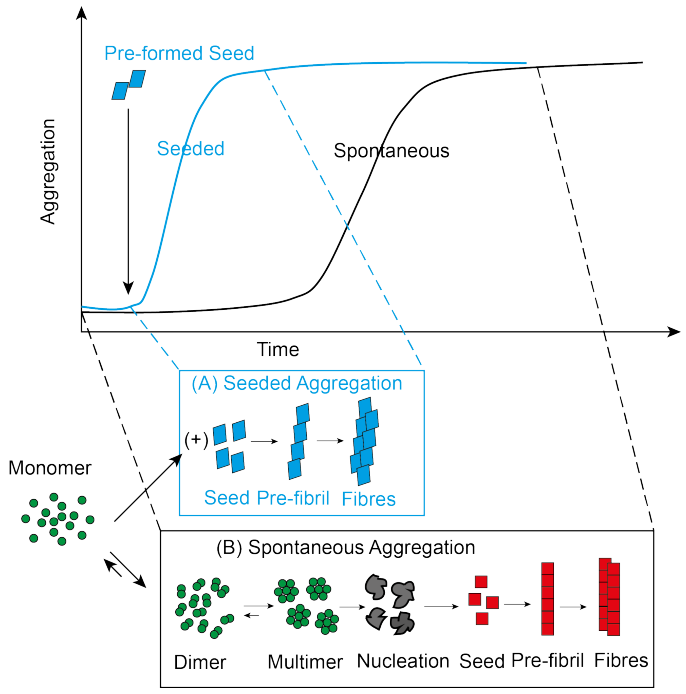

Fig.- 1.14: Schematic model of seeded fibril growth. (**A**) Preformed Seed added to the assay called as seeded aggregation (cyan curve). (**B**) Spontaneous aggregation (black curve).

1.8 Amyloid Beta seeding assays

The working principle behind seeding assays have been explained in detail in the "Seeded Fibril Growth" section (Introduction, Section 1.7.2). Seeding assays can detect oligomers and fibrils, which are produced years or decades before the onset

of clinical symptoms and substantial brain damage in AD (Buchhave et al. 2012). The major advantage of using seeding assay is that, *in-vitro* seeding experiments have shown that seeded fibril growth preserves the molecular structure of the seed (Petkova et al. 2005; Paravastu et al. 2009; Lu et al. 2013). This molecular structural information might help in defining targets to inhibit amyloid formation and accumulation in the brain. All Aβ seeding assays utilize thioflavin-t fluorescence to monitor Aβ aggregation. The assays are performed mostly in a 96 well plate format with multiple replicates, as amyloid aggregation kinetics is heterogeneous. Table-1.1 summarizes current developments in seeding assay literature and gives information on the nature of Aβ seed source, Aβ substrate used, assay condition parameters and characterization techniques used in the assay.

Assay Name	Aβ Seed (derived)	Aβ Substrate	Fragmentation Of Seed	Methods	Ref.
Fibril Amplification Assay-I#	Human Brain Purified	Aβ40	Fibril Sonication	Th-T, TEM, NMR	(Paravastu et al. 2009)
Kinetic Aggregation Assay*	Mammalian cell culture media & mice brain homogenate	Aβ40	Fibril Sonication & Assay Agitation	Th-T	(Du et al. 2011)
Fibril Amplification Assay- II#	Human Brain purified	Aβ40	Fibril Sonication	Th-T, TEM, NMR	(Lu et al. 2013)
Aβ-PMCA*	Human CSF / Oligomers	Aβ42	Assay Agitation	Th-T	(Salvador et.al, 2014)

Table- 1.1: Aβ seed amplification and characterization assays. (* Indicates Aβ detection / quantification and # indicates Aβ detection and characterization)

1.8.1 Fibril amplification assay- I

In this assay (Paravastu et al. 2009), Aβ fibrils seeds are extracted from the frontal lobe brain tissue obtained from autopsy using a Aβ purification protocol described earlier (Roher & Kuo 1999). This assay was designed on the basis of a previous study, where it was shown that preformed Aβ40 fibrils can propagate their molecular conformations when seeded to the soluble Aβ40 (Petkova et al. 2005; Paravastu et al. 2008b). Using the fibril amplification assay, it was demonstrated that fibrils extracted from the brain tissue of the diseased AD patients can be used to seed the isotope-labeled soluble Aβ40 substrate to generate isotope-labeled fibrils in sufficient quantities for NMR characterization studies. Greater fibrillar homogeneities were observed in the samples seeded from patients as compared to the unseeded *de-novo* aggregated control sample (Paravastu et al. 2009).

However, this assay has several limitations like only synthetic Aβ40 substrate peptide could be used to capture the *in-vivo* brain-Aβ conformation. Moreover, NMR studies performed by the same group have also shown that *in-vitro* Aβ42 fibrils did not seed the soluble Aβ40 peptide and hence concluded that brain-seeded Aβ40 fibrils mostly likely arose from Aβ40 seeds and not Aβ42 seeds in the brain (Lu et al. 2013). The other disadvantage of this assay is that the brain aggregated-Aβ extraction protocol involves many steps where denaturants and detergents are used. This multiple protocol can alter, modify or select out a particular Aβ conformation from the brains and detergents traces can potentially alter and interfere with Aβ oligomerization kinetics *in-vitro* in the assay (Rangachari et al. 2006).

1.8.2 Kinetic aggregation assay

This assay (Du et al. 2011) is a selective and sensitive method for quantifying Aβ load from complex biological samples. The kinetic aggregation assay uses synthetic Aβ40 as the substrate peptide. The assay is able to quantitatively detect seeding competent Aβ aggregates in mammalian cell culture media, from *C. elegans* lysate

and in mouse brain homogenate. The added seed samples are sonicated and PK-digested before added for seeding. Sonication is performed to increase the seed concentration and PK digestions to inactivate other proteins, which can potentially interfere with the aggregation in the assay.

The aggregation was monitored by thioflavin-T and analyzed in terms of lagtime. It was found that the assays can quantify Aβ seeds in a concentration and time dependent manner even in the presence of complex biological samples (Du et al. 2011). This is the first established seeding assay analogous to Colby's seeding assay for prions (Colby et al. 2007). The limitations of the assay are: It uses only synthetic Aβ40 as the substrate peptide, which is not known to capture the Aβ42 aggregate conformation (Lu et al. 2013; Pauwels et al. 2012). The assay does not employ any characterization technique to show any differences between the *de-novo* aggregated and the bio-seeded Aβ aggregates.

1.8.3 Fibril amplification assay- II

This assay (Lu et al. 2013) is more sophisticated version of the fibril amplification assay described earlier (Paravastu et al. 2009). The purification of Aβ seed from the brain involved fewer extraction steps, preserved more components of the brain tissue and permitted pure NMR samples to be generated in a single seeding step from smaller quantities of brain tissue. Aβ seeds were purified from the brains of two AD patients with distinct clinical histories. When the seeds were added to the assay with synthetic Aβ40 as the substrate and allowed to seed the fibril growth, the resultant fibril structures showed a single predominant Aβ40 fibril structure in each patient; however, the Aβ40 fibril structures were different from one another (Lu et al. 2013). The critical limitations of this assay are that it only uses synthetic Aβ40 as the substrate. In the same study, the authors declared that *in-vitro* Aβ42 fibrils did not seed the monomeric Aβ40 substrate in their assay; thereby declaring that the seeding of the substrate could have only occurred by Aβ40 fibrillar seeds.

1.8.4 Aβ-PMCA (Protein Misfolding Cyclic Amplification)

This is the first study, where Aβ42 peptide has been used as the substrate to detect Oligomeric-Aβ from CSF (Salvadores et al. 2014). This assay exploits the nucleation polymerization of Aβ oligomers along with fragmentation property (intermittent agitation) to form new seeds, that can seed in the assay. The original PMCA protocol was originally developed to replicate the misfolding and aggregation of the prion protein (PrP^{Sc}) implicated prion disease (Morales et al. 2012), the same methodology was adapted to the Aβ in Aβ-PMCA. PMCA traditionally uses sonication as a mechanical force for fragmentation to break fibrils, however as shown by Caughey and colleagues, sonication can also be replaced by a strong agitation to achieve similar results using a procedure called QuIC (Quake-induced conversion) (Atarashi et al. 2011). In Aβ-PMCA, strong intermittent agitation has been used to fragment the fibrils, which increase the number of seeds, available for seeding in the assay. This assay can detect up to 3 fmol of Aβ oligomers clearly and easily distinguishable from that observed in absence of Aβ seeds *in-vitro* (Salvadores et al. 2014). Using CSF, this assay is able to distinguish AD patients from control individuals affected by a variety of other neurodegenerative disorders or non-degenerative neurological diseases with an overall sensitivity of 90% and specificity of 92%. The limitations of this method, however has been that; it can only be used as a detection technique and not for amplification of *in-vivo* brain-Aβ42 conformational structure. As this assay is not compatible to utilize brain homogenate as seeds like the kinetic aggregation assay, thereby cannot be used to amplify the brain-Aβ conformation. This is because, Aβ42 aggregation kinetics is difficult to control under the influence of brain homogenate cellular debris and accessory components and that is one of the reasons, why CSF material was only used to seed the substrate Aβ42 in the Aβ-PMCA.

1.9 The Research Question

In summation to what has been published so far in literature, it can be speculated that proteopathic diseases such as Alzheimer's disease, Parkinson's disease, Huntington's disease, amyotrophic lateral sclerosis and prion diseases are increasingly being realized to have common disease pathological propagation by seeding mechanism like prions (Cushman et al. 2010; Jucker & Walker 2013; Stohr et al. 2012).

In AD, Aβ40 levels in humans are roughly 5-fold larger than Aβ42 levels. However, Aβ42 is often considered important in AD, because of its strong propensity to aggregate *in-vitro* (Bitan et al. 2003; Yan & Wang 2006). In *in-vivo* studies, Aβ42 peptides were also suggested to be more neurotoxic and may generate more free radical damage than Aβ40 (Klein et al. 1999). Due to the strong amyloidogenicity of the Aβ42 peptide and irreproducibility of aggregation kinetic data, many labs around the world have described this peptide as “Peptide from Hell” (Finder & Glockshuber 2007). Currently, in the literature there are only methods to amplify and characterize the *in-vivo* brain-Aβ aggregate using synthetic Aβ40 as the substrate peptide using seeding assays. However the limitations of these assays are that, Aβ40 substrate cannot capture the Aβ42 conformation in the brain (Pauwels et al. 2012; Lu et al. 2013; Kuperstein et al. 2010).

The exact nature of the Aβ42 AD seed, in the brain still remains a conundrum and a bottleneck to be solved in the AD field. To this time, there have been no high-resolution atomic measurements of fibrillar structures of Aβ *in-vivo* fibrils, which leads us to the question of whether the structural conformations observed in *in-vitro* preparations are faithful representations of those found *in-vivo*? This presses the need to develop a seeding assay that can conformationally template the brain aggregated-Aβ 42 structures for characterization studies. This assay must use recombinant Aβ42 as its substrate as synthetic forms lends itself to a variety of substitutions and modifications along with intrinsic adducts that severely affect the oligomerization kinetics (Finder et al. 2010). These intrinsic impurities can interfere

with the conformational templating mechanism, making the assay fibril samples incompatible for seeding studies. Establishing such an assay, will improve overall understanding of brain aggregated-Aβ conformations and how these conformations seed and lead to AD condition. So, far no studies have clearly indicated or characterized a particular Aβ42 species or conformation that can act as a seed and progress AD condition in the brain. Thus, our study is a first attempt to distinguish and characterize the brain-Aβ from the *in-vitro* spontaneously aggregated *de-novo* Aβ fibrils by developing an Aβ42- conformational seeding assay.

2 Aims and Objectives

The mechanism of conformational conversion of soluble Aβ to fibrillar Aβ by seeding is still a poorly understood phenomenon. Several studies have attempted to understand the seeding mechanism by developing seeding assays. These assays mostly utilize synthetic Aβ40 peptide as the substrate (Paravastu et al. 2009; Du et al. 2011; Lu et al. 2013; Spirig et al. 2014) except for this assay (Salvadores et al. 2014), where synthetic Aβ42 is used as the substrate. However, there are no studies in literature that utilize recombinant Aβ42 used as the substrate to amplify the *in-vivo* brain aggregated-Aβ conformation. This is crucial as Aβ42 peptide is known to be the main culprit and the toxic conformation in Alzheimer's disease (Irie et al. 2005; Bitan et al. 2003). Our research has addressed this critical bottleneck by developing the Aβ conformational seeding assay (Aβ-CSA) using recombinant Aβ(1-42)M35L as the substrate and *in-vivo* transgenic mice brain aggregated Aβ as seeds.

The first objective of this work was to develop a standardized approach by establishing a thioflavin-t fluorescence based in-vitro Amyloid Beta (Aβ) seeding assay using recombinant Aβ(1-42)M35L as the substrate and in-vitro aggregated Aβ as seeds. This assay must be able to detect Aβ seeding in a seed concentration and time dependent manner. The key parameters that can influence the Aβ aggregation kinetics in this assay will be investigated. In particular, these include (i) Substrate Aβ concentration (ii) Concentration of Aβ seed detectable in the assay (iii) Aggregation buffer composition (iv) Assay plate-reader parameters like Agitation, Read Interval. To optimize these parameters in a systematic manner in the assay, an analytical method will be developed to determine the lagtime of aggregation from the raw kinetic data.

The second objective of this work is to transfer the knowledge from the established Aβ seeding assay and then add transgenic mice brain-Aβ extracts as seeds in the form of brain homogenate. This step requires standardizing and abrogating factors that are detrimental to Aβ aggregation and conformational seeding. In addition, this step should also ensure that, there is no interference of brain homogenate debris on

the seeding mechanism in the assay.

Finally, the third objective is to characterize differences between the brain seeded and *de-novo* spontaneously aggregated Aβ fibrillar end products from the assay by (i) Aβ seeding kinetics (ii) TEM Investigation and (iii) Acoustic SSA (Selective Shear Amplification) technique of fragmenting the fibrils to assess fibril fragmentability by its seeding capacity in the assay.

3 Material and Methods

Materials

3.1 Instrumentation and Consumables

A list of all instruments lab apparatus and consumables used during this thesis can be found in table- 3.1 below.

Instrument / Consumables	Manufacturer
Autoclave	(Top7000PST, Sauter)
De-ionized water generation	Millipore Systems
Electron Microscope	Zeiss Libra 120 plus
Fluorescence Spectrometer	TECAN M-1000
Incubator	Thermo Scientific Heraeus
Mass Spectrometer	Bruker Daltonics
Micro-centrifuge	Eppendorf Desktop
Mid-bench Centrifuge	Sigma (4K15C)
pH Meter	Thermo Electron
Shaker	Eppendorf Thermo Mixer
Spectrophotometer	Thermo (Helios-Omega)
Thermoshaker	Infors HT
UV Spectrometer	Helios-Omega UV-Vis
Ultra-centrifuge Rotor	Beckmann
Ultrasonifier (Cell-Lysis)	Bandelin Sonopuls
Ultrasonifier (MODIFIED)	Misonix S-4000
Ultrasonifier Horn	Misonix
Ultra-centrifuge Device	(Discovery, Sorvall)
96 Well Lids (Transparent, low profile lid)	Greiner Bio
96 Well PP plate (Flat bottom, Non-sterile)	Greiner Bio
Centrifuge tubes	Beckman (Polycarbonate)

Column packing Frits	Isolute
Falcon tubes (PP)	Corning
Filter membrane	Millipore (0.2μm)
Glass bottles	Schott
Micro-Cuvettes	Bio-lab
Micro-Tubes (PP)	Eppendorf (1 & 1.5ml)
Needles	(18G & 23G)
Pipette Tips	Safe Seal Biozyme / Tip One
Pipettes	Eppendorf Professional +
Sealing Para film	Parafilm, USA
Single use columns	Isolute Accessories
Tubings	Tygon Saint Gobain
Ultra-centrifuge	(Discovery, Sorvall)

Table -3.1: List of Instrumentation and Consumables used in the Study

3.1.1 Enzymes

Proteinase-K (Merck), Protease Inhibitor (Roche)

3.1.2 Bacterial Strain

BL21 (DE3) from Strategene

3.1.3 Chromatography Material

Chelating Sepharose Fast flow (GE Lifesciences) (Lot - 10179318) and Toyopearl SP-650M (Tosoh Bioscience)

3.1.4 Recombinant Peptides

Aβ(1-42)M35L and Aβ(1-40)M35L

3.1.5 Phospholipid and Dyes

Phospholipid 1,2-dihexanoyl-*sn*-glycero-3-phosphocholine (DHPC) was purchased from Avanti Polar Lipids, USA. Thioflavin-T dye (Merck), Commassie dye (Bio-Rad).

3.1.6 Transgenic Mice Brain Homogenates

Mice	Cage id	Euthanization Age	Lab/ Company
APP/PS1 (TG)	42#1268	6 months	Matthias Jucker Lab
APP/PS1 (WT)	42#1260	6 months	Matthias Jucker Lab
APP-23 (TG)	23#1057	N.A	Matthias Jucker Lab
APP-23 (WT)	23#1049	N.A	Matthias Jucker Lab
BL6	-	8 weeks	Harlan

Table- 3.2: Transgenic AD Mice and other models used to make brain-homogenate

3.1.7 Buffers to Setup the Assay

Composition of the aggregation buffer used in the study are as the following shown in the table- 3.3. Thioflavin-T* dye is added freshly 10-15 minutes before starting the aggregation reaction. The protein elution buffer is used to elute the protein from the cation-exchange column. The standard PBS is used for homogenizing the brains used in this study (Table- 3.2).

Buffer Name	Constituents	Concentration / pH
2X Aggregation Buffer (AB)	Tris. HCl	400mM
	NH_4OH	50mM
	Thioflavin-T*	100μM
	pH	7.7
Protein Elution Buffer	NH_4OH	50mM
	pH	11

Standard PBS	NaCl	137mM
	KCl	2.7mM
	Na2HPO4 • 2 H2O	10mM
	KH2PO4	2.0mM
	pH	7.4

Table- 3.3: Commonly used buffer in the Study (* in the text above)

All the buffers are prepared fresh and filtered through 0.2μm Millipore filters and consumed within two weeks.

Methods

3.2 Recombinant Protein Expression and Purification

3.2.1 Plasmids

The Plasmids given below (Table- 3.4) are used in this study. Dr.Thorsten Lührs and Frau. Stefanie Loss engineered these plasmids in the year 2007 at HZI.

Sr.No	Vector	Fusion Construct	Features
1	pETRO 2.31	6x His- $(NANP)_{19}$ - RSM-Aβ (1-42) M35L by Dr.Thorsten Lührs	N-Terminal Hexa His-TAG and engineered cyanogen bromide methionine cleavage site at the N-terminus of the Protein of interest
2	pETRO 2.31	6x His- $(NANP)_{19}$ - RSM-Aβ (1-40) M35L by Dr.Thorsten Lührs	N-Terminal Hexa His-TAG and engineered cyanogen bromide methionine cleavage site at the N-terminus of the Protein of interest

Table – 3.4: Vector Aβ constructs used in the study

There are several elements contained in this protein sequence construct detailed in the figure- 3.1. The Amino terminus contains a hexa-histidine tag for Immobilized metal ion affinity chromatography (IMAC) purification on the nickel chelate column. The -NANP- sequence tag is repeated 19 times. This tag is bulky and a highly hydrophilic segment, which occurs, in the surface protein of parasite plasmodium falciparum. It has been integrated due to its high expression with E.coli, and it renders the amyloid protein soluble in aqueous solutions. The Methionine has been strategically introduced at the start of the Aβ (M35L) sequence, to facilitate cleavage of the protein construct by Cyanogen Bromide (Döbeli et al. 1995; Thorsten et al. 2005). The Vector plasmid map of Aβ(1-40)M35L is given in the figure -3.1. The

Vector plasmid is the same for Aβ(1-42)M35L is the same as the Aβ(1-40)M35L except that it codes for 2 more amino acids in the C-terminus.

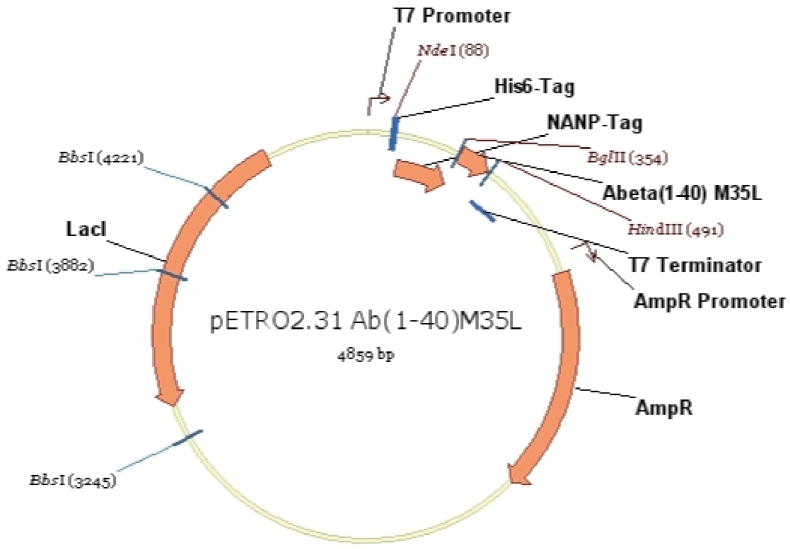

Fig.- 3.1: Vector construct of Aβ(1-40)M35L

3.2.2 Protein Expression Bacteria

BL21 (DE3) competent E.coli strain cells are used in this study for high-level protein expression and easy induction. These cultures are initially sub-cultured and later maintained as stock of 100 µl cell suspension aliquoted in small eppendorf tubes (1.5mL), which are flash frozen and stored at -80 °C until further use. The genotypic description of the construct is given below:

E.coli Strain	Genotypic Construct	Source
BL21 (DE3)	F^- ompT gal dcm lon $hsdS_B(r_B^- m_B^-)$ λ(DE3 [lacI lacUV5-T7gene 1 ind1 sam7 nin5])	Stratagene

3.2.3 Bacterial Transformation and Culturing

Transformation of BL21 (DE3) was done by quick heat shock method and was plated onto (LB) Agar plate containing the antibiotic ampicillin. The constituents of the LB

agar are given in the table- 3.5.

Medium	Composition
Lysogeny Broth (LB)	1% (w/v) Tryptone, 0.7% (w/v) NaCl, 0.5% (w/v) yeast extract, adjusted to pH 7.5
LB-Agar ^{Amp}	Lysogeny Broth + Ampicillin (100μg/mL), 1.5% (w/v) agar-agar

Table- 3.5: Composition of Lysogeny Broth and Lysogeny Agar

Bacterial cells suspension aliquot were transferred to ice bath from -80 °C storage. The 100µl of BL21 (DE3) cell suspension in the aliquot was allowed to thaw on ice for 10 minutes. 40-50ng of the vector plasmid from table- 3.4 was transferred into the BL21 (DE3) thawed suspension on ice under the clean bench. After pipetting the vector plasmid, the suspension is incubated on ice for 15 minutes. After incubation, the suspension is transferred onto LB ^{Amp} –Agar petri plate under the clean bench hood and the suspension is spread over the agar surface with the help of sterile glass beads shaking. The glass beads are later discarded and the LB ^{Amp} –Agar petri plate is transferred into 37°C incubator overnight (14-15 hours) until colonies are detected in the plate. The culture medias and buffers used in this work are explained in the table- 3.6, 3.7 and 3.8. Both the culture media and the buffers used have been heat sterilized by autoclaving (121°C, 2 bar, 20 min). Heat sensitive media ingredients were sterile filtered (0.2µM pore size, Millipore). Antibiotics and MEM Vitamins (Sigma-Aldrich 100x) in the media are added after the media cooled down to less than 50°C.

Media	Medium	Main Function
Pre-culturing Media	ZYP-7050	Colony multiplication
Auto-Inducing Media	ZYP-5052(Studier 2005)	Protein Expression

Table- 3.6: Media used to culture recombinant bacterial cells

Both the **ZYP-7050** and **ZYP-5052** medias only differ by a presence of lactose in the later and absence in the former.

Media Ingredients	Concentration
Tryptone	1%
Yeast Extract	0.5%
Na_2HPO_4	25mM
KH_2PO_4	25mM
NH_4Cl	50mM
Na_2SO_4	5mM
$MgSO_4$	2mM
Trace Elements (1000x)	O.2x
MEM Vitamins (100x)	2x
Antibiotics (Ampicillin)	(1:1000) 1μg/mL

Table- 3.7: Composition of Culture Medias

The carbon source in media **ZYP-7050 is Sugar 5050 Mix** and for **ZYP-5052** is **Sugar 5052 Mix.** The composition of the sugar mixes is shown in the table 3.8.

	Ingredients	Concentration
Sugar 5050 Mix	Glycerol	0.5%
	Glucose	0.05%
Sugar 5052 Mix	Glycerol	0.5%
	Glucose	0.05%
	Lactose	0.2%

Table- 3.8: Carbon source used in the culture medium

Methods to express the recombinant protein were adopted from the auto inducing media protocol established by (Studier 2005). The methods were standardized for Aβ protein expression in this work (Data not shown).

Pre-Culturing

Transformed bacterial colony is cultivated for gene expression and plasmid amplification. A transformed single colony of bacteria from the agar plate is inoculated into ZYP-7050 pre-warmed (37°C) pre-culture media described in the table 3.7 and 3.8. This media is handled in culture flasks (500ml) with baffles and is placed in a shaker (Infors HT) at 37°C, shaking at the speed of 180RPM. The Media is cultured; until the bacterial cell growth reaches the exponential phase to the OD^{600} between 4 to 5. It took around 7-8 hours to reach this OD.

Main Culturing

Inoculation of pre-cultured bacterial material into auto-inducing media is called as main culturing. The composition of the main culture or auto-inducing medium is discussed in the table 3.7 and 3.8. The Auto-inducing main culture is pre-warmed to 37°C and cells from pre-culture media are inoculated to a starting OD^{600} of 0.1. The main culture flasks are large volume culture flasks (1000ml) with baffles and placed inside shaker at 37°C with vigorous shaking at 200 RPM. In the main culture medium, the bacterial cells are induced by the lactose sugar activating the Lac Operon containing the DNA of the protein of interest and thereby resulting in desired protein expression.

Bacterial Harvesting

Bacterial cells from the main culture are harvested when they reach the OD^{600} of 6-7. The main culture media is centrifuged (6000g, 10 minutes, 4°C) in 1000ml centrifuge flasks and the pellets recovered are stored at -80°C not more than 3 months before used for pellet protein purification.

3.2.4 Recombinant Protein Purification

An Inclusion body purification of the Aβ protein is performed from the harvested pellet. The pellet is resuspended by constant magnetic stirring in “Buffer G” at room

temperature for 1 hour. The composition of “buffer G” is given below. The volume of “buffer G” added to re-suspend the pellet is ten times the mass of the pellet. After one hour, the suspension is then sonicated for 16 minutes (ON:OFF= 0.5s: 0.5s, 150 Watts) (Bandelin Sonopuls TT13/F2). The ultrasonication shear force ruptures the bacterial cells, and the sonicated suspension is centrifuged at 18,000g for 30 minutes. Centrifugation, pellets down the cell debris and now the protein remains in the supernatant in a denatured state.

Solution/ Buffer	Composition	Company
Buffer G	6M Guanidine-HCl, 10mM Tris-HCl, 100mM NaPi, pH = 8.0	Sigma-Aldrich

IMAC Denatured Protein Purification

IMAC stands for Immobilized Metal ion Affinity Chromatography. The protein rich supernatant is incubated of Ni-Sepharose equivalent to the mass of the weighed harvested pellet. The Ni-Sepharose is stored in 20% ethanol solution. It is equilibrated with “Buffer G” before adding to the supernatant from the earlier step. The supernatant suspension with the Ni-Sepharose is slowly stirred in a beaker using a magnetic stirrer at room temperature for 1 hour.

Material	Composition	Company
Chelating Sepharose Fast flow (Lot No.- 10179318)	Nickel ($NiSO_4$) is Immobilized to chelating Sepharose by protocol provided by the company	GE-Amersham

In the incubation step, the Nickel is able to capture the His-tagged expressed protein from the supernatant. The suspension is briefly spinned at 1000g for a minute to recover the Ni-Sepharose laden with the expressed protein and the supernatant is discarded. The expressed protein laden Ni-Sepharose sediment is re-suspended in 10 times volume of Ni-sepharose in “Buffer G” and is washed by centrifugation-sedimentation method (1000g /1 Minute) for 4 times discarding the supernatant and

resuspending the pellet at each step. The Sediment is then re-suspended in 8M Urea and washed for 4 times by the same method. This is followed by one time wash with de-ionized Milli-Q water. Later, the sediment is washed 4 times with 40% Acetonitrile. After discarding the supernatant, 3.4% Formic Acid volume is added to the volume of Ni-Sepharose sediment. A solution containing 40% Acetonitrile and 3.4% Formic acid is then added in equal volume to the Ni-Sepharose sediment, mixed, and allowed to incubate for 5 minutes at room temperature. The Solutions and buffers required in this step are summarized in the table- 3.9.

Chemical / Buffers	Composition	Company
Urea	8M Urea Solution	Merck
Acetonitrile	40% Acetonitrile	J.T.Baker
Formic Acid	<98% Pure	Roth

Table- 3.9: Chemical materials used IMAC protein purification

Expressed Protein Elution and Quantification

Added formic acid results in the pH change and the pH change induces the liberation of His-Tags from the immobilized Nickel. For Aβ(1-42)M35L, the suspension is centrifuged and the supernatant containing the protein is filtered by filter paper (Pall Life-science). 3-4 fractions of the protein are eluted by further adding 40% Acetonitrile + 3.4% formic acid solution. In the case of Aβ(1-40) M35L elution, the protein laden Ni-Sepharose is loaded onto a column, packed by frits on both ends, and the protein is eluted drop by drop. The concentration of the expressed protein is determined by UV absorbance. The fractions of high yield and purity are combined together and the protein concentration is adjusted between 20-25mg/ml using 40% Acetonitrile and 3.4% formic acid solvent. To this fraction, equal volumes of <98% Formic Acid (Roth) analytical grade is added to denature the expressed protein completely, bringing the final protein concentration down to ~10-12.5 mg/ml.

Cyanogen Bromide Cleavage

As explained in plasmids section (Refer, Section- 3.2.1), the expressed protein can

be cleaved at the starting Methionine position, which precedes the Aβ sequence (M-DAEFRHD….). Cyanogen bromide is added to the protein fraction at the concentration of 50 mg/mL and incubated for 3-4 hours at room temperature to achieve efficient peptide cleavage to separate the desired Aβ peptide from the -NANP- expression tag. The cleaved protein mixture is aliquoted, flash freezed and stored at -80°C and used within 6-8 months.

Chemical	Concentration	Company
Cyanogen Bromide (BrCN)	5M BrCN Stock	Sigma-Aldrich

Cation Exchange Chromatography

Ion exchange chromatography is a technique that allows the separation of ions and polar molecules based on their charge. The cleaved raw protein solution consists mixture of the Aβ peptide (Hydrophobic) and the –$NANP^{19}$ (Hydrophilic) tag repeat. The stationary cation exchange material displays a negatively charged functional group, which are able to retain the positively charged cations. To separate the Aβ peptide from the raw peptide mixture, cation exchange chromatography method is used. The materials and buffers required for cation exchange chromatography are summarized in the table- 3.10.

Buffer	Composition	Company
Buffer A	1% Acetic Acid	Roth
Buffer B	1% Acetic Acid, 20% Acetonitrile, 1M NaCl	Roth, JT Baker, Merck
Buffer C	1% Acetic Acid, 20% Acetonitrile	Roth, JT baker
Buffer D	50mM Ammonium Hydroxide (pH 10-11)	Fluka

Table- 3.10: Materials and Buffers used in the Ion-exchange chromatography

10-12 mg of the cleaved raw peptide containing approximately 50% Formic Acid is diluted to 0.7% Formic Acid with de-ionized Milli-Q water. This solution is loaded

drop-by-drop onto the cation exchanger column (2mL – Toyopearl SP-650M) and equilibrated with Buffer A. After loading the column with the peptide, the column is washed with 5 CV of buffer-A, buffer-B and buffer-C. Before elution, the column is washed with 2CV wash with Buffer A and finally eluted with Buffer D. The fractions are collected in micro-uv cuvettes and protein concentration is determined in the cuvette fractions. The fractions with higher protein purity are combined together and maintained on ice until further purification by ultra-centrifugation.

Ultracentrifugation Purification

The combined fractions of the peptide are then purified by ultra-centrifugation. The protein is pipetted in 5ml Beckmann rotor polycarbonate tubes and ultra-centrifuged (Order Ref- 349622, Lot- P202MPI) at 1,68,000g for 1 hour at 4°C. After centrifugation, the concentration of the protein is determined by UV- absorbance. After concentration determination, the protein is stored on ice until further use.

3.2.5 Peptide Quantification by UV Absorbance

The physico-chemical parameters of the expressed Aβ peptides and Aβ peptides used in this study are summarized in the table- 3.11. The parameters were calculated using program called as PROTPARAM (Walker 2005) found in the web (www.expasy.org).

Protein	Amino-Acids	MW (kDa)	pI	ε_{280} (M^{-1} cm^{-1})
Aβ(1-42)M35L	42	4496.0	5.31	1490
Aβ(1-40)M35L	40	4311.8	5.31	1490

Table- 3.11: Physico-chemical parameters of the protein purified

From the information in the table- 3.11, we can calculate the protein concentration using Lambert Beer law. The concentration of the protein was determined by absorption of the protein at 280nm against the protein constituent buffer. ε_{280} refer to the molar extinction coefficient expressed in units of M^{-1} cm^{-1}, at 280nm measured in water. By dividing molar extinction coefficient by molecular weight, the result gives 1

unit of absorbance gram per liter of the protein. With molecular coefficient, molecular weight and absorbance at 280nm we can determine the concentration of the protein.

3.2.6 Characterization of Peptide by Mass Spectrometry

ESI-MS / MALDI-TOF-MS was performed to verify the mass, intactness and salt contamination in the recombinantly produced protein. Fresh soluble protein of high concentration and high pH (10-11) was always used for analysis for accurate results. For MALDI-TOF-MS, the molecular masses were determined in the positive-ion mode on a Bruker Ultraflex time-of-flight mass spectrometer (Bruker Daltonics GmbH).

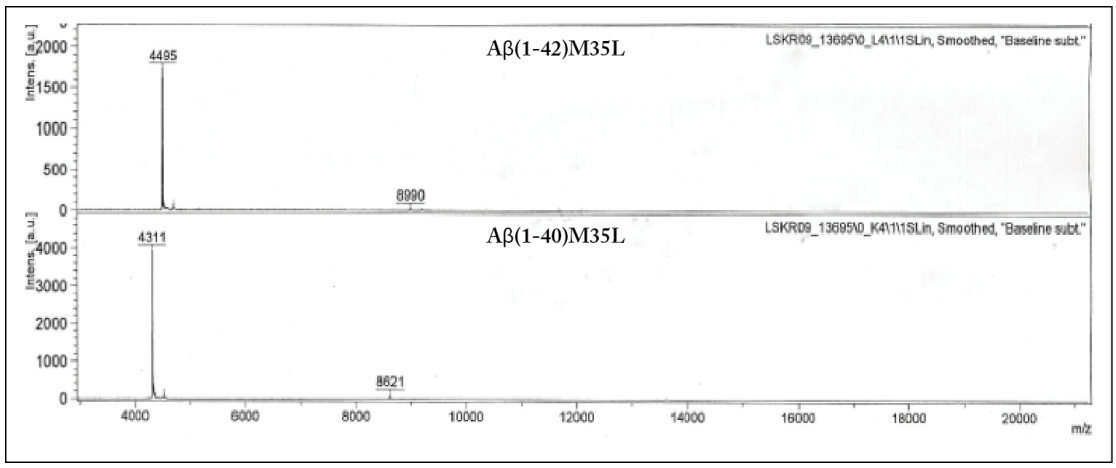

Fig.- 3.2: Mass Spectroscopic (MS-ESI) Analysis of Aβ(1-42)M35L (Top) showing a molecular mass of 4495 Daltons and Aβ(1-40)M35L (bottom) showing a mass of 4311 Daltons.

Manfred Nimtz, Anja Meier and Undine Felgenträger performed Mass spectrometry measurements at the institute (HZI, Braunschweig). Freshly prepared soluble Aβ from ultracentrifugation was analyzed by MS-ESI to verify the molecular mass, protein intactness and salt contamination from cation-exchange purification. Mass spectrometric analysis of purified Aβ(1-42) M35L and purified Aβ(1-40) M35L peptides (Fig.- 3.2) are well inside agreeable molecular weight limit with peaks at 4495 Da and 4311 Da respectively. Presence of a single peak indicates intactness of the purified protein. The consequent step was to select the right substrate concentration of Aβ's to use in the amyloid seeding assay.

3.3 Other Methods

3.3.1 Preparation of Phospholipid DHPC

DHPC encompasses two hexanoic acid chains and a choline headgroup (Fig.- 3.3). Stock solutions of DHPC (1,2-dihexanoyl-*sn*-glycero-3-phosphocholine), were prepared by solubilizing the phospholipid powder in 2X Aggregation Buffer (400mM TRIS-HCl; 50mM NH4OH; pH 7.7). DHPC stock solutions were prepared using lipid specific density; volume, mass and concentration calculations to achieve desired stock concentration. DHPC is highly hygroscopic and hence prepared under nitrogen cabinet and later the stock solution (200mM) is mixed at room temperature placing on a rotation wheel on slow rotation for 4-5 hours for dissolving lipid solids completely. Care must be taken to avoid frothing the DHPC stock solution while dissolving.

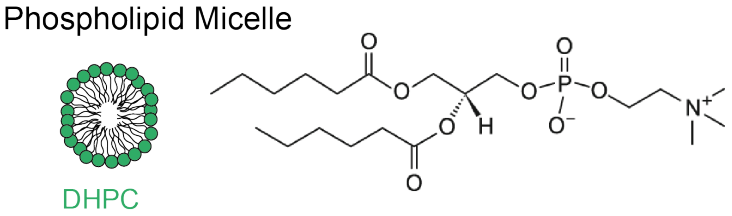

Fig.- 3.3: Structure of Lipid Micelles (DHPC)

3.3.2 Preparation of Amyloid Beta Seeds

Aβ Seeds are preformed fibrillar / oligomeric form of Aβ peptide. They are classified into two from where they have been generated or derived. Two types of Seeds used in this study are: (i) *De- novo* Seeds and (ii) Brain aggregated-Aβ seeds.

De-novo Fibrillar Seeds

Freshly Soluble Aβ at high concentration (100μM) is allowed to aggregate spontaneously at 100μM in 1X Aggregation buffer at room temperature and allowed to equilibrate for ca. 2-3 weeks. The concentration of the peptide is kept high (100μM) to facilitate accelerated fibril formation. There are two types of *de-novo*

aggregated fibrils used as seeds in our study, they are: (i) Aβ(1-42)M35L fibrillar seeds and (ii) Aβ(1-40)M35L fibrillar seeds. The *de-novo* fibrillar seeds are formed under quiescent condition at room temperature.

Brain Aggregated-Aβ Seeds

Brain Aβ seeds are Aβ accumulates deposited in the brain of transgenic mice used in this study (Refer, Table- 3.2). Brain Seeds are prepared by homogenizing the brain of transgenic mice. 10% Brain Homogenate is prepared by homogenizing the brain by needle-syringe homogenization method in 1X PBS buffer. Syringe homogenization procedure is initially performed with few strokes with 18G needle and later few strokes with 23G needle on ice. After homogenizing, the brain homogenate is spinned down at 3000g for 5 minutes at 4°C. The supernatant is carefully pipetted and collected in aliquots, flash freezed and stored at -80°C until further use. The 10% Brain Homogenate are used as brain- Aβ seeds later in the assay.

3.3.3 Proteinase-K Digestion of Brain Homogenate

Brain homogenates are Proteinase-K (PK) digested to inactivate the native cellular proteases present in the brain homogenate. This is done to prevent the cellular proteases from digesting the soluble Aβ added as substrate in the assay. The total protein content in the brain homogenate is determined using Bradford assay (~5-6 mg/ml). 1:500 of PK is added w/w to the determined total protein content in the brain homogenate. The *in-vivo* brain aggregated Aβ aggregates are PK digestion resistant (Stohr et al. 2012) and hence PK does not affect the *in-vivo* aggregated Aβ in the brain. The PK digestion reaction is carried on at room temperature for 2 hours on a thermo-shaker (25°C, 100 RPM). The PK is inactivated by boiling the sample at 95°C on a heating block for 10 minutes and subsequently cooling it on ice. Later, this PK digested brain homogenate is added to the assay as a source of brain derived Aβ seeds.

3.4 Thioflavin-T Fluorescence Spectroscopy

3.4.1 Experimental Setup

Fluorescence spectroscopic measurements were carried out in TECAN M1000 Fluorescence plate reader controlled by Tecan i-control software. A 96 well plate (Black Polypropylene, Greiner Bio, Flat bottom, Non-sterile) was used for the assays. The reaction is pipetted into the micro-wells, leaving aside the borders of the 96 well-plate to avoid plate-edge effects. The plate is closed with a 96 well plate transparent lid (Greiner Bio, Transparent, low profile lid) and sealed with paraffin wax tape for insulation to avoid evaporation and transpiration. The temperature of device during the measurement is maintained at constant temperature of 25°C and the readings are recorded in the range between 24.5°C – 25.5°C.

Thioflavin-t fluorescence intensity is measured in the 96 well-plate at 488 nm after excitation at 442 nm using a Tecan (M1000) spectrofluorometer plate reader. For both, excitation and emission, a bandwidth of 5 nm was used and multiple readings were obtained per well (4 x 4, border 1000 µm) in a circular pattern. A single flash was used with a flash frequency of 400Hz. Some experiments are recorded under quiescent mode and some under agitation mode to ensure homogeneity in sample representation during measurements. The 96 well plate was linearly agitated for 10 second with 5 mm linear amplitude. This agitation enables fragmentation of Aβ aggregates to form seeds in the assay, which accelerates the seeding in the assay. The gain was set manually in the range 90-105 and the Z-position (~ 21500 µm) is adjusted manually before starting of the measurements. The kinetic cycle for measurements was programmed from 10-40 minutes as mentioned for each experiment.

3.4.2 Starting Amyloid Beta Aggregation Reaction in the Assay

Soluble Aβ obtained after ultracentrifugation purification is solubilized in high pH buffer- D (50mM NH_4OH, pH 11). The Aβ peptide remains soluble and usable for

assay within 2-3 hours on ice after purification. For aggregation and seeding studies in the assay, the pH of Aβ peptide is brought down to 8.1. This is done using the 2X Aggregation buffer (400mM Tris-HCl in 50mM NH_4OH, pH 7.7). The 2x aggregation buffer stock is added to the desired concentration of soluble substrate Aβ in equal volumes leading to final 1X aggregation reaction condition (200mM TRIS, 50mM NH4OH, pH 8.1) in the assay. Adjusting the pH of the 2X Aggregation buffer can vary the final pH of the aggregation reaction condition. Thioflavin-T compound is added approximately 3 times the concentration of protein to the reaction mix (~90μM). The phospholipids and thioflavin-t dye to be added in the assay are first solubilized in the 2X aggregation buffer to the desired concentration and then added to the substrate Aβ peptide in equal volume to start the aggregation reaction. This strategy has been used in order to reduce the experimental time delay between the start of aggregation and recording the fluorescence measurement *in-vitro*.

3.4.3 Data Parsing and Smoothing for Lagtime Analysis

The data is measured using the TECAN M1000 device. The data is digitally recorded in a Microsoft excel sheet file (Fig.- 3.4). The excel sheet contains quantitative fluorescence intensity measurements recorded in time intervals from the user selected wells of the 96 well plate. The data is acquired in kinetic cycles as programmed by the user in the TECAN proprietary i-control software.

The generated raw data is parsed by a macro excel file. The “Parse” macro extracts the time interval mean values generated from the multiple reads (Fig.- 3.4A) and prints them onto a summary tab in the excel file (Fig.- 3.4B). The macro processed data is saved as a summary tab in the excel sheet file. Later, the kinetic data recorded from each well corresponding to the reactions is plotted against the time domain in a scatter plot and analyzed for the quality of the aggregation data. It was generally found that reactions with added seed produced systemic fluctuations in the aggregation data (Fig- 3.5A). We were able to get rid of the fluctuations used a filtering algorithm discussed in the next section.

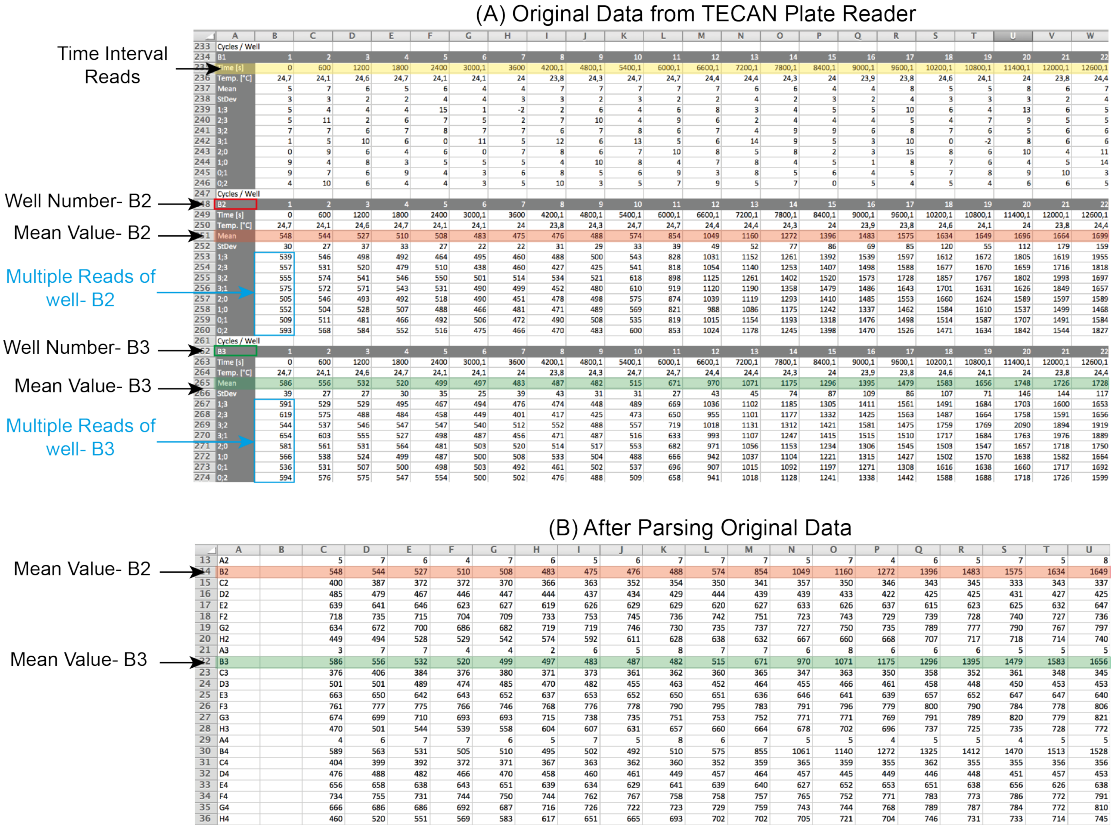

Fig.- 3.4: Parsing and creating summary from original raw data from TECAN device.

Savitzky-Golay Signal Smoothing

Signal smoothing is widely used to increase the signal to noise ratio of a signal without distorting the signal a lot. The goal of smoothing is to remove rough fast changing components of the signal and highlight slow changes in value for that it is easier to see trends in the data. There are different filters available to perform signal smoothing (i) Moving Average filter (ii) Savitzky-Golay (SG) filter. The moving average filter is good at rejecting noise but introduces transient effects in the process and the processed data from the filter lags behind the original data. This lag is due to the delay introduced by the smoothing filter. This delay needs to be taken care of explicitly in this case as we are evaluating the aggregation lagtime of reactions.

To track data more closely and to account for transient effects we chose Savitzky-Golay filter also known as digital smoothing polynomial filter or least squares smoothing filter to smooth our data. SG filter performs polynomial fitting to segments of data known as frames. They are particularly effective for data smoothing and are

typically used to smooth out noisy data that even without noise span a large range of frequencies. SG filters tend to preserve the high frequency components of the data while smoothing it. The Savitzky-Golay filter method essentially performs a local polynomial regression to determine the smoothed value for each data point. This method is superior to adjacent averaging because it tends to preserve features of the data such as peak height and width, which are usually attenuated by adjacent averaging.

One approach for smoothing the time series data is to replace each value of the series with a new value, which is obtained from a polynomial fit to 2n+1 neighboring points (including the point to be smoothed), with n being equal to, or greater than the order of the polynomial. A second order polynomial fit with 17 data points was designed for the moving frames SG filter. The data consists of a set of n $\{x_j, y_j\}$ points (j = 1, ..., n), where x is an independent variable (time) and y_j is an observed value (fluorescence units). They are treated with a set of m convolution coefficients, C_i according to the expression given below equation [**1**].

$$Y_j = \sum_{i = -(m-1)/2}^{i = (m-1)/2} C_i \, y_{j+i} \qquad (m+1)/2 \le j \le n - (m-1)/2$$

For an 17-point smoothing quadratic polynomial, m = 17, i = (-8, -7, -6, -5, -4, -3, -2, -1, 0, 1, 2, 3, 4, 5, 6, 7, 8) and the j^{th} smoothed data point Y_j, is given by this equation [**2**] in the excel spreadsheet as below:

$$Y_j = (- 21 * y_{j-8} - 3.5 * y_{j-7} + 14 * y_{j-6} + 26.5 * y_{j-5} + 39 * y_{j-4} + 46.5 * y_{j-3} + 54 * y_{j-2} + 56.5 * y_{j-1} + 59 * y_j + 56.5 * y_{j+1} + 54 * y_{j+2} + 46.5 * y_{j+3} + 39 * y_{j+4} + 26.5 * y_{j+5} + 14 * y_{j+6} - 3.5 * y_{j+7} - 21 * y_{j+8}) / 483$$

Where C_{-8} = -21 / 483, C_{-7} = -3.5 / 483, C_{-6} = 14 / 483… etc. The convolution coefficients values used for smoothing are -21, -3.5, 14, 26.6, 39, 46.5, 54, 56.5, 59,

56.5, 54, 46.5, 39, 26.5, 14, -3.5 and -21. The formula filter of window size 17 is moved over the data points and smoothed data points are obtained for the same data. However, the (m-1)/2 points at the start and end of the series cannot be calculated using this process, hence the raw data is artificially extended by adding, in reverse order, copies of the first $(m - 1)/2$ points at the beginning and copies of the last $(m - 1)/2$ points at the end.

For all the data points on the Fluorescence-time F(t) aggregation curves (black and red) with set of n $\{x_j, y_j\}$ points (Fig- 3.5A), the Savitzky-Golay equation [2] is moved in 17 - frames to derive the filter smoothened values (Y_j) and later plotted against time (Fig- 3.5B). Data smoothing was only done, when there was an increase in noise levels compared to signal, required for determining the aggregation lagtime (e.g.- as in figure 3.5A).

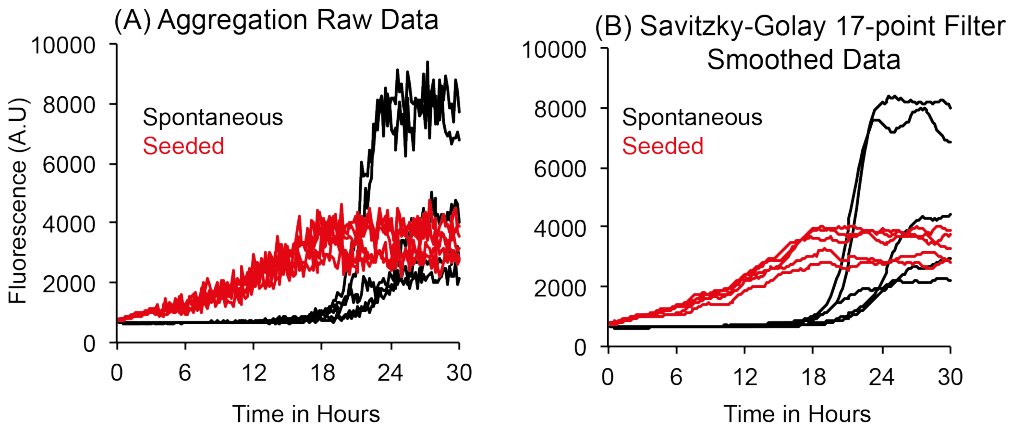

Fig- 3.5: 17- point Savitzky-golay smoothing. (**A**) Indicates raw data from spontaneous aggregation. (**B**) Indicates the same data after Savitzky-Golay filter smoothing.

3.4.4 Determination of Lagtime

The starting time point of aggregation of the peptide or the length of the lag phase is referred to as the lagtime (t_{lag}). There are several methods used to determine the lagtime of amyloid aggregation. A frequently used way to measure the lagtime is to extrapolate the slope of maximal growth rate of the aggregation curve (F_t) back to the time axis and use the intersection with the fluorescence baseline as the value for the starting point of aggregation (Fig.- 3.6). Maximal aggregation rate (K_a) is taken to be

the slope of the linear portion of the aggregation kinetic curve (F_t), visualized by the red dotted line in fig- 3.6. The intercept of this maximal slope line with the time-axis is determined as the lag-time (t_{lag}) of aggregation for that particular aggregation reaction (Auer & Kashchiev 2010).

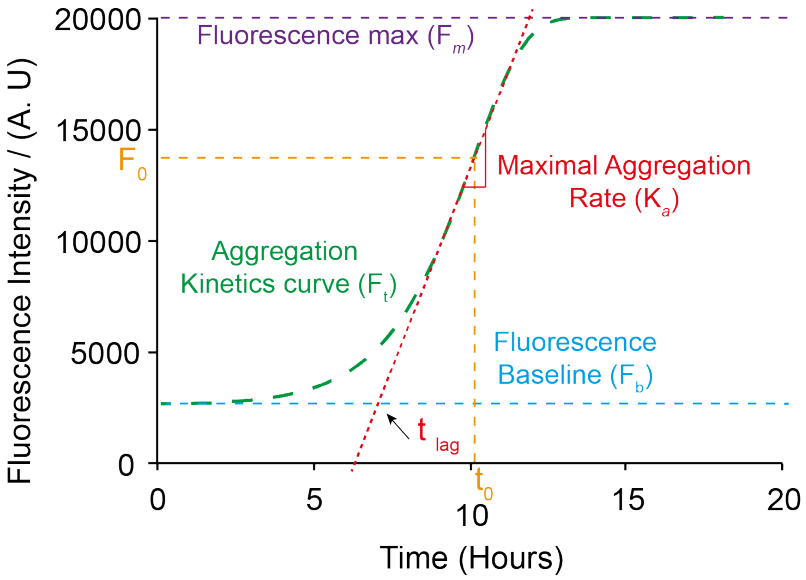

Fig.– 3.6: Determination of Lagtime (t_{lag}). The green curve trace represents the aggregation kinetic data time-point curve F(t). The dotted redline shows the maximal growth rate (K_a). The maximal aggregation rate (K_a) is determined with the aid of the F(t) inflection point co-ordinates t_0 and F_0. Partly adapted from (Auer & Kashchiev 2010).

The maximum rate of aggregation (K_a) is calculated by finding the maximum slope of the F(t) curve by using a moving slope formula in excel with a window size of 5 aggregation data points. The moving slope formula calculates the best fit for the 5 points and it is extended over the entire data points in the series. Later to determine the intersection of the maximal slope with the time axis to calculate the lagtime (t_{lag}), the y- intercepts of the F(t) curve data points corresponding to the maximal slope line are calculated using the intercept formula in the excel. Now, determining the x-intercept of the maximal slope (K_a) becomes easier using the slope-intercept straight-line equation [**3**] as given below:

$$y = mx + b$$

Where, y is equation of the straight line, m is the slope, “x” is the x-intercept and “b” is the y-intercept. The baseline of the F(t) curve averaging the first five data points is

subtracted with the y-intercept to get the real value of the y- intercept “b”. To determine the x-intercept (t_{lag}), the value of y is substituted to 0 and then values for the maximal slope “m” and the corresponding value of the y-intercept “b” are substituted in the formula.

3.5 Characterization of Amyloid beta aggregates

3.5.1 Transmission Electron Microscopy (TEM)

The electron microscopic analysis was done with the energy-filtered transmission electron microscope (EF-TEM) Zeiss Libra 120 plus Zeiss Oberkochen, Germany), running at 120 kV and with 1 µA emission current. Images were recorded within a magnification range of x12500 to x50000 with a 2048 x 2048 cooled CCD-camera (SharpEye, Tröndle, Moorenwies, Germany) under the regime of the iTEM software package (OSIS, Münster, Germany) in the 'elastic bright field mode', using an energy slit width of 10 eV. Protein fibril sampling copper grids were layered with butvar foil, air-dried and C-coated from carbon thread by resistance evaporation, using a BalTec MED020 (BalTec, Liechtenstein), and were glow-discharged from air for roughly 10 seconds.

TEM of Aβ aggregates

Aβ fibrils were adsorbed to freshly glow-dischared C-butvar foils for usually 60 seconds at ambient room temperature. The fibril concentrate was maintained at 134mg/ml deduced from the initial monomeric peptide concentration. They were shortly blotted with filter paper (Schleicher & Schüll, Dassel, Germany). The preparate was then immediately touched to a drop of 1 % (w/v) uranyl acetate; pH 4.0 and was blotted within 3 to 5 seconds and air-dried before TEM analysis. Electron microscopy experiments were performed in close collaboration with Dr. Heinrich Lünsdorf (HZI, Braunschweig).

3.5.2 Acoustic SSA Setup

Fragmentation of Aβ aggregates by Acoustic SSA (Selective Shear Amplification) was performed using instrument (Misonix S-4000, Qsonica LLC, USA) with Microplate Probe (Horn). Dr.Thorsten Lührs along with Felix Deluweit, HZI, assembled the acoustic SSA setup; the construction and the working principles have been described in detail in Felix's PhD thesis. Ultrasound is propagated via a series of compression and rarefaction waves induced in the molecules of the medium through which it propagates. In application of sufficiently high power, the rarefaction cycle may exceed the attractive forces of the molecules of the liquid and in this way the cavitation- bubbles are formed in the medium.

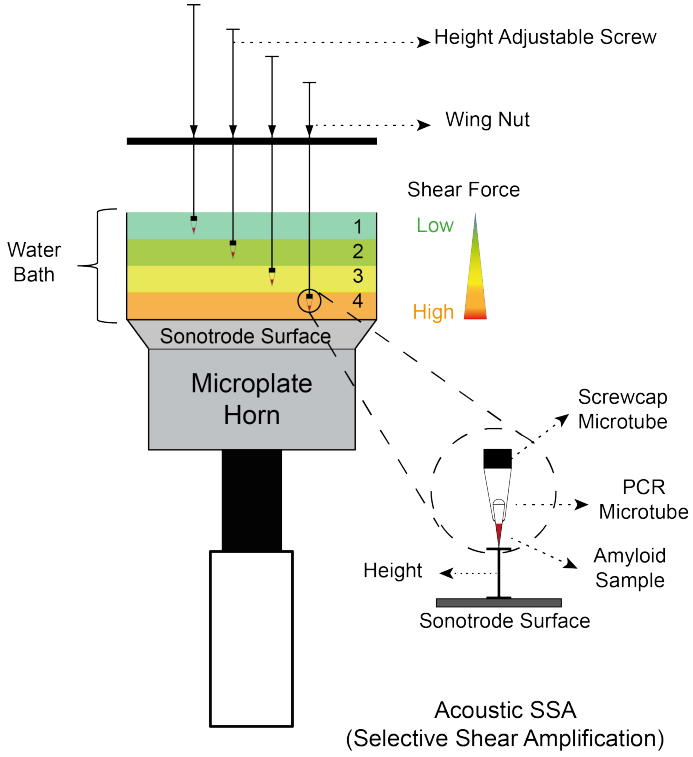

Fig.- 3.7: Working Principle and experimental setup of Acoustic SSA (Selective Shear Amplification)

When these cavities collapse in successive compression cycles, it generates energy in the medium. Such violent collapses of bubbles can generate large shear forces in the bulk medium that could be used for homogenous mixing, particle dispersion and polymer fragmentation. High energies are generated when these bubbles collapse

and these occur more in number closer to the sonotrode surface. The cavitation bubbles decreases, as we move away from the surface of the sonotrode. This phenomenon is used to control the shear forces acting on the sample to be fragmented by adjusting the heights (using screws) away and near from the sonotrode surface (Fig. 3.7). The nearest region to the sonotrode surface experiences more force and it successively decreases as we increase the height (Level 4→ Level 1) with the help of the screw-nut arrangement (Refer Figure- 3.7).

Fragmentation of Aβ fibrils using Acoustic SSA

The amyloid fibril sample is pipetted into a PCR tube (100μL), this tube is inserted into a screw-cap microtube with a cut bottom, which acts as a holder for the PCR tube. The holder tube exposes the conical surface of PCR tube to the temperature controlled sonicator water bath (Fig.- 3.7). A Screw is attached to the cap of the microtube, which acts a height adjuster when screwed clock or anticlockwise. Each 360° turn in the screw corresponds to 1mm increase or decrease in height from the sonicator probe surface. Different ON:OFF sonication shear timings along with periodic number of cycles are used to fragment the Aβ aggregate material. After sonication, the samples are stored on ice bath. The fibril samples under study were always sonicated at the same position to prevent variance in applied sonication force due to positional effects on the sonotrode surface. To understand more about positional effects in detail, one can refer Felix Deluweit PhD thesis, where the working of the Acoustic SSA has been standardized. The fragmented amyloid material is later seeded to the Aβ conformational seeding assay (Aβ-CSA) to assess the extent of fragmentation. Optimally fragmented fibrils would generate more seeds that can efficiently seed the substrate peptide in the assay as compared to non-optimally fragmented fibrils, which would inefficiently seed for the same seed concentration. These differences can be observed analyzing the aggregation kinetics of the reactions.

4 Results

4 Experimental Strategy

A three-step strategy was used to achieve the Aims (Refer Chapter –II Aims and Objectives). The experimental strategy has been explained in detailed in the schematic (Fig.- 4.1).

1. To Develop an *In-vitro* based Aβ seeding assay to distinguish Spontaneous and Seed driven Aβ aggregation exploiting the amyloid nucleated polymerization and seeding mechanism.

2. Transfer the technical knowledge from the developed seeding assay to seed and conformationally amplify the brain aggregated -Aβ from the brain homogenate added reactions. The assay must also be flexible for screening different biological conditions that can modulate Aβ aggregation so as to abet seeding and amplification of brain aggregated-Aβ conformation.

3. To biophysically characterize spontaneous aggregated Aβ and *in-vivo* mice brain seeded Aβ aggregates by investigating morphological differences using TEM and fibril fragmentability differences using Acoustic- Selective Shear Amplification (Acoustic-SSA) technique.

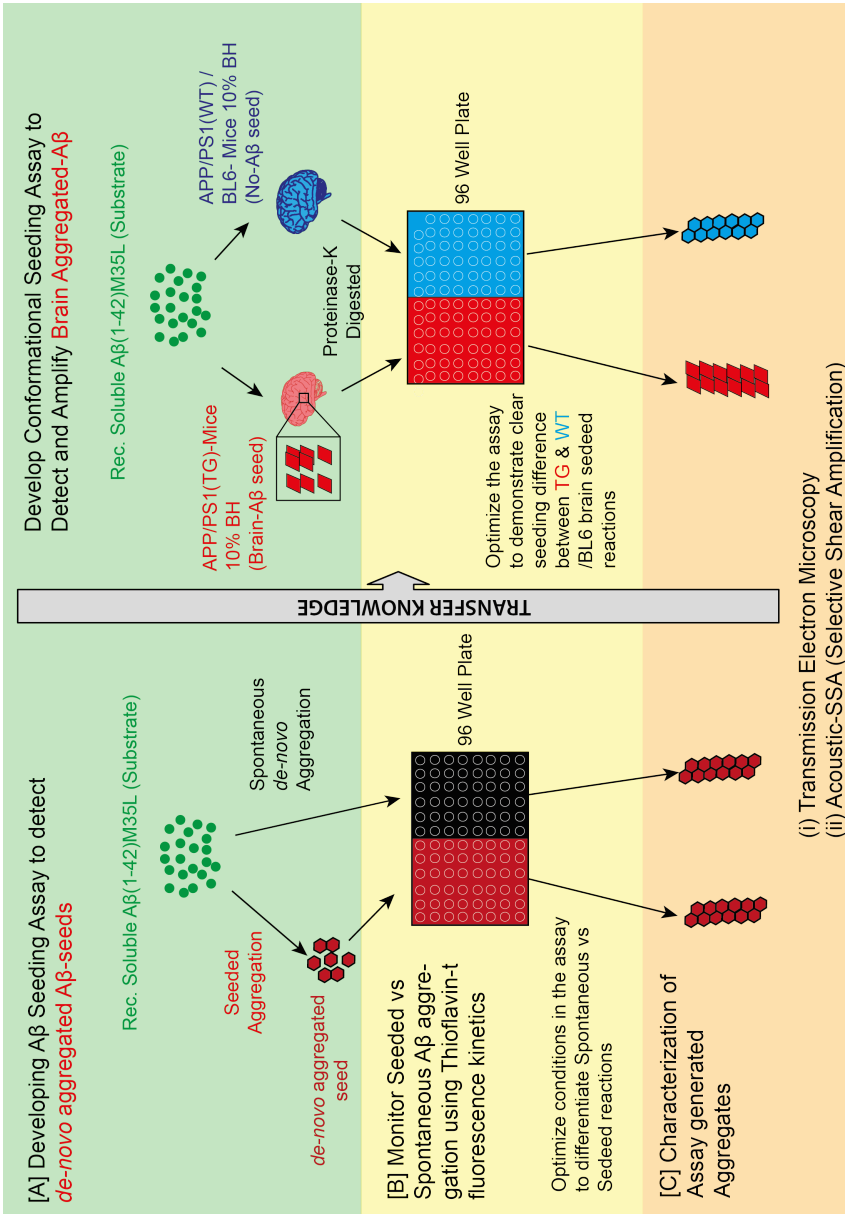

Fig.- 4.1: Schematic Representation of Assay Development. (**A**) Development of seeding assay to detect *in-vitro* Aβ seed (**B**) Distinguish Seeding and Spontaneous aggregation using thioflavin-t fluorescence kinetics data. (**C**) Characterization of Amyloid aggregated reactions using (i) Electron Microscopy (ii) Acoustic-SSA. Transfer the knowledge from using *in-vitro* aggregated Aβ seeds in the assay to using *in-vivo* brain aggregated-Aβ as seeds in the form of brain homogenate.

4.1 Development of Aβ Seeding Assay

Development of the Aβ seeding assay requires standardization and optimization of parameters like (i) Reproducible recombinant production of soluble Aβ peptide [Aβ(1-40)M35L and Aβ(1-42)M35L]. (ii) Optimization of substrate Aβ peptide concentration and Aβ-seeding in the assay. (iii) Optimization of buffer conditions for reproducible Aβ peptide aggregation (iv) Standardization of assays parameters like plate read interval, aggregate fragmentation by adjusting agitation and (v) A consistent way to analyze lag times.

4.1.1 Aβ Fibrillation is Substrate Concentration Dependent

Spontaneous fibrillation kinetics of Aβ peptides was investigated at varying micro molar substrate concentrations in the assay. Soluble Aβ(1-42) M35L & Aβ(1-40)M35L were freshly prepared by cation exchange and ultracentrifugation as described in detail (Ref. Methods, Section 3.2.4). Soluble Aβ peptides are diluted to 50μM, 40μM, 30μM and 20μM in the standard aggregation buffer (200mM TRIS-HCl; 50mM NH_4OH; pH 8.1) and pipetted in a 96 well plate to start the Aβ aggregation reaction (Refer, Methods, Sec. 3.4.2). Each reaction cohort contains ten replicates. Each single sigmoidal aggregation trace represents fluorescence intensity versus time of one aggregation reaction from a single well (Fig.- 4.2). The raw aggregation kinetic data of Aβ(1-42)M35L and Aβ(1-40)M35L reactions are presented in the Fig.- 4.2(A) and 4.2(B) respectively. The data recording parameters of the plate reader device for this experiment was set to reading interval frequency of 40 minutes, Gain-105 (manual) and data was recorded under quiescent conditions. The lagtime of aggregation were determined as explained here (Refer 3.4.4). Henceforth, all the aggregation data will be analyzed and presented in this scatter plot format with determined lag times on the Y-axis and the investigation parameter on the X-axis (Fig.- 4.2C).

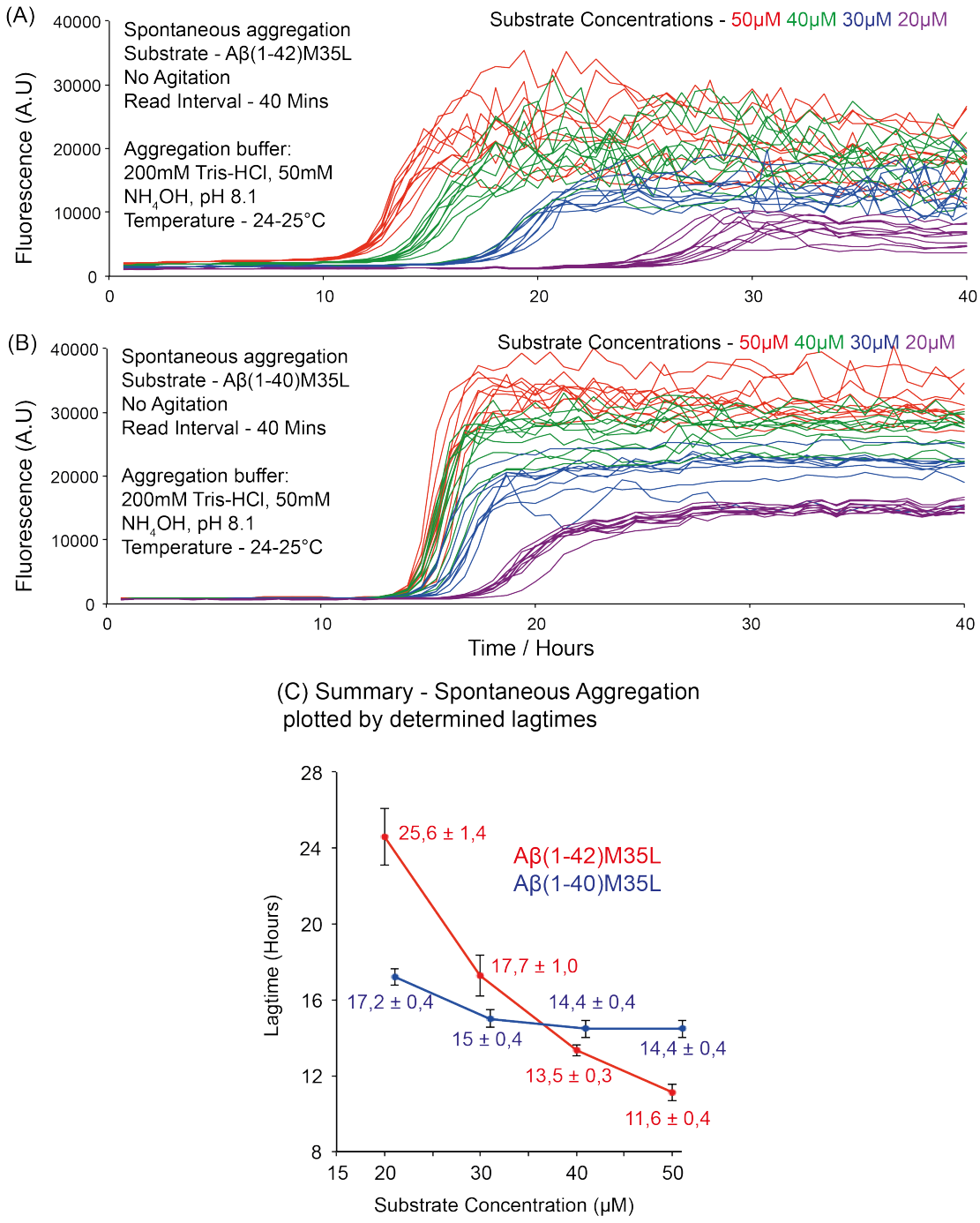

Fig.- 4.2: Concentration dependent spontaneous aggregation of Aβ in the assay. (**A**) Aβ(1-42)M35L and (**B**) Aβ(1-40)M35L in varying substrate concentrations of 50,40,30 and 20μM showing time and protein concentration dependent fibrillation. (**C**) The red trace corresponds to determined aggregation lagtimes of Aβ(1-42)M35L and the blue trace corresponds to aggregation lagtimes of Aβ(1-40)M35L peptide. The error bars indicate standard deviation from the median of lagtimes. N=10, replicates per reaction cohort.

The spontaneous aggregation lagtimes of Aβ(1-42)M35L at varying substrate concentrations shows concentration and time dependent aggregation. Increase in

substrate concentration resulted in decreased lagtime and vice-versa. Aβ(1-40)M35L aggregation has flat lagtime response to increase in substrate concentrations from 50-30μM, and the lagtime marginally increases at 20μM concentration. Although both the substrate peptide differ by only two amino acids by show a clear variability in substrate concentration dependent aggregation. This result also shows that Aβ(1-42)M35L is more aggregation prone and amyloidogenic compared to Aβ(1-40)M35L. 30μM of Aβ peptide substrate concentration is chosen as the ideal concentration for the assay as higher substrate concentrations increases the propensity for spontaneous Aβ peptide aggregation leading to reduction in lagtime and low substrate concentrations can lead to arbitrary nucleation among the replicates of Aβ spontaneous aggregation. The substrate concentration changes in the assay system can significantly alter the resoluting capacity to map lagtime differences between the spontaneous and the seeded reactions. Increase in substrate can enhance spontaneous primary nucleation to dominate over the added seed nucleation. The next step was to select the appropriate pH for the substrate aggregation in the assay system.

4.1.2 Aβ aggregation kinetics is highly pH sensitive

Change in pH is known to affect amyloid aggregation kinetics and morphology in literature (Fraser et al. 1991). To discern and select an optimal pH condition for the aggregation assay, aggregation kinetics of Aβ(1-42)M35L & Aβ(1-40)M35L was monitored under varying pH conditions adjusted in the aggregation buffer. Soluble substrate Aβ's were diluted to 30μM in aggregation buffer corresponding to final pH values in the range 8.1 to 9.1. The pH values of the range were precisely measured using a pH meter and corresponded to 8.1, 8.27, 8.42, 8.56, 8.74, 8.93, 9.16 and 9.48.

The Aβ's aggregation reactions were set to the above-mentioned pH conditions with 5 replicates per pH value. Reading interval frequency was maintained at 40 minutes, Gain was adjusted to 90 (manual) and data was recorded under quiescent conditions. Fig.- 4.3(A) shows spontaneous aggregation of Aβ's under varying

aggregation buffer pH's on the "X-axis" and final plateau fluorescence intensity on the "Y-axis". Fig. 4.3(B) displays aggregation of Aβ's under varying pH conditions on the "X-axis and determined aggregation lagtimes on the "Y-axis".

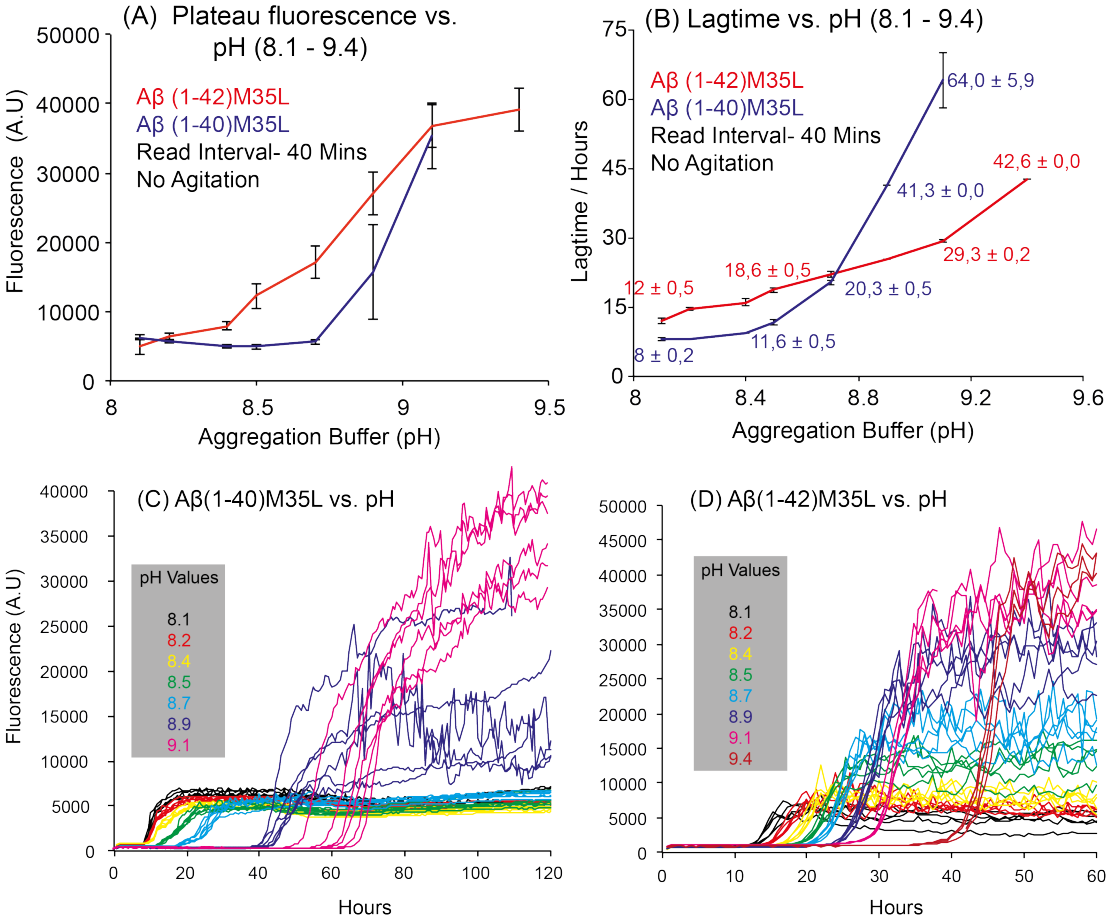

Fig.– 4.3: Effect of pH on Aβ fibrillation at 30μM substrate concentration. For A and B, Red curve indicates Aβ(-42)M35L peptide and blue indicates Aβ(-40)M35L peptide. (**A**) Aggregation of Aβ's under varying pH conditions correlated to Final plateau fluorescence intensity and (**B**) Aggregation lagtimes. The raw kinetic data is presented for Aβ(1-40)M35L (**C**) and for Aβ(1-42)M35L (**D**). (N=5) for each reaction, error bars indicate standard deviation from the median recorded values.

The observed trend is consistent with literature, where Aβ aggregation are known to be affected by change in pH condition. Increasing pH is known to retard aggregation propensity and aggregation is stronger closer to the pI (Isoelectric Point) of the peptide. This result, offers a glimpse into linear increase in thioflavin-T fluorescence intensity with an increase in pH values (Fig.- 4.3 C&D). The pH dependent aggregation kinetics of both Aβ(1-42)M35L and Aβ(1-42)M35L substrates are distinct in the assay. This is due to the presence of two extra hydrophobic amino acids at the C-terminal of Aβ(1-42)M35L peptide.

TEM micrographs were further analyzed to correlate to the kinetic changes observed for the Aβ's samples at pH 8.1 and 9.1 (Refer, Results, Section- 4.4.1, Fig.- 4.12 and 4.13). From this experiment, it was decided to maintain the pH of the aggregation buffer at pH 8.1, as aggregation propensity at this pH was reproducible and optimal and did not influence the formation of oligomeric aggregates that could induce formation of a particular Aβ fibril type in the assay.

4.1.3 Soluble Aβ's Reciprocally Delay Each Other's Spontaneous Aggregation and Aβ42 fibril Does Not Seed Substrate Aβ40

In AD condition, Aβ peptides and its truncations are found aggregated in the brains. An increase in Aβ42:Aβ40 ratios seems to coincide with more threatening forms of the disease. Co-incubation kinetics of Aβ peptides in varying stoichiometric ratios along with cross-seeding was performed to understand the transition and seeding dynamics involved between the substrate Aβ peptides and seeding in the assay.

Soluble Aβ substrates were diluted to 30μM and mixed in stoichiometric ratios [Aβ(1-42)M35L : Aβ(1-40)M35L] as (10:0/ 7:3/ 5:5/ 3:7 and 0:10) in the aggregation buffer. These mixtures were allowed to aggregate spontaneously and with and without *de-novo* aggregated Aβ seeds (Ref. Sec 3.3.2) added to them by logarithmic dilution from 5 - 0.00005μM. There were two replicates for the seeded reactions and four replicates for the spontaneous reactions. Plot- 4.4(A) and 4.4(B) contain Aβ(1-42)M35L and Aβ(1-40)M35L *de-novo* seeded respectively at varying stoichiometric mixtures of Aβ substrate peptides. The reading interval for this experiment was reduced to 25 minutes from the earlier 40 minutes and reads were acquired under quiescent condition.

With the increase in frequency of reading interval in the assay to 25 minutes from the earlier 40 minutes, there is decrease in the lagtime of the spontaneous aggregation for substrate Aβ(1-42)M35L by a factor of half (Fig.- 4.4) compared to earlier experiments (Refer, Fig.- 4.2 & 4.3). This decrease in lagtime is due increase in the frequency of plate movement while taking the measurements. This movement results

in mild agitation, which accelerated the soluble Aβ substrate aggregation. Aβ(1-42)M35L and Aβ(1-40)M35L spontaneously aggregate approximately at similar lagtimes between 6 to 8 hours under the mentioned assay conditions (Refer- Fig.- 4.4). Inhibition of Aβ(1-42)M35L spontaneous aggregation is observed in the presence of soluble Aβ(1-40)M35L substrate and vice versa. Increasing the stoichiometric concentration of soluble Aβ(1-42)M35L with soluble Aβ(1-420)M35L substrate or vice versa leads to increase in aggregation lagtime indicating inhibition of aggregation. It is clear from the above observations, that soluble Aβ's reciprocally delay spontaneous aggregation of each other in concentration dependent manner (Fig.- 4.4A & B).

Aβ(1-42)M35L *de-novo* aggregated fibrils are able to seed Aβ(1-42)M35L substrate protein in a concentration and time dependent manner. The Aβ(1-42)M35L fibrils seeding was found to be more Aβ(-142)M35L substrate dependent in the stoichiometric ratio mixtures where Aβ(1-42)M35L dominated in this assay (Fig.- 4.4B). However, there is a weak seeding effect observed for Aβ(1-40)M35L fibrils seeding the soluble Aβ(1-40)M35L and Aβ(1-42)M35L substrate (Comparing, Fig- 4.4A with Fig.- 4.4B, also refer SD, Fig.- 7.1 and 7.2). This could be very well due to floccular morphology of the Aβ(1-40)M35L fibrils, that could be visually confirmed.

The established Thioflavin-T based Aβ seeding assay works as proof of principle to detect minutest amount of Aβ42(M35L) fibrils, even in the nanomolar ranges. The next step was to add *in-vivo* brain homogenate from AD transgenic mice as seeds in the assay. This would enable seeding and amplification of the *in-vivo* brain aggregated-Aβ seed specific conformational template to the soluble Aβ(1-42)M35L substrate peptide in the assay. The raw kinetic data for this experiment has been presented in the supplementary section (Refer, SD, Fig.- 7.1 & 7.2).

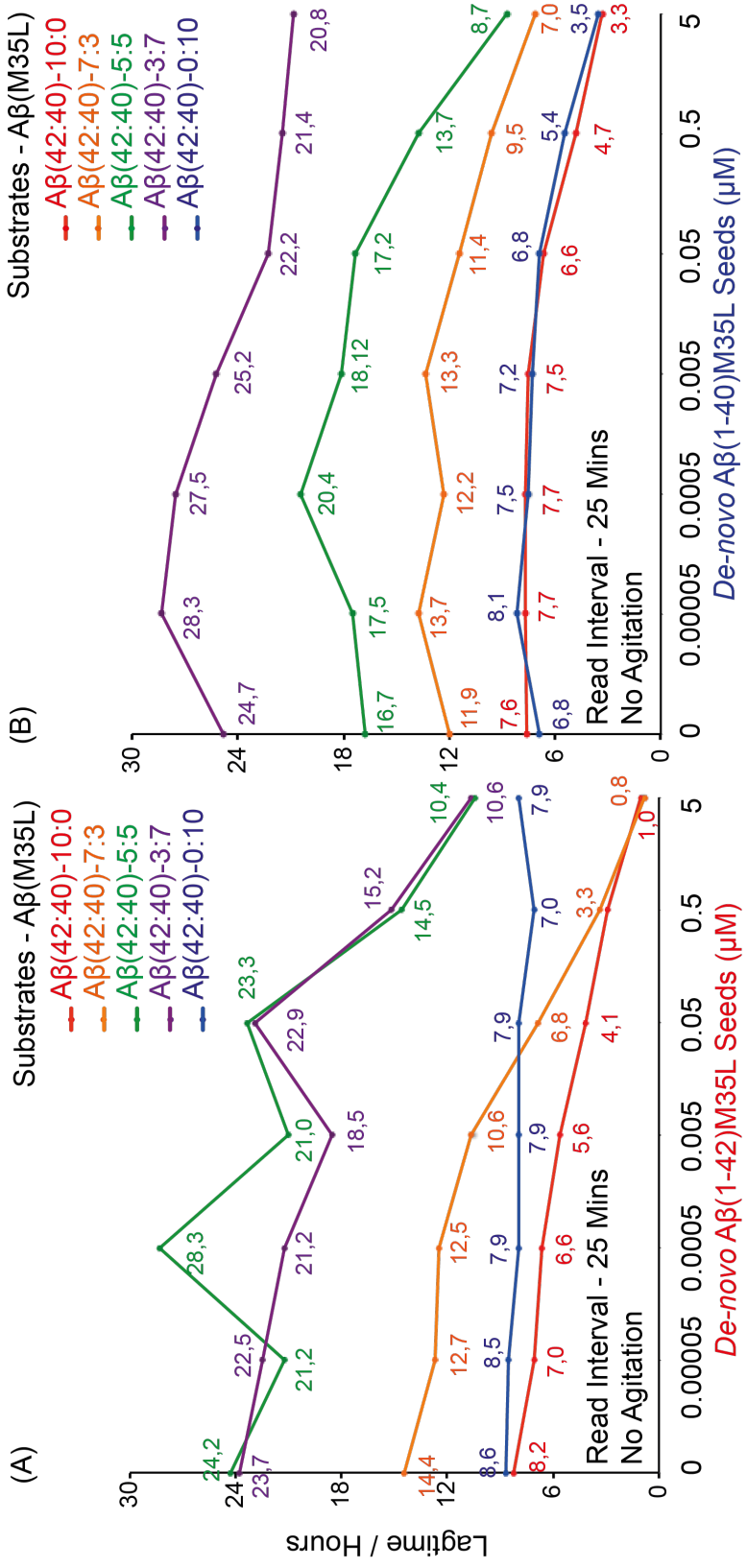

Fig.- 4.4: Stoichiometric Aβ substrate ratio mixtures in spontaneous aggregation (N=4) **and seeded** (N=2) with logarithmically decreasing (0.5μM-0.00005μM) *de-novo* Aβ seed. (**A**) Seeded with *de-novo* Aβ(1-42)M35L fibrils and (**B**) Seeded with *de-novo* Aβ(1-40)M35L fibrils. The Seed concentrations are plotted on the "X-axis" and the determined median lagtimes on the "Y-axis".

4.2 Brain homogenate retards Aβ aggregation in the assay

After establishing the assay to detect the *de-novo* generated seeds. The next step was to add the *in-vivo* brain aggregated -Aβ containing APP/PS1(TG) brain homogenate (BH) as seed to the assay. The *in-vivo* brain aggregated-Aβ is anticipated to seed the soluble substrate Aβ(1-42)M35L in the assay as analogous to the *de-novo* aggregated fibrillar seeds.

Preparation of BH seed suspension to be added as seed in the assay is described in detail (Refer, material Methods, section 3.3.2). The wild-type (WT) mice and BL6 BH are added to the assay as a material for negative control. The BH material as a seed is added to the assay in two ways. Adding 10% brain homogenate seed directly to the assay in the presence of (i) Protease Inhibitor (PI) or (ii) by Proteinase-K (PK) digestion of the added brain homogenate.

4.2.1 Brain homogenate seeding with 2X Protease Inhibitor

Protease Inhibitor (PI) is a cocktail of protease inhibitors that are excellent inhibitors of serine and cysteine proteases present in the cells. They can protect soluble substrate Aβ peptide from cleavage by cellular protease present in the brain homogenate added as a seed to the assay. PI was used two times more than the manufacturer (Roche) recommended concentration in the brain aggregated- Aβ seeding experiment in the assay.

Soluble Aβ(1-42)M35L substrate was diluted to 30μM in the aggregation buffer containing 2X Protease Inhibitors and added with the brain homogenates [BL6, APP/PS1(TG/WT)]. APP/PS1(TG) brain is known to contain higher fraction of brain aggregated Aβ42 seeds, which can seed the soluble Aβ(1-42)M35L substrate in the assay. Six replicates representing each reaction cohort was used in this experiment. PBS is added as an additional control in the assay, as the 10% brain homogenate is prepared in the standard PBS buffer. Brain homogenate is added at 0.075% and 0.1% concentrations to total reaction volume. In this experiment, the kinetic read

interval was set to 10 minutes with 10 seconds agitation between each read. The agitation parameter along with increase in frequency of read interval (10 minutes, from the earlier 25 minutes) was introduced in the assay, as without agitation the aggregation did not occur, when the brain homogenates were added (Data not shown). Agitation resulted in better mixing of Aβ reactions inside the well, leading to homogenous fluorescence intensity measurements in the well. Agitation additionally introduces fragmentation of formed aggregates and even the added fibrils / seeds in the system accelerating the aggregation kinetics in the system. This results in the increase in the population of seeds that can act as growing ends to accelerate aggregation (Refer, Introduction, Section- 1.7).

Introducing agitation for 10 seconds in combination with 10 minutes read interval, dramatically reduces the spontaneous aggregation lagtime of Aβ(1-42)M35L to a factor of half (Lagtime of ca. 4 hours) (Refer Fig.- 4.5C) as compared to 25 minutes read interval with no shake program (Lagtime ca. 8 hours) (Refer, Fig.- 4.4A&B). No seeding activity was detected between (TG) vs. BL6 or WT at both 0.075% and 0.1% brain homogenate concentrations (Refer, Fig.- 4.5A&B). Overall, there was increase in the lagtimes of the aggregation in all reactions was observed, wherever brain homogenate was added when compared to non-brain homogenate added reactions. Increase in brain homogenate concentration (from 0.075% to 0.1%) increased the aggregation lagtime in a concentration and time dependent manner (Compare, Fig.- 4.5A&B). There is a large standard deviation recorded in the lagtime values recorded among the of APP/PS1(TG) seeded reactions indicating that the aggregation was spontaneous and not influenced by the brain aggregated-Aβ seed from the brain homogenate. From this experiment, it is clear that amyloid nucleation and aggregation processes are very sensitive and vulnerable to addition of brain homogenate, which retards the substrate Aβ aggregation in the assay. There was no detectable effect on Aβ(1-42)M35L spontaneous aggregation in the presence of protease inhibitor or PBS on in the assay. The kinetic raw aggregation data for this assay has been shown and explained in the supplementary section (Refer, Supplementary Data, Fig.- 7.4).

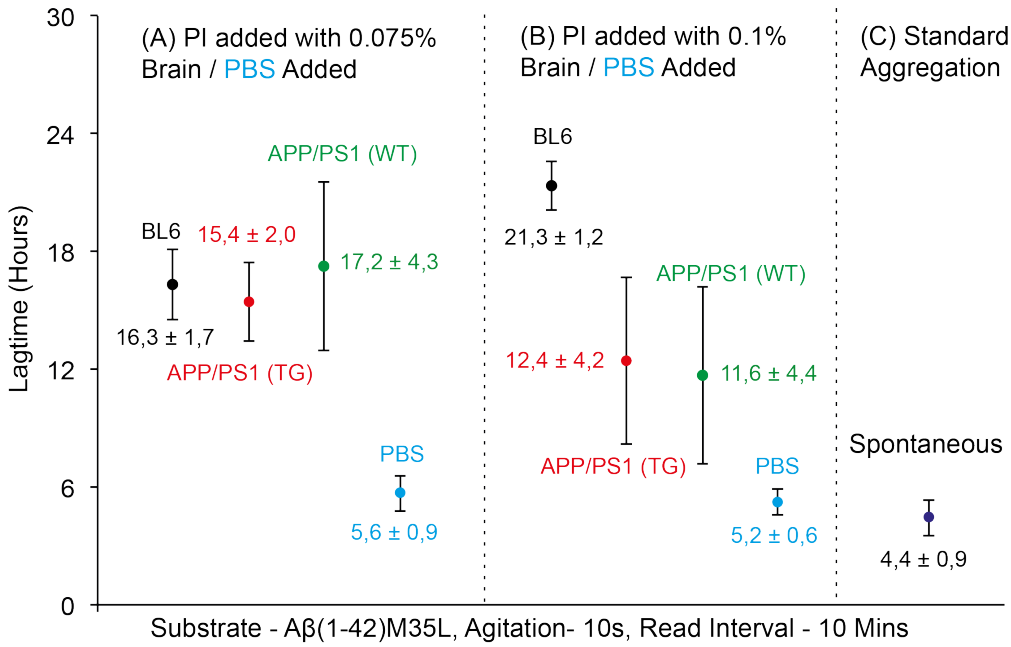

Fig.- 4.5: Brain homogenate seeding with 2X Protease Inhibitor. (**A**) Brain homogenate APP/PS1 (TG/WT) and BL6 added at 0.075% (v/v) as seed and a same volume of PBS is added as negative control. (**B**) Brain homogenate APP/PS1 (TG/WT) and BL6 added at 0.01% (v/v) as seed and a same volume of PBS is added as negative control. (**C**) Spontaneous Aggregation of the substrate without protease inhibitor. The error bars indicate standard deviation from the median of lagtimes analyzed. (N=5, for all the reactions).

In summary, addition of brain homogenate as seed in the assay retarded aggregation of Aβ substrate in the assay. In the absence of added protease inhibitors, the aggregation reaction is completely inhibited in the assay (Data not shown), as the cellular proteases from the brain homogenate cleaved the soluble Aβ substrate in the assay. Retardation of aggregation in the presence of brain homogenate added reaction was considerably observed despite adding high amount of protease inhibitors in the assay. This pressed the need for using an alternative Proteinase-K (PK) digestion, which is a stronger proteinase digestion enzyme.

4.2.2 PK digestion abrogates the retardation effect of brain homogenate

Proteinase-K (PK) is a broad-spectrum serine protease enzyme. PK was added (1:500) w/w adjusted to total protein content in the brain homogenate. The protein content in the 10% brain homogenate was estimated using a Bradford assay. The protein concentration in the brain homogenate was estimated to be ca. 6 microgram per microliter. Brain homogenate is incubated with PK (1:500) at room temperature

for 2 hours and later heat inactivated by boiling the mixture at 95°C for 10 minutes and later placing it on ice bath (Ref. Section, 3.3.5). Freshly prepared soluble Aβ(1-42)M35L substrate is added to this mixture and diluted to 30μM final concentration in the aggregation buffer. 10% APP/PS1 (TG/WT) brain homogenate fraction is added at 1% and 2% in the assay after PK digestion. Standard PBS is added as the negative control, as the brain homogenate is homogenized in the PBS buffer. *De-novo* Aβ(1-42)M35L fibrillar seed (1μM) is spiked in standard PBS, to ascertain the effect of PK digestion on *de-novo* fibrillar seeds. Each reaction cohort in this experiment was performed with 6 replicates (Fig.- 4.6). The error bars indicate standard deviation from the median of the determined lagtimes. The kinetic reading parameters included: 10 minutes read frequency interval with 10-seconds shake (agitation) before each read.

The overall observed lagtime analyzed for brain homogenate added reactions in the assay are approximately in the same regimes of spontaneous aggregation without the brain homogenate (Lagtimes of ca. ±2 hours). This result indicates that PK digestion can annul the effect of brain material induced aggregation retardation induced in the assay to a considerable extent. Comparing PK digestion to Protease inhibitor addition (Fig.- 4.5), it is evident that PK digestion of the BH in the assay is a more promising approach to deal with the BH induced retardation effect in the assay. However, no seeding activity was still detected between the APP/PS1(TG) and APP/PS1(WT) brain seeded samples (Fig.- 4.6A&B), despite increasing the brain homogenate seeding concentration to 0.2% (Fig.- 4.6 B) in the assay. Increasing the brain homogenate concentration from 0.1% to 0.2% in the assay system marginally increased the detected lagtimes owing to higher brain material load in the assay. The *de-novo* spiked Aβ(1-42)M35L fibrillar seed (1μM) in the PBS buffer (0.1% & 0.2%) was found to be PK resistant (Fig.- 4.6A&B), as it could still actively seed the soluble Aβ(1-42)M35L substrate in the assay as observed in the standard seeding reactions without PK digestion (Fig.- 4.9C). The raw kinetic data for this experiment is available in the supplementary section (Refer, Supporting Data, Fig.- 7.4).

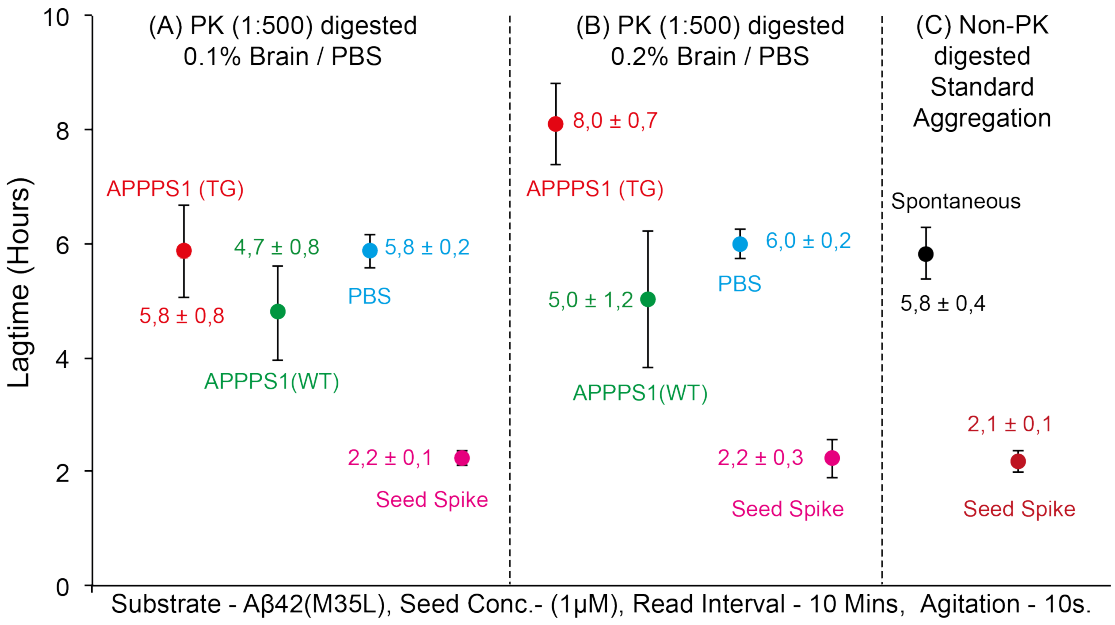

Fig.- 4.6: **Addition of Proteinase-K (PK) digested brain homogenate seed in the assay**. (**A**) Represents analyzed lagtimes of reactions seeded with 0.1% PK digested Brain homogenate APP/PS1 (TG/WT) added as seeds, along with PBS and spiked *de-novo* seed in PBS buffer. (**B**) Represents analyzed lagtimes of reactions seeded with 0.2% PK digested brain homogenate APP/PS1 (TG/WT) added as seeds, along with PBS and spiked *de-novo* Seed in PBS buffer. (**C**) Standard spontaneous and seeded aggregation of Aβ(1-42)M35L in aggregation buffer without PK digestion. Error bars indicate standard deviation of analyzed lagtimes from the median value. (N=5, for all the reactions)

The seeding difference between the APP/PS1(TG) and the APP/PS1(WT) brain homogenate seeds could not be detected suggesting that the brain homogenate components like native proteins and membranes, might be suppressing the seeding capabilities of the Aβ fibrils present in the TG mouse brains. Later, it was decided to screen for phospholipid conditions in the seeding assay that can mimic the membrane-like *in-vivo* brain environment. Another possibility, why the brain seed did not seed in the assay, could also be due to the low concentration of added brain-Aβ seed, which could not dominate and compete with the concomitant (spontaneous) Aβ nucleation and aggregation. Therefore, it was hypothesized that, membrane-like conditions would mimic the brain biological environment, where the kinetics of aggregation and seeding could be different compared to *in-vitro* aggregation in the assay. It was hypothesized that the lipid condition could aid in conformational brain aggregated-Aβ seeding in the assay.

4.3 Mimicking Phospholipid Condition in the Assay

Brain aggregated-Aβ seeding activity did not occur by introduction of brain homogenate in the assay under standard buffer conditions with both protease inhibitors addition and by proteinase-k digestion. This gave rise to an idea of mimicking *in-vivo* biological conditions *in-vitro* by adding lipid membranes-like condition in the assay. The membrane-like condition was hypothesized to interact akin to cellular membranes in the brain, where synthesis of Aβ and seeding activity could be much more efficient as compared to standard *in-vitro* conditions in the assay. This phospholipidic milieu will enable to understand and investigate kinetics of Aβ spontaneous and seeded aggregation in membrane-like conditions in the assay.

Another, plausible reason why brain-Aβ could not seed in the assay could also have been due to, low availability of brain aggregated-Aβ seeds in the brain homogenate added to the assay. Low concentration of brain-Aβ seeds could have not been sufficient to robustly compete and dominate over the spontaneous aggregation of substrate Aβ(1-42)M35L in the assay. To overcome this bottleneck, we would need an experimental assay condition, where the primary nucleation of the substrate Aβ is specifically suppressed. This would enable brain aggregated -Aβ seed added to the assay to compete and seed robustly over the primary concomitant nucleation of the substrate Aβ. To investigate these membrane-like conditions *in-vitro*, screening of phospholipid was carried on in the assay system so far established.

4.3.1 Phospholipid DHPC suppresses substrate Aβ primary nucleation and enables Aβ seeding in the assay

DHPC (1,2-dihexanoyl-*sn*-glycero-3-phosphocholine) is a short-chained phospholipid molecule and an excellent phospholipid model system to study effects of lipid interactions on Aβ aggregation (Dahse et al. 2010). DHPC is added in the assay to monitor the Aβ oligomerization kinetics. To 30μM Aβ(1-42)M35L soluble substrate concentration in the Assay, DHPC was added in incremental steps of 1mM from 0-6mM in both spontaneous and *de-novo* added seed condition. *De-novo* Aβ(1-

42)M35L fibrillar seeds were spiked at a concentration of 0.25μM in this experiment (Fig.- 4.7). There are five replicates for each reaction in the experiment. The kinetic recording parameters for the experiments are 10 minutes reading interval with 10s agitation before each read. The gain was set manually to value 95.

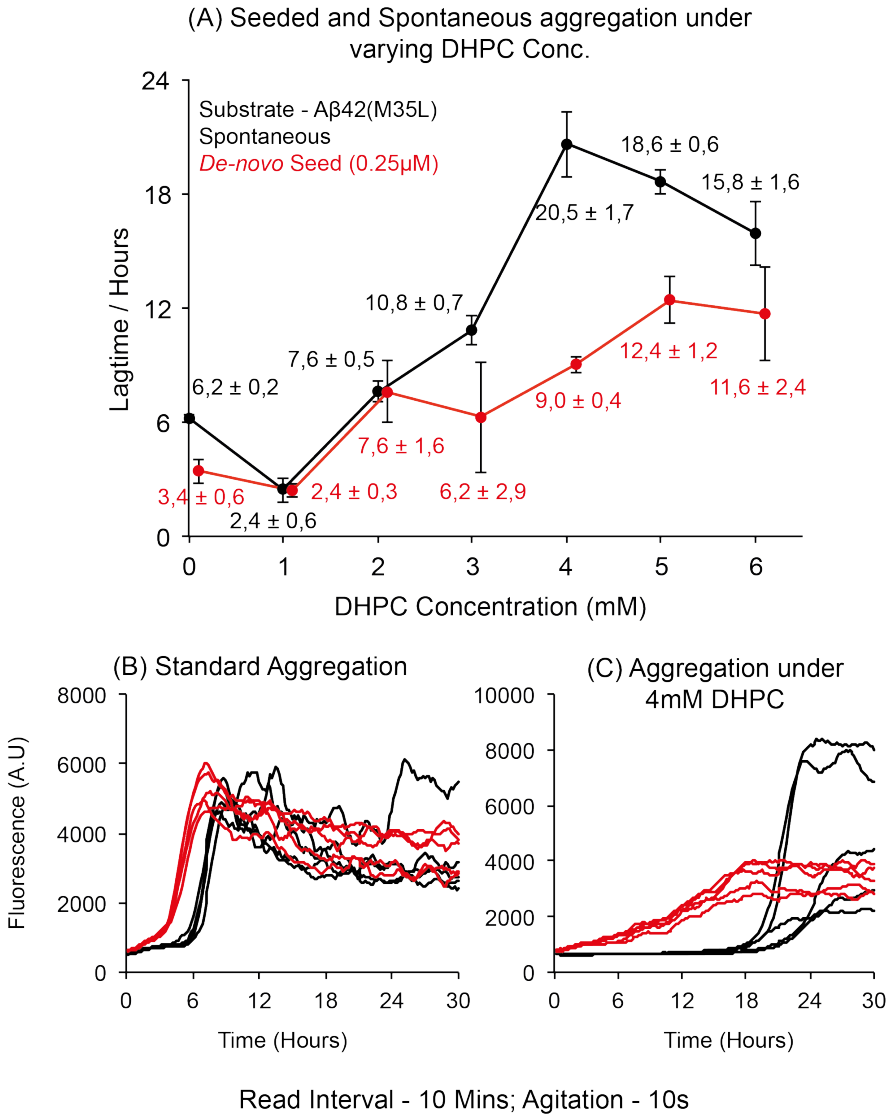

Fig.- 4.7: **Addition of DHPC in the assay under spontaneous and *de-novo* seeded condition** (N=5). (**A**) Aggregation of Aβ(1-42)M35L under varying concentrations of DHPC (0-6mM). (**B**) Standard aggregation and (**C**) in the presence of 4mM DHPC. Black curve indicates the spontaneous and the red curve indicates seeded aggregation. Error bars indicate standard deviation from the median lagtime values analyzed.

Varying concentrations of DHPC is mixed with 30μM Aβ(1-42)M35L with both spontaneous / *de-novo* Aβ(1-42)M35L fibrils, the data is presented in Fig.- 4.7A. DHPC screening in the assay demonstrates that the Aβ aggregation and seeding

kinetics is strongly affected by the phospholipid DHPC at different concentrations (Fig.- 4.7A). However, the nature of these effects precisely depends on the concentration of DHPC used in the assay. At 1mM DHPC, there is a strong influence of the DHPC on soluble Aβ(1-42)M35L substrate and its subsequent seeded reaction evidenced by accelerated aggregation. There are no seeding differences detected between the seeded and the spontaneous aggregation at 1mM DHPC condition in the assay. In the ranges from 2 to 6mM DHPC, the Aβ spontaneous aggregation is impeded indicated by increasing lagtime up to 4mM and then gradually starts declining at 5mM and 6mM DHPC concentration in the assay (Fig.- 4.7A). There is significant increase in the lagtime values of spontaneous Aβ aggregation at 4mM DHPC concentration ~20 hours as compared to the spontaneous at ~6 hours (Fig.- 4.7B&C). Differences in seeding activity in the presence and absence of 4mM DHPC is shown as fluorescence intensity kinetic data (Refer, Fig.- 4.7B&C). The kinetic raw data has been smoothed using 17-point Savitzky-Golay filter. The raw kinetic data for this experiment has been provided in the supplementary data section of this thesis (Refer, Supplementary Data, Fig.- 7.5).

DHPC also considerably affects the seeded aggregation in the assay system. The seeded aggregation kinetics is indistinguishable from spontaneous aggregation at 1mM and 2mM DHPC having no seeding resolution. Seeding resolutivity denotes the quantitative difference in determined lagtime between the spontaneous aggregation and the seeded aggregation reaction. The seeding resolutivity gradually starts to increase at 3mM and 4mM DHPC and later decreases at 5mM and 6mM DHPC. The seeding resolutivity of the assay is maximum at 4mM DHPC condition, approximately 4 times the seeding resolutivity compared to the standard spontaneous and seeded aggregation.

It was a serendipitous finding that; DHPC at 4mM suppressed spontaneous and seeded aggregation by more than 3 fold compared to standard spontaneous and seeded aggregation reaction and enabled higher seeding resolutivity in the assay (Refer, Fig.- 4.7B&C). From these observations, it was decided to add 4mM DHPC in the assay to increase the seeding resolutivity in the system. Higher seeding resolutivity is crucial in the seeding system as it grants a broad lagtime window to

detect lower dilution of added seed in the assay. The next step was to test the effect of 4mM DHPC in the presence / absence of brain homogenate in the assay and determine the seed detection limit in the assay by logarithmically diluting out the seeds. This would help in understanding the dynamics of seeding mechanism in the presence and absence of brain homogenate in the assay.

4.3.2 Assay can detect low concentration of Aβ-fibrils spiked to the brain homogenate

This experiment was designed to investigate the comparative seeding sensitivities between brain homogenate added and standard seeding reactions in the assay. The aim was to understand the aggregation kinetics and seed detection in the presence and absence of 0.1% BL6 brain homogenate added in the assay system under 4mM DHPC condition. *De-novo* Aβ(1-42)M35L fibrillar seeds are logarithmically diluted from 250nM to 2.5pM and mixed with / without 0.1% BL-6 brain homogenate in the aggregation buffer (Fig.- 4.8B). Later they are PK digested and added as seed in the assay to 30μM soluble substrate Aβ(1-42)M35L with (Fig.- 4.8B&C) and without (Fig.- 4.8A) 4mM DHPC. Spontaneous Aβ aggregation with 4mM DHPC in the presence and absence of 0.1% brain homogenate is performed as controls in this assay (Fig.- 4.8C). The aggregation data for the substrate Aβ(1-42)M35L in the presence of only 4mM DHPC* (Fig.- 4.8C ii) is appropriated from the last experiment (Refer, Results, Section- 4.3.1). There are 5 replicates to each reaction cohort in this assay. All the reactions in this assay are PK digested except for spontaneous aggregation of substrate Aβ(1-42)M35L in 4mM DHPC (Fig.- 4.8C ii). Error bars indicate standard deviation from the median of determined lagtimes. The assay parameters of this experiment are: 10 minutes reading interval with 10 seconds agitation before each read. The raw kinetic data for this experiment has been provided in the supplementary section (Refer, Supplementary Data, Fig.- 7.6).

The assay could detect spiked *de-novo* Aβ seed reliably up to 25pM in the presence of 0.1% brain homogenate under the 4mM DHPC condition. There are profound seeding differences in lagtimes between reactions with / without 0.1% brain

homogenate. Seeding lagtime times are longer for reactions with 0.1% brain homogenate (Fig.- 4.8B i) compared to reactions without brain homogenates (Fig.- 4.8B ii). This significant difference in lagtimes can be attributed to presence of added brain homogenate material that interferes with the amyloid spontaneous and seeded nucleation. In the next step we used the brain material from the AD transgenic mice APP/PS1 (TG /WT) and APP-23 (TG/WT), PK digested and add them as seed in the assay with 4mM DHPC condition.

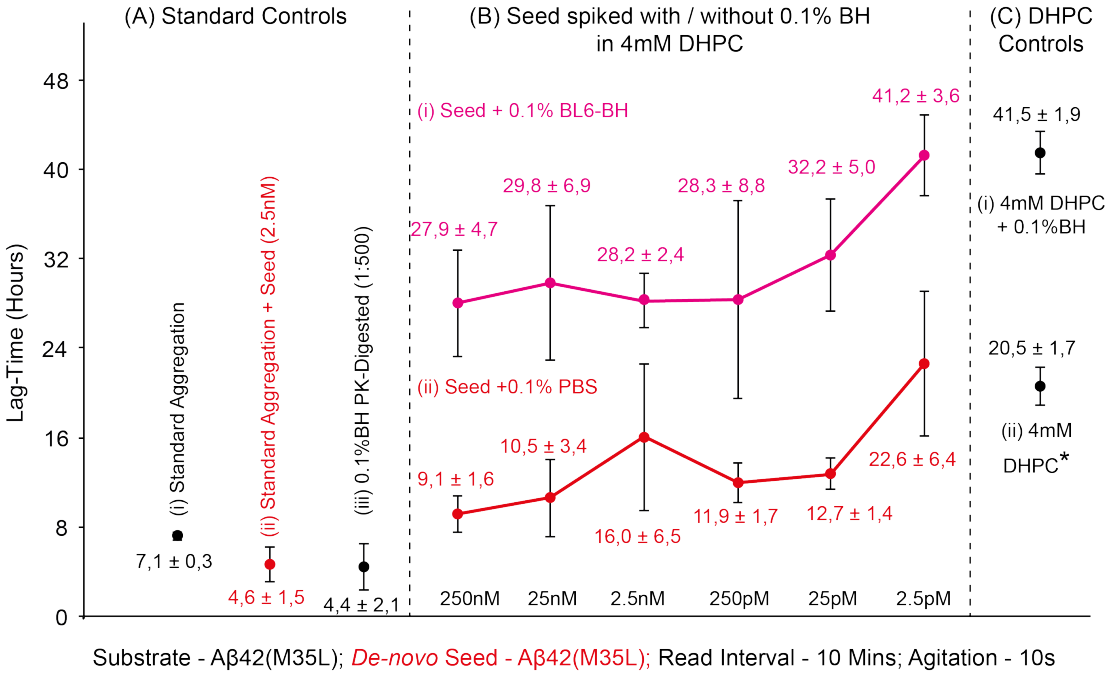

Fig.- 4.8: **Detection of *de-novo* spiked Aβ seed in the assay**. (**A**) Standard controls in Aggregation buffer (i) Spontaneous aggregation. (ii) 2.5nM *de-novo* seeded reaction and (iii) 0.1% BH PK-Digested. (**B**) Logarithmically diluted seed (250nM- 2.5pM) with 4mM DHPC seeded in the (i) presence and (ii) absence of 0.1% brain homogenate. (**C**) Substrate Aβ spontaneous aggregation in the (i) presence and (ii) absence of 0.1% brain homogenate under 4mM of DHPC. Error bars indicate standard deviation from the median lagtime values determined. (N=5). (* Indicates data from the previous experiment)

4.3.3 APP/PS1(TG) Brain Aggregated-Aβ seeds in the assay

With the combined knowledge of PK digestion and phospholipid DHPC condition in the assay; APP/PS1(TG/WT), APP23(TG/WT) and BL6- brain homogenates were added as seeds in the assay. 0.2% brain homogenate material was first PK digested (1:500), PK inactivated, and stored on ice. This mixture is later added as seeds to the

soluble Aβ(1-42)M35L substrate in the assay. APP/PS1 (TG) brain contains Aβ material (Aβ42:Aβ40) in (70:30) ratio and APP23(TG) contains (30:70) ratio (Meyer-luehmann 2006). APP/PS1(TG) brain homogenate material contains more Aβ42 seed material, so in principle it was hypothesized to seed the Aβ(1-42)M35L substrate in the assay. The APP/PS1(WT) and APP23(WT) brain material forms the negative control for the transgenic mice brain that does not contain any Aβ aggregates. The BL6 brain homogenate is additionally added as a negative control.

The assay is setup by mixing the 30μM soluble Aβ(1-42)M35L with the PK digested brain homogenate and 4mM DHPC is added before starting the reaction (Fig.- 4.9C,D & E). DHPC is not added to the cohort A (Fig.- 4.9A) and they contains standard aggregation controls like (i) Standard spontaneous Aβ aggregation (ii) Spontaneous Aβ aggregation in PK digested aggregation buffer and (iii) 0.2% BL6 brain material PK digested and added to Aβ substrate. Cohort B presents aggregation controls in the presence of 4mM DHPC (i) Spontaneous Aβ aggregation (ii) Spontaneous Aβ aggregation in PK digested standard aggregation buffer (iii) 0.2% PBS added to spontaneous aggregation buffer. Cohort C contains 0.2% PK digested brain homogenate seeded reactions with 4mM DHPC (i) APP/PS1(TG) and (ii) APP/PS1(WT). Cohort D contains 0.2% PK digested brain homogenate seeded reactions with 4mM DHPC (i) APP23(TG) and (ii) APP23(WT). The last reaction cohort E contains 0.2% PK digested BL6 brain homogenates and added with 4mM DHPC. The kinetic aggregation data is recorded with 10 minutes reading interval with a 10 seconds agitation before each read. The gain for this experiment was set to 90 (manual). There are 6 replicates for all the reactions in this experiment. Error bars indicate standard deviation from the median of detected lagtimes. The raw kinetic data for this experiment has been included in the supplementary data section of this thesis (Refer, Supplementary Data, Fig.- 7.7).

The aggregation kinetics of the APP/PS1(TG/WT) and BL6 seeded reactions were monitored (Fig.- 4.10A). From the kinetics it can be clearly observed that APP/PS1(TG) brain homogenate seeded the soluble substrate Aβ(1-42)M35L in the assay. The APP/PS1(TG) seeded reaction (Fig.- 4.10A, red trace) also displayed

higher fluorescence intensity as compared to APP/PS1(WT) or BL6 brain homogenate seeded reactions.

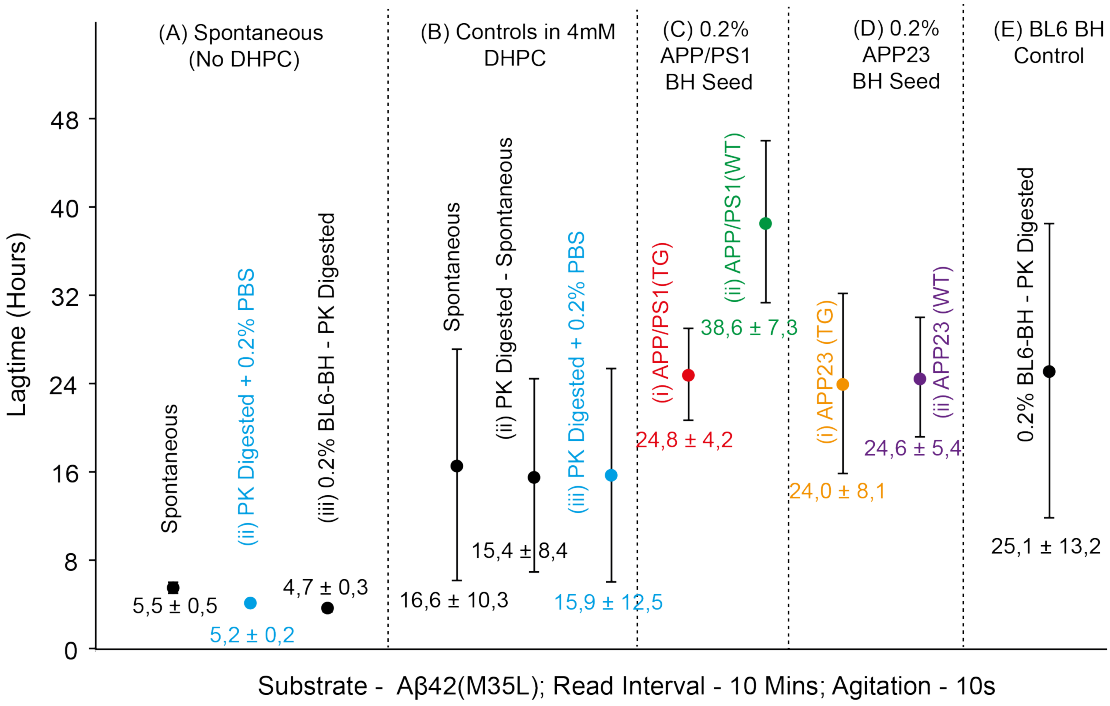

Fig.- 4.9: **Seeding of Brain homogenates in the Assay.** (**A**) Standard aggregation controls (i) Substrate spontaneous (ii) Substrate Spontaneous PK digested PBS and (iii) 0.2% BL6 brain material PK digested spontaneous aggregation. (**B**) DHPC (4mM) aggregation controls (i) Substrate spontaneous aggregation (ii) Substrate spontaneous PK digested buffer and (iii) Substrate spontaneous with PK digested PBS. (**C**) 0.2% APP/PS1 (TG/WT) brain PK digested and seeded in the assay with 4mM DHPC. (**D**) 0.2% APP23 (TG/WT) brain homogenates PK digested and seeded in the assay with 4mM DHPC. (**E**) 0.2% BL6 brain homogenate PK digested and seeded in the assay with 4mM DHPC. (N=6). Error bars indicate standard deviation from the median lagtimes.

The higher fluorescence in APP/PS1(TG) seeded reactions along with the reduction in aggregation lagtime compared to the APP/PS1(WT) added reactions indicates that the brain aggregated Aβ from the APP/PS1(TG) mice brain homogenate seeded in the assay. The brain-Aβ seeding with higher fluorescence is also observed in the fibril amplification assays utilizing Aβ40 substrate (Paravastu et al. 2009; Lu et al. 2013). The seeding can be further confirmed by observing the seeded aggregation kinetics of replicates moving together as a bundle with lesser standard deviation between them (Fig.- 4.10A).

The data from the negative control brain homogenate [APP/PS1(WT) and BL6]

added reactions with 4mM DHPC bear close resemblance to spontaneous aggregation with a larger spread and higher standard deviation among the replicates. APP23 (TG) brain homogenate did not seed in the assay (Fig.- 4.10B), this might be due to the difference in molecular composition of Aβ seeds present in the APP23(TG) brain. The *in-vivo* brain aggregated-Aβ experiment has been repeated multiple times and in all the experiments, it was found that only APP/PS1(TG) brain material seeded in the assay and APP23(TG) did not seed the soluble Aβ(-42)M35L substrate. Seeding activity was not observed, when 0.1% brain material was used to seed the Aβ(1-42)M35L substrate in the assay (Data not shown).

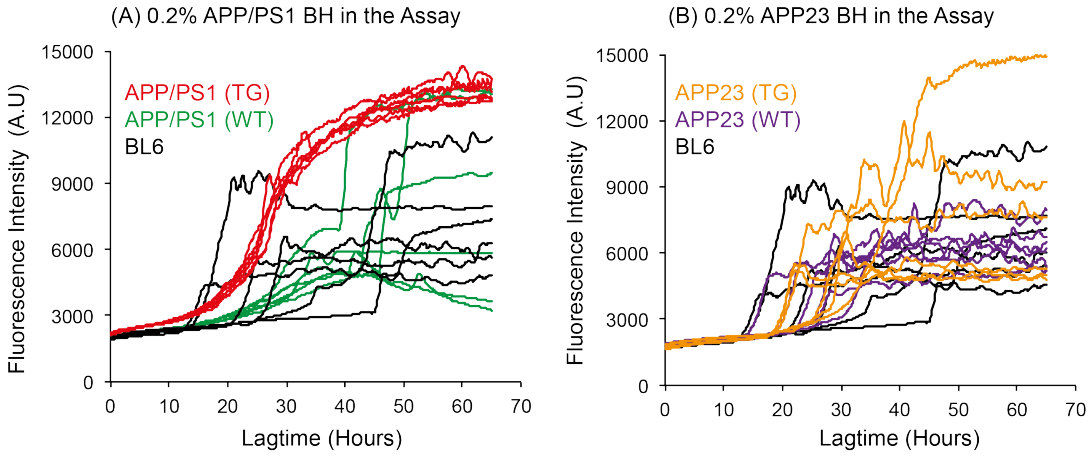

Fig.- 4.10: **APP/PS1(TG/WT), APP23(TG/WT) and BL6 Brain Homogenate Seeding**. PK digested 0.2% brain homogenate were seeded in the assay with 4mM DHPC. (**A**) Raw aggregation kinetics of APP/PS1(TG) (Red), APP/PS1(WT) (green) and BL6 (black) reactions and (**B**) APP23(TG) (orange), APP23(WT) (violet) and BL6 (black).

The seeding in the assay was considerably improved by introducing a number of measures that reduced the time delay between the digestion of the brain seed material and production of the recombinant soluble Aβ(1-42)M35L substrate from cation-exchange purification. A mild agitation using the thermo-shaker during the PK digestion of the brain homogenate greatly improved the brain aggregated-Aβ seeding in the assay (Fig.- 4.11). PK digestion of brain homogenates and introduction of phospholipid DHPC (4mM) in the assay enabled APP/PS1(TG) brain aggregated -Aβ to seed and conformationally amplify in the assay with soluble Aβ(1-42)M35L as the substrate. The amplification was further confirmed by TEM of the aggregates (Refer,

Section- 4.4.2). The seeding was possible, as DHPC micelles at 4mM significantly suppressed the substrate Aβ spontaneous nucleation thereby giving an edge to conformational seeding to occur from the brain aggregated-Aβ seed even at low concentration in the assay.

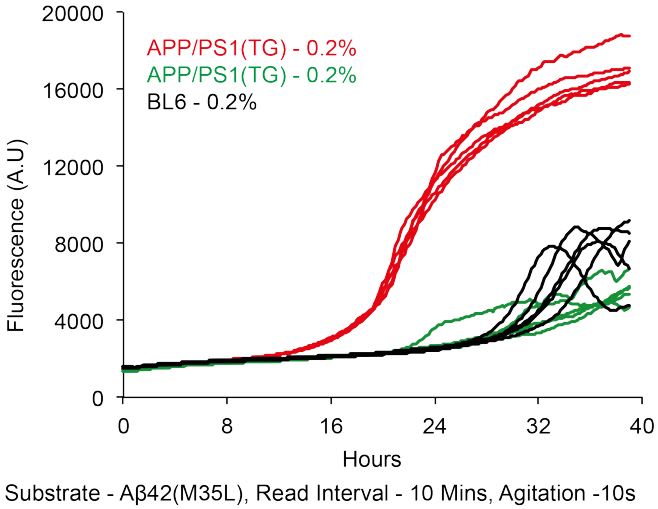

Fig.- 4.11: **Improved APP/PS1(TG) brain aggregated-Aβ seeding**. The data has been smoothed using a 17-point Savitzky-Golay filter. Gain = 90 (Manual)

4.4 Characterization of Aggregates by Negative Staining Transmission Electron Microscopy (TEM)

Negative stain TEM is a relatively rapid method to investigate, morphological fibrillar characteristics of amyloid proteins at a molecular level. To study the morphological differences between the aggregates that are generated in our assay, the final aggregated reaction samples were examined by TEM.

4.4.1 Aggregation Buffer pH Affects Aβ-fibril Morphology

To analyze the effect of pH on Aβ fibril morphology, the final *in-vitro* aggregated samples from the assay were used to investigate morphological differences using TEM. For TEM analysis, grids were prepared by the methods as described here (Methods, section 3.5.1). The age of the aggregate samples were approximately 200 hours post aggregation when analyzed in this study. The mechanism of formation of fibrils and its intermediates has been explained in detail (Introduction, Section 1.7). Overall, from the micrographs (Fig.- 4.12 & 4.13), we can see that Aβ(1-42)M35L and Aβ (1-40)M35L form fibrils, oligomers and other intermediate aggregate structures.

Aβ(1-42)M35L *de-novo* spontaneously formed fibrils (red arrows) and oligomers (green arrows) at pH 8.1 are detected at moderate (200nm) and higher (100nm) magnification (Fig.- 4.12A&B). The Aβ(1-42)M35L fibril sample at pH 8.1 overall displays fibrils with thin, fragile, rod-like, linear with lateral branching morphologies with oligomers loosely associated with them (Fig.- 4.12A and insets A1 & A2). Oligomers are found loosely associated to the fibrils observed with higher magnification in (Fig.- 4.12B, inset B1 and B2).

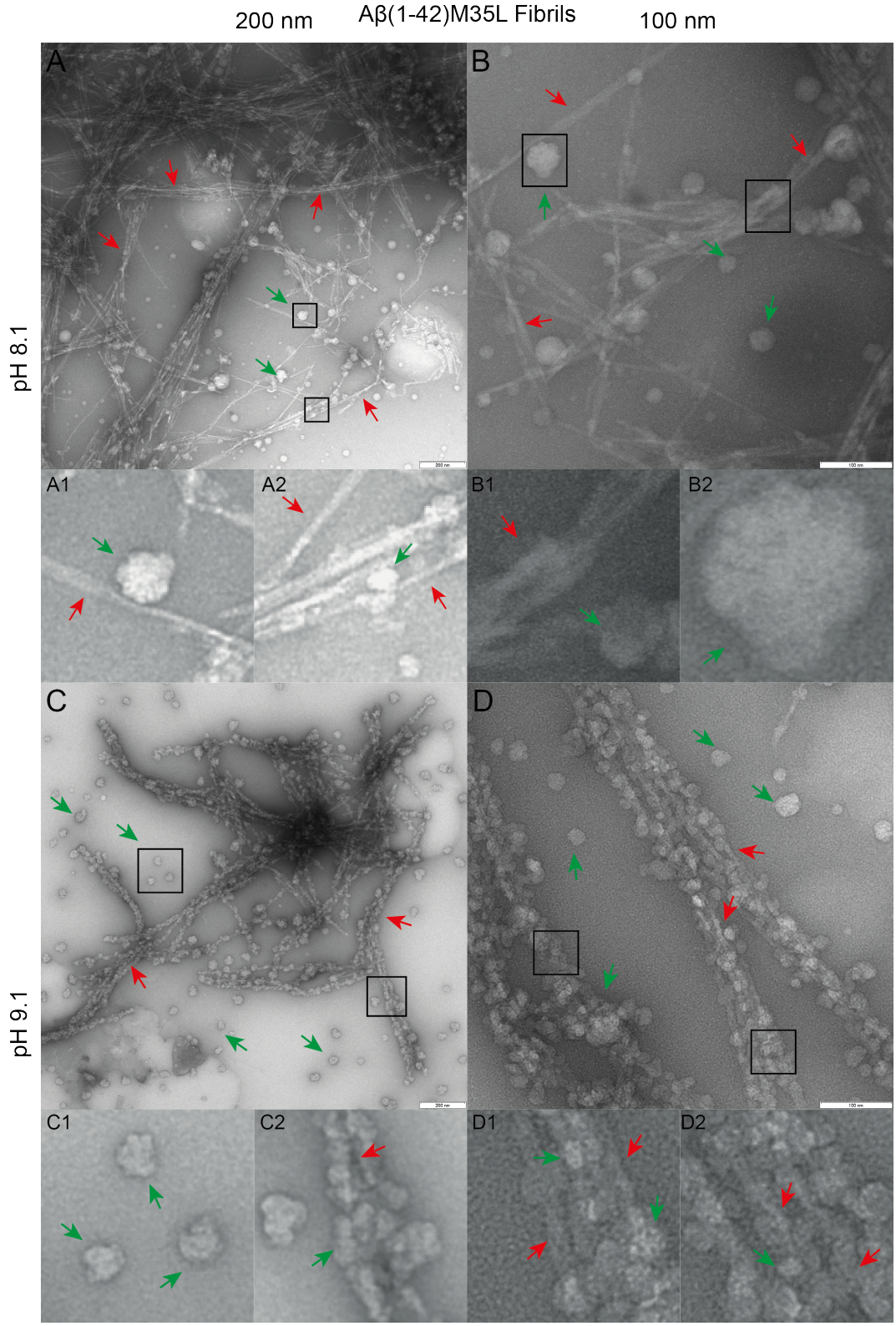

Fig.- 4.12: Effect of pH on Aβ(1-42)M35L fibril formation. TEM study at medium (200nm) (**A&C**) and higher (100nm) (**B&D**) magnifications. TEM micrographs correspond to Aβ(1-42) M35L at pH's 8.1 (**A & B**) and 9.1 (**C & D**). Red arrows indicate the fibrils and the green arrows indicate oligomers in the micrographs. The inset stamps display detailed view of marked morphological structures. The white bar in the right bottom indicates the scale of magnification.

Fibrils and oligomers of Aβ (1-42)M35L are similarly detected at pH 9.1 (Fig.- 4.12C & D). The oligomeric population predominates in the sample as compared to the fibrils at pH 9.1 (Fig.- 4.12C; inset C1 and C2). At higher magnification, large amounts of oligomers are densely clustered to fibrils like beads on a string (Fig.- 4.12D; inset D1 and D2). The size of Aβ(1-42)M35L oligomers ranges from ca. 30 - 40nm in diameter observed at both pH's 8.1 and 9.1 samples.

The Aβ(1-40)M35L spontaneous *de-novo* aggregates at pH 8.1 forms dense fibers (cyan arrows) running like cables in contact with, each other (Fig.- 4.13A&B). Fibers are predominantly seen, which look organized, smooth with periodic twist and occasionally overlapping each other (Fig. - 4.13A&B, inset A1 and B2). At closer inspection, fibrils are observed twisted and twined with one another at regular internodal spacing of ca. 7 - 10nm. The pairs of such fibrillar motifs combine and run over each other (Fig.- 4.13B and inset B2). Oligomers (green arrows) are detected in the sample and in general are scattered and sometimes bounded to fibrils with sizes ranging from ca. 15 - 25nm in diameter. The Aβ(1-40)M35L peptide at pH 9.1 forms thick and linear cluster of fibers which appear tightly twisted and intertwined with each other densely embedded by oligomers (Fig.- 4.13C& D; insets C1 and D1). Oligomers (green arrows) were observed densely packed to into the fibrillar structures protruding on the surface (Fig.- 4.13 D1) and sometimes sparsely distributed independently in the sample probe (Fig.- 4.13C and inset C2).

This result gives a clear indication that change in pH results in morphological differences in the aggregated Aβ protein. The differences have been succinctly summarized here (Table- 4.1). Increase in pH clearly leads to increase in population of oligomers detected in the sample. From these observations, it can be safely indicated that increase in oligomeric populations leads to increase in fluorescence emission spectra values observed in the assay (Refer, Fig.- 4.3). In order to reduce the effect of pH in forming oligomers in the assay, it was decided to limit the pH of the aggregation buffer in the assay to pH 8.1.

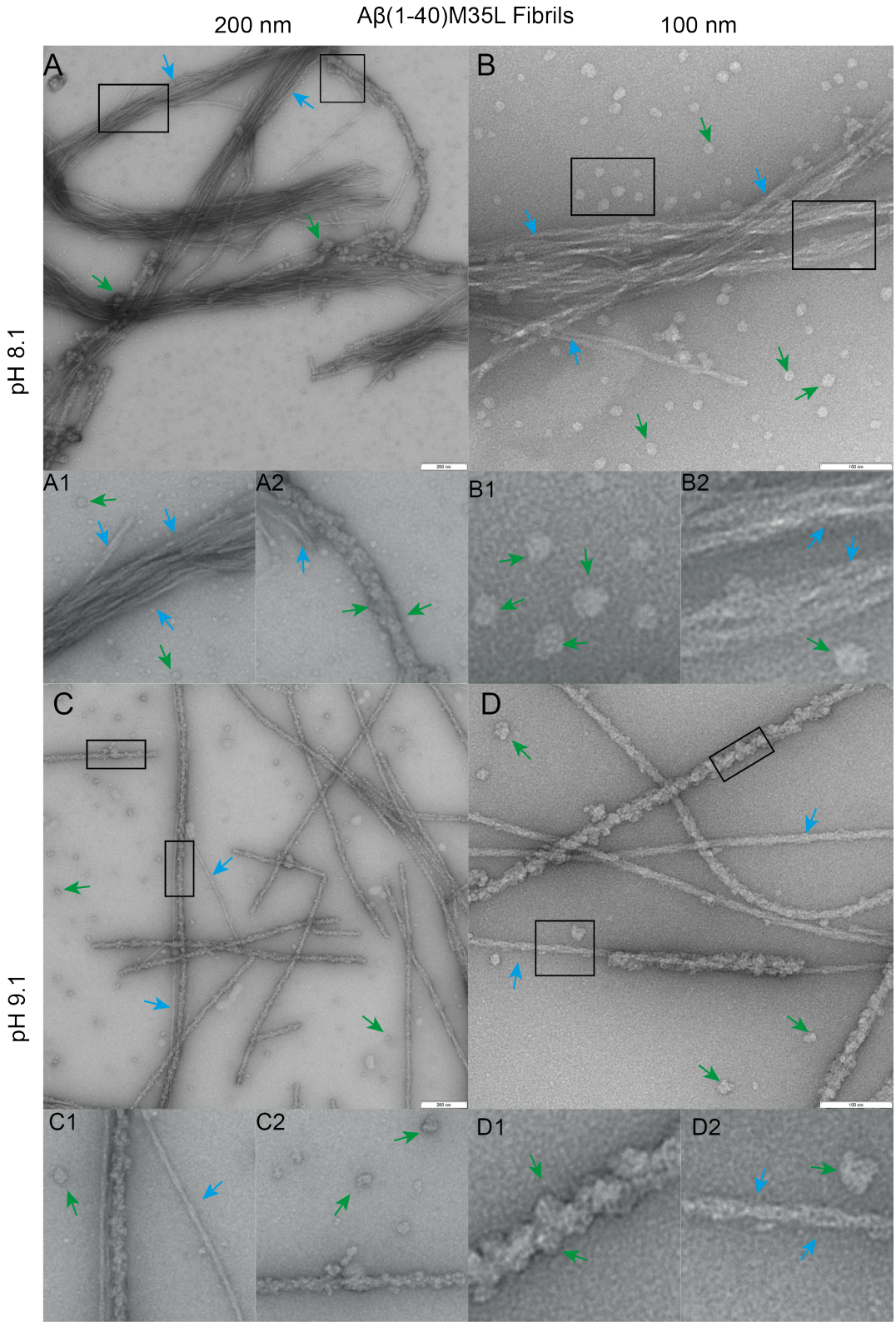

Fig.- 4.13: **Effect of pH on Aβ(1-40)M35L fibril formation**. TEM study at medium (200nm) (**A&C**) and higher (100nm)(**B&D**) magnifications. TEM micrographs correspond to Aβ(1-40)M35L at pH's 8.1 (**A&B**) and 9.1 (**C&D**). Cyan arrows indicate the fibrils and the green arrows indicate oligomers in the micrographs. The inset stamps display a detail view of marked morphological structures. The white bar in the right bottom indicates respective scales.

By adjusting the aggregation buffer to pH 8.1 in the assay system, the duration of each experiment and its data acquisition time could be overall reduced within a day by reduction in lag-phase of aggregation.

	Amyloid Beta *de-novo* aggregates at pH's 8.1 and 9.1	
Type	Aβ(1-42)M35L (pH 8.1)	Aβ(1-40)M35L (pH 8.1)
Fibrils	Higher fibrillar population, appear thin, fragile, rod-like and linear with multiple lateral branching morphologies.	Smooth and dense fibers, individual fibrils running parallel like flat cables and striated in appearance.
Oligomers	Sparsely scattered in the sample, Oligomer size (~30-40nm)	In general scattered, but sometimes found tightly bound to fibrils. Sizes range from (~15-25nm).
Special features	Oligomers loosely associated with fibrils and fibrillar heterogeneity observed.	At closer magnification, periodic twisting of fibrils are observed with an inter-nodal spacing of ~7-10nm.
	Aβ(1-42)M35L (pH 9.1)	Aβ(1-40)M35L (pH 9.1)
Fibrils	Thick Fibers, barely visible as beaded by oligomers	Thick and linear cluster of fibers, appearing tightly twisted and intertwined
Oligomers	Higher Oligomeric population, Oligomer size (~30-40nm)	Oligomers are interspersed in the sample with sizes ranging from ~15-25nm
Special features	Oligomers densely clustered alongside the fibril length like beads on a string.	Fibers are densely embedded by oligomers and sometimes also found naked

Table - 4.1: Morphological comparison of *de-novo* spontaneously aggregated Aβ sample

4.4.2 Distinct Morphological Differences are Observed in APP/PS1(TG) Seeded and Control Brain Homogenate Added Reactions

TEM grids were prepared from APP/PS1(TG/WT) and BL6 brain homogenate seeded aggregates from the assay. The sample age was approximately 84 hours when the TEM analysis was carried out. The final aggregation reactions products from the assay are referred to as 1st Generation (1G) as they are seeded from the mice brain homogenate seed added to the substrate Aβ in the assay. Once the aggregation process is deemed to be complete by reaching the plateau phase the Aβ aggregates are adsorbed to freshly prepared carbon butvar foils (Refer, section 3.5.1) and the TEM preparates are analyzed at 2μM, 500nm and 200nm resolution. A slim white line seen on the right bottom side of each micrograph represents the reference scale (Fig.- 4.14 & 4.15).

In the BL6-1G aggregate sample at 2μm resolution (Fig.- 4.14 A&B), we can observe small cluster of fibers that appear thread-like and knotty in appearance indicated by red arrows. Oligomeric Aβ species are observed uniformly distributed and consistently negatively stained (green arrows). Oligomers are also found occasionally bound to the fibrils. Some pre-fibrillar amyloid material is also observed in the sample indicated by cyan arrows (Fig.- 4.14 A, B and inset B1). Clusters of massively clumped fibrils adsorb more dye and appear intensely stained (Fig.- 4.14 A1). On closer examination of BL6 homogenate seeded reactions (Fig.- 4.15A) at medium magnification (500nm), the fibers appear flexible, moderately thick and intertwined with each other. At higher (200nm) resolution Fig. 4.15 (B), the intertwined fibrils look twisted with each other with internodal spacing observed at regular intervals (Fig.- 4.15B & inset B1). There are also short and thick fibers observed displaying different and distinct morphologies occasionally found in the sample showing higher sample heterogeneity. In our observation, there were no major morphological differences detected between BLG-1G and APP/PS1(WT)-1G seeded sample probes (Fig.- 4.14 C&D and Fig.- 4.15 C&D). The APP/PS1(WT)-1G aggregate macromolecular and morphological features look rather similar to those of the BL6-1G probes at all the analyzed magnifications (2μM, 500nm and 200nm).

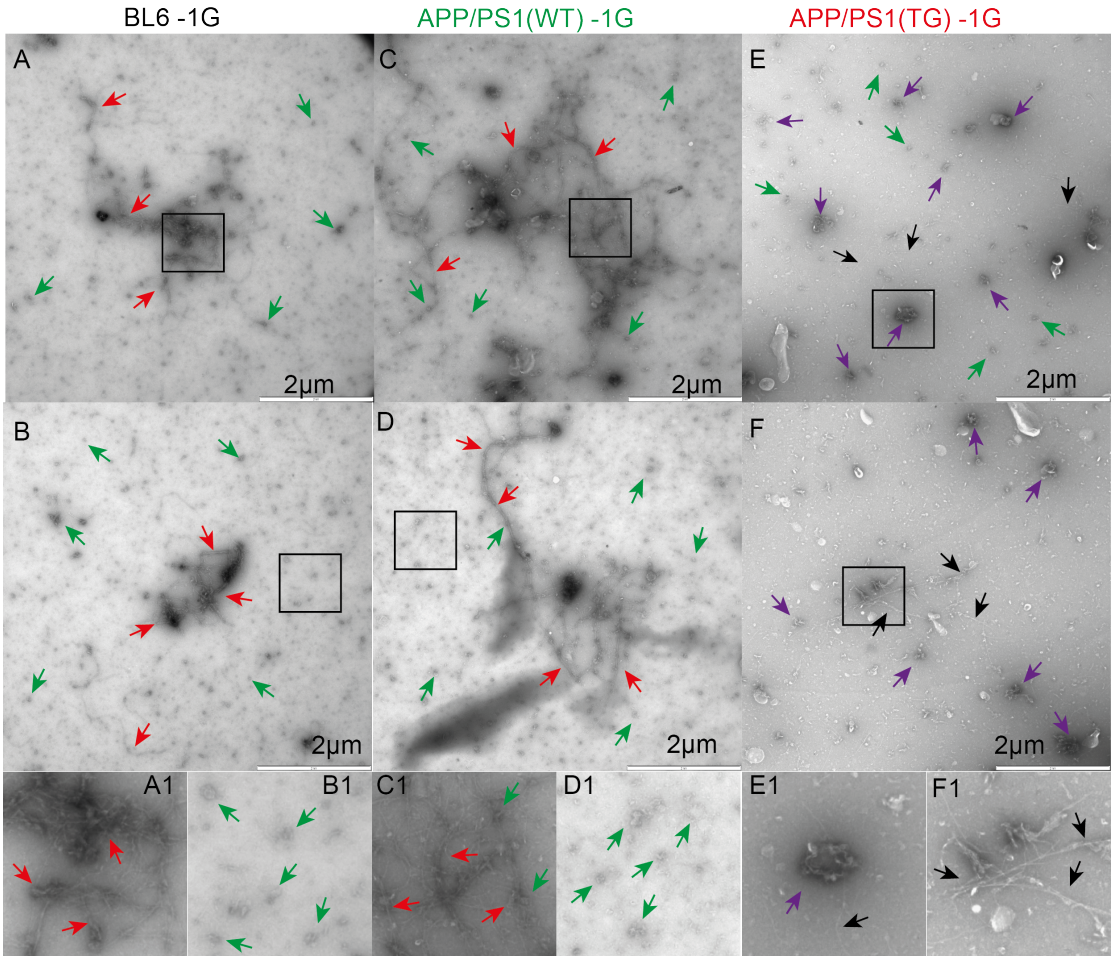

Fig.– 4.14: TEM micrographs of brain seeded reactions (**A-F**) at lower magnification 2µm. Red arrows indicate fibrillar material and green arrows indicate oligomeric species. The black arrows indicate APP/PS1(TG) fibrils and purple ones indicate prefibrillar oligomers. The insets include detailed molecular features analyzed in the micrographs. The white slim line below the micrographs indicates the scale (2µm). (**A &B**) represents BL6 brain homogenate-seeded reaction; **A1** &**B1** are insets showing detailed features of micrographs. **C and D** micrographs are 0.2% APP/PS1(WT) brain material seeded reactions, **C1** and **D1** show insets of detailed features of micrographs C and D. **E and F** are micrographs of 0.2% APP/PS1(TG) brain seeded reactions, showing detailed insets of features in **E1** and **F1**.

In APP/PS1(TG) seeded samples (Fig.- 4.14 & Fig.- 4.15E&F), large prefibrillar oligomeric structures are found coalesced together ranging from ca. 150-300nm in diameter (Fig.- 4.14E&F). These structures are found to adsorb more negative-stain indicated by purple arrows in (Fig.- 4.14 E&F). These pre-fibrillar oligomeric structure look like ball of yarn coalesced together with oligomers. These larger pre-fibrillar oligomers were absent in the BL6-1G or APP/PS1(WT)-1G aggregate samples. A close view of these large prefibrillar oligomers is provided in the insets (Fig.- 4.14E1). Small oligomeric structures were rarely detected in the APP/PS1(TG)-1G samples as compared to its strong background presence in BL6-1G and APP/PS1(WT)-1G

samples indicated by green arrows in (Fig.- 4.14 A,B,C&D, and also detailed view in insets B1&D1). The small oligomers that are observed in abundance in APP/PS1 (WT) and BL6 brain homogenate seeded samples (Refer Fig. 4.14A,B,E &F) are rarely to be observed in APP-PS1(TG) seeded samples.

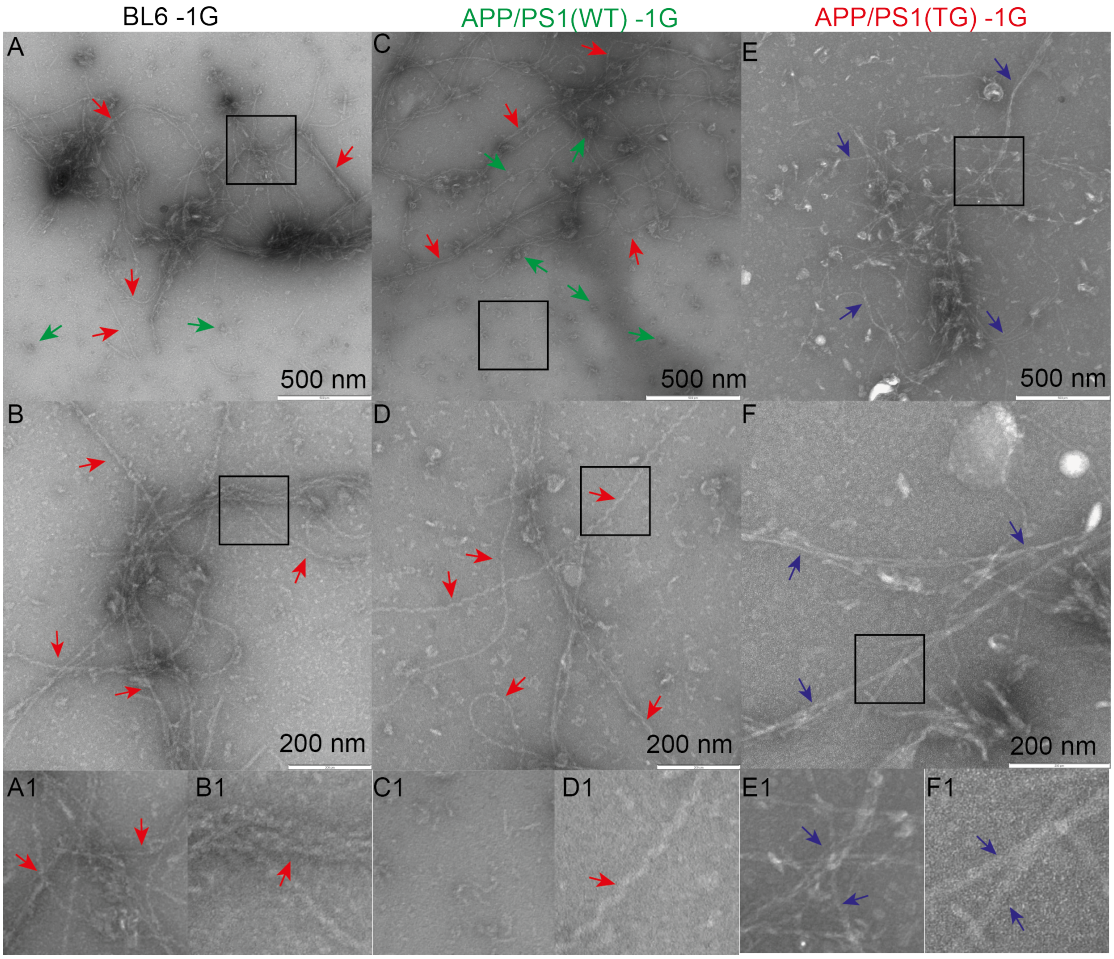

Fig.– 4.15: TEM micrographs of brain material seeded reaction in the Assay (**A-F**) at higher magnifications (scale 500nm and 200nm). Red arrows indicate fibrillar material and green arrows indicate oligomeric species. **A and B** micrographs represent BL6 BH seeded reactions at different magnifications. **C and D** micrographs represent APP/PS1(WT) BH seeded reactions at different magnifications. **E and F** micrographs represent APP/PS1(TG) BH seeded reactions at different magnifications. The blue arrows indicate APP/PS1(TG) fibrils and purple ones indicate prefibrillar oligomers. The insets include detailed molecular features analyzed in the micrographs.

The fibrillar content was hardly observed in APP/PS1(TG)-1G sample in comparison to APP/PS1(WT) and BL-6 seeded samples. At medium magnification (500nm), very few thin but short and slender fibrils were observed (Fig.- 4.14F and inset F1). At higher magnification (200nm), these fibrils appeared like fiber-optic filaments, rigid, needle-like appearance and straightened up with no periodic twisting features or

flaccid features (Refer, Fig.- 4.15 E, F and detailed features insets E1&F1). Fibrillar heterogeneity was not clearly observed in the APP/PS1(TG)-1G aggregates. They are found to be laterally associated with each other which is distinctly in contrast to BL6-1G and APP/PS(WT)-1G aggregate sample probes. TEM analysis for same cohort of aggregates but from a an another *in-vivo* brain homogenate seeding experiment revealed the similar morphological features as explained here. The differences between the fibrillar morphologies among the brain-seeded samples have been succinctly summarized using a table- 4.2 below.

	Brain Seeded Aggregate Sample Probes	
Type	APP/PS1(WT)-1G & BL6-1G	APP/PS1(TG)-1G
Fibrils	(i) Thick, flexible, thread-like, knotty appearance, fibrillar crossovers at regular intervals, pre-fibrillar aggregates also detected. (ii) Fibrillar heterogeneity clearly observed	(i) Sporadically detected, thin, needle-like, slender, laterally arranged and fragile. (ii) Fibrillar heterogeneity not observed.
Oligomers	Large population of small oligomers producing a strong spongy-like background	Large pre-fibrillar Oligomeric structures appearing like ball of yarn appearance (150-300nm). Smaller oligomers rarely found.
Special Features	Oligomers are found independently as well as sparsely bound to the flexible fibrils	Small oligomers were rarely found and oligomeric binding to fibril was absent.

Table. - 4.2: Morphological comparison brain homogenate seeded Aβ.

4.5 Acoustic SSA Distinguishes Fragmentability of Aβ Aggregates

Formation of matured fibers and aggregates with time results in the reduction of seeding capacity of Aβ aggregates. Fragmentation of aggregates by ultrasonication has been known in literature to increase the seeding capacity (Petkova et al. 2005; Fritschi et al. 2014). When fragmented, these fibrillar aggregates generate seeds

because of the fragmentation of fibril structure. Although, this method has been used to fragment the amyloid aggregates to increase the seeding capacity. Specific mechanical fragmentation of Aβ fibrils by controlled sonication as a characterization technique to distinguish structural conformations has yet not been reported. This study is one of the first initial attempts to understand the specific fibrillar mechanical stability of Aβ conformations using a novel Acoustic-SSA technique. This technique has been explained in detail in Acoustic SSA section (Refer, Material-Methods, Section 3.5.2). Controlled fragment is achieved by adjusting the height of the sample away from the sonicating sonotrode surface. The fragmented Aβ sample is then seeded to the seeding assay and monitored for seeding kinetics.

4.5.1 *De-novo* aggregated Aβ fibrils optimally fragment at 1.5mm height in the Acoustic-SSA setup

A proof-of-the-concept experiment of fragmentation by ultrasonication using Acoustic SSA was carried out, using *de-novo* aggregated Aβ(1-42)M35L spontaneous quiescent fibrils. The method of operation of sample preparation and Acoustic-SSA has been explained in detail (Refer, Section 3.5.2). The *de-novo* aggregated Aβ(-42)M35L fibrillar seeds were non-sonicated / sonicated at different heights (0.5, 1.5, 4.5 and 9.5) mm above from the flat horn of the sonicator probe surface.

The height was varied using the screw and the wing-nut arrangement. The position of the sample holder is always kept constant relative to sonotrode surface, owing to positional effects observed by Dr. Felix Deluweit (SBIB, HZI) in prions amplification experiments using the Acoustic-SSA method. The sonication settings are: 30 seconds total ON time with 10 pulses (3 second per pulse) and 7 seconds quiescence gap between each pulse. The fragmented *de-novo* Aβ seed material is logarithmically diluted to (3, 0.3, 0.03 and 0.003)μM and added to PK digested 0.2% BL6 brain homogenate in aggregation buffer and then seeded to soluble Aβ(1-42) M35L substrate with 4mM DHPC in the assay (Fig.- 4.16).

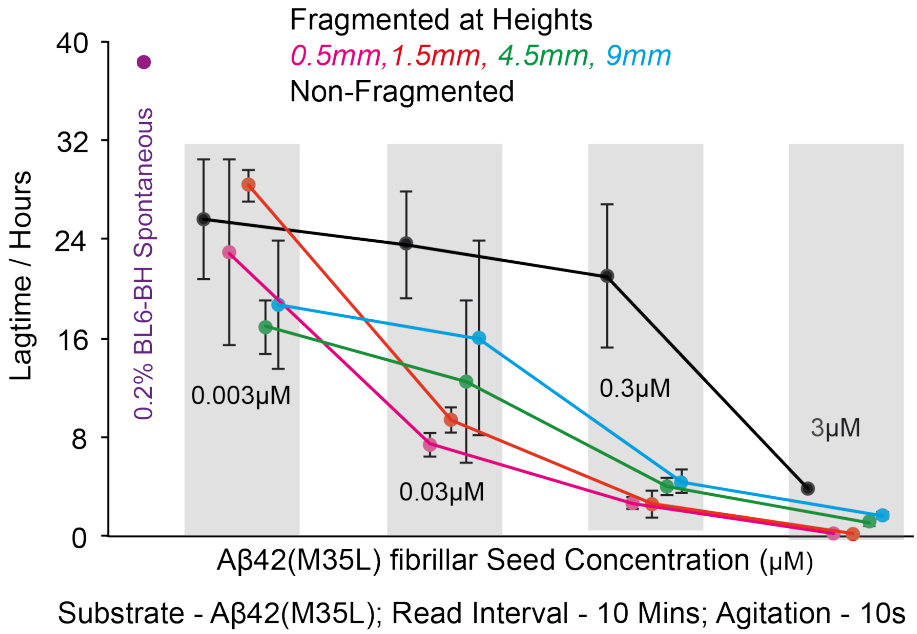

Fig.- 4.16: Controlled fragmentation of *de-novo* Aβ(1-42)M35L fibrils by Acoustic-SSA. Fragmented / Non-fragmented fibrils at different heights and seeded in assay by logarithmically diluting out the Seed. The spontaneous aggregation of the substrate Aβ(1-42)M35L on the top extreme left. The error bars indicate standard deviation from the median values of the detected lagtimes. (N=4)

There are four replicates for each reaction in this experiment. The seeds are then mixed with soluble Aβ in the assay and are analyzed for aggregation lagtimes (Fig.-4.16). The error bars indicate standard deviation from the median values of the analyzed lagtimes. The assay parameters used in recording kinetics are 10 minutes read interval with 10 seconds agitation before the start of each read. The gain used in recording the data is 95 (manual). Fig.– 4.17 displays the fluorescence intensity raw kinetic data of the assay. The Y-axis represents the fluorescence in arbitrary units and the X-axis represents time in hours. The kinetic aggregation data has been smoothed using a 17-point Savitzky-Golay filter.

The non-sonicated *de-novo* seeded reactions in the assay only seed at high concentration (3µM). With the lowering of seed concentration, the seeding resolution (concentration and time dependent seeding activity) is abruptly abolished and aggregation becomes random in the assay. Sonication shear force applied to the sample is height dependent, higher shear force is experienced closer to the sonotrode horn probe and lesser force away from the probe. Fibrils exposed to sonication shear force fragment and generate seeds. These seeds are added in the

assay to assess the fibril mechanical fragmentability under specific sonication forces.

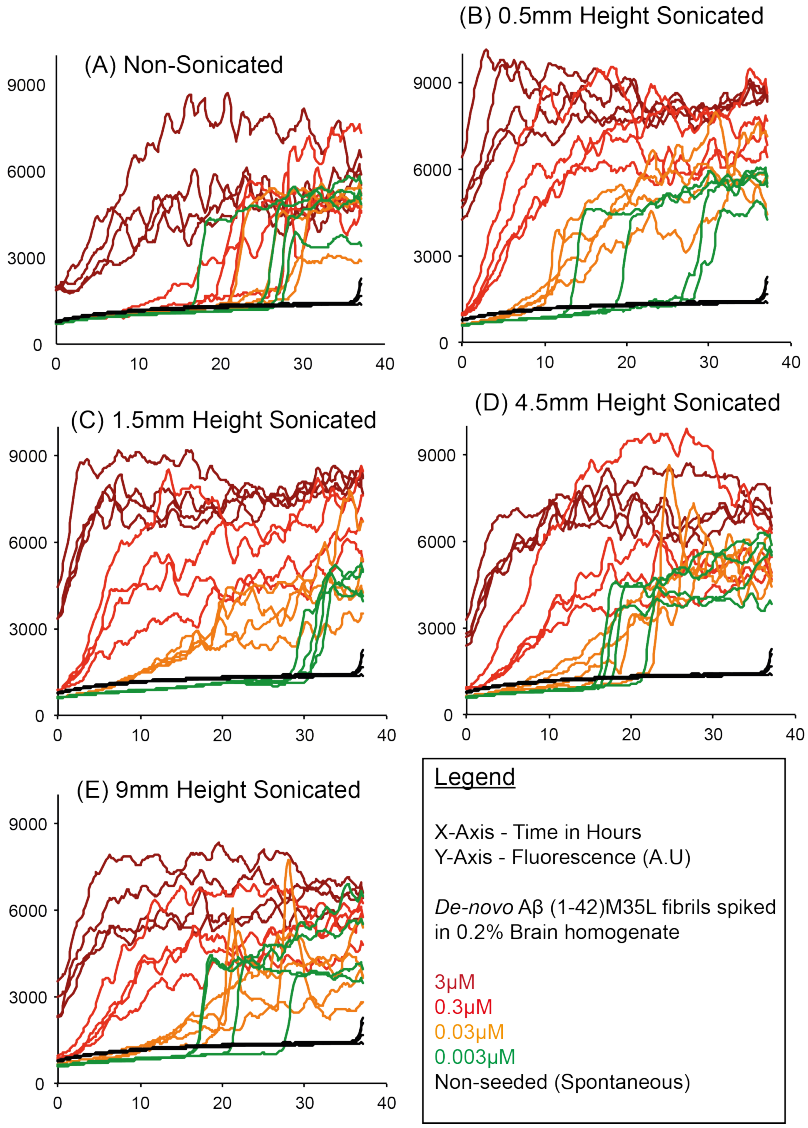

Fig.- 4.17: *De-novo* Aβ(1-42)M35L fibrils fragmented using Acoustic-SSA. Aggregation data of fragmented T-fibrils using Acoustic-SSA at different heights and seeding at different concentrations in the assay. (**A**) Non-sonicated and seeded. (**B**) Ultrasonicated at 0.5mm and seeded. (**C**) Ultrasonicated at 1.5mm and seeded. (**D**) Ultrasonicated at 4.5mm and seeded. (**E**) Ultrasonicated at 9mm and seeded. (N=4). The curves are smoothed using an 17-point Savitzky-Golay filter. The Y-axis represents the fluorescence intensity in arbitrary units and the X-axis represents time in hours.

Scanning the height range, it was observed that 1.5mm was the optimal height for sonication of *de-novo* Aβ(1-42)M35L fibrils. The optimal fragmentation of the *de-novo* Aβ(1-42)M35L fibrils can be inferred by the determined lagtimes that gives information on the seeding resolutivity of the logarithmically diluted seeds in the assay. The 1.5mm sonicated samples seed until the last logarithmic dilution

(0.003μM) with concentration to time dependence. This is only possible, when fibrils are optimally fragmented to seeds that can seed even in lowest dilution titer. From the knowledge derived from fragmentation by sonication of *de-novo* Aβ(1-42)M35L spontaneous quiescent fibrils, it was possible to apply the same methodology to APP-PS1(TG/WT) and BL6 seeded reactions to asses their mechanical fibril fragmentability.

4.5.2 APP/PS1(TG)-1G Fragmented Aggregates Seed Poorly in Assay

The APP/PS1(TG/WT) and BL6 brain homogenate seeded reaction aggregates are referred to as APP/PS1(TG/WT)-1G and BL6-1G, 1G refers to its first generation. The BL6-1G and APP-PS1 (TG /WT)-1G age-matched Aβ fibril material at 1μM were fragmented by sonication at 0.5mm height for 30 / 60 seconds in the acoustic-SSA setup. After fragmentation, they were seeded to soluble Aβ(1-42)M35L substrate with 4mM DHPC in the assay. There are 5 replicates for each reaction cohort in the assay. The parameters used for monitoring are 10 minutes read interval with 10 seconds agitation before the start of each read. The raw kinetic and fluorescence intensity data for the assay is presented with time domain on the X-axis and fluorescence intensity values on the Y-axis (Fig.- 4.18).

Seeding activity is observed distinctly in BL6-1G and APP/PS1(WT)-1G fragmented aggregates in the assay. They display similar seeding kinetics in the aggregation assay both processed at 30 and 60 seconds sonication time and at 0.5mm height in the Acoustic-SSA (Fig.- 4.18A,B,D&E). APP/PS1(TG)-1G fragmented and seeded reactions under the same conditions (0.5mm height , 30/60 sonication time) have a late lag phase, indicating poor availability of seed concentration required for seeding in the assay (Fig.- 4.18C&F).

The poor availability of seed in the APP/PS1(TG) could have been due to mild or excessive fragmentation of the aggregate in the Acoustic-SSA conditions that could have resulted in either poor generation of seeds or depolymerization of the TG-1G seed structure itself. Fragmentation of the aggregate is both depend on the processing time and the applied intensity of sonication force. The processing

fragmentation time was increased from 30 seconds to 60 seconds; but still there was no improvement in seeding effect of APP/PS1(TG)-1G material (Fig.- 4.18C&F). Rather increasing the processing time only worsened the seeding activity indicated by the randomness in lagtime of aggregation (Fig.- 4.18F).

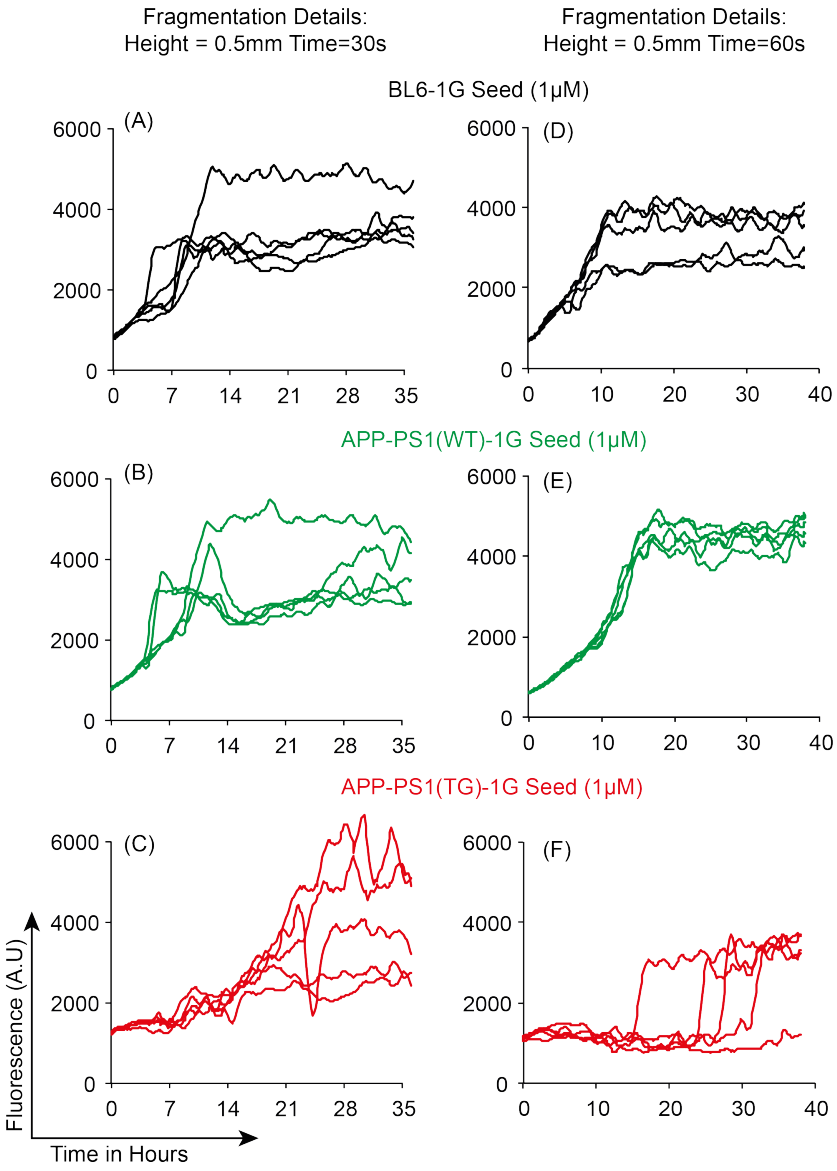

Fig.– 4.18: Difference in Seeding Kinetics after Fragmentation in Acoustic-SSA. Kinetic data of APP-PS1(TG/WT)-1G and BL6-1G fibril (1µM) fragmentation at 0.5mm height for 30/60 seconds using Acoustic-SSA. BL6-1G fragmented for 30 and 60 seconds at height 0.5mm and seeded in the assay (**A&D**). APP/PS1(WT)-1G fragmented for 30 & 60 seconds at height 0.5mm and seeded in the assay (**B&E**). APP/PS1 (TG)-1G material fragmented for 30 and 60 seconds at height 0.5mm and seeded in the assay (**C&F**). (N=5) The data has been smoothed with 17-point Savitzky-Golay data smoothing filter.

While, BL6-1G and WT-1G fragmented seeds showing similar seeding kinetics in the assay at both 30 and 60 seconds fragmentation processing time (Fig.- 4.18 A, B, D&E). Increasing the processing time to fragment the APP/PS1(TG)-1G was also tested, but still it did not seed in the assay (Refer, Supplementary Data, Fig.- 7.8). The height set in this experiment (0.5mm) was the lowest point where maximal shear forces can be applied to the sample in the acoustic SSA. Increasing the height to reduce the applied shear force on the sample was also performed on APP/PS1(TG)-1G samples and it still did not generate seeds to seed in the assay (Refer, Supplementary data, Fig.- 7.9). The seeding kinetics differences between brain aggregated-Aβ seeded APP/PS1-TG-1G and the *de-novo* aggregated [APP/PS1(WT)-1G and BL6-1G] arises due to the fibril mechanistic fragmentational differences encoded in its molecular structure. This indicates to presence of a specific brain aggregated -Aβ molecular conformation from the APP/PS1(TG) brain that has conformationally seeded in the Aβ-CSA (Conformational Seeding Assay). Polymorphic Aβ having different rates of fragmentation in the presence of shear forces has already been shown in the case of Aβ40 fibrils (Qiang et al. 2013). And, this study is the first one to show initial indications of difference in fibril fragmentability between brain aggregated-Aβ seeded fibrils and *de-novo* aggregated Aβ42 fibrils.

5 Discussions

Investigation into the pathogenic agent in Alzheimer's disease has lead researchers to arrive to a common speculation that Aβ peptide aggregation and accumulation is a dominant disease biomarker. Since a decade many studies have strongly indicated that Aβ can also act like prions propagating by conformational seeding and maintaining a distinct Aβ strain (Watts et al. 2014; Stöhr et al. 2014; Lu et al. 2013; Hatami et al. 2014; Aguzzi 2014; Spirig et al. 2014) (Also, Refer, Introduction, Section 1.5). Currently, there is enough credible evidence to suggest that AD could be transmissible in the same sense as in prion diseases (Meyer-luehmann 2006; Eisele et al. 2010; Langer et al. 2011; Stohr et al. 2012; Hamaguchi et al. 2012; Rosen et al. 2012; Morales et al. 2015). Similar to prions strains, Aβ peptide is also known to adopt polymorphic conformations *in-vivo* depending on the aggregation environmental conditions and several other factors (Cohen et al. 2015; Nilsson et al. 2007). To this date, the *in-vivo* specific Aβ structure in the brain still continues to be an major bottle neck in the field.

In order to amplify and characterize the *in-vivo* specific Aβ conformation in the brain, our project primarily focuses on developing an Aβ Conformation Seeding Assay (Aβ-CSA) using Aβ42 as a substrate. The first goal of the project was to enable conformational seeding of the brain aggregated-Aβ to the soluble Aβ42 substrate in the assay. The aggregation in the assay was monitored by thioflavin-t fluorescence kinetics. Later, the aggregates derived from the assay were characterized by negative staining TEM and Acoustic-SSA (Selective Shear Amplification) technique. Acoustic-SSA is a novel fragmentation technique that exploits the fibril mechanistic property to fragment and form seeds when selective sonication energy is applied.

5.1 Developments of Aβ-fibril amplification and seeding assays

Several *in-vitro* based seeding and fibril amplification assays have been reported in literature (Refer, Introduction, Section- 1.8). A study by Tycko and co-workers in the year 2005 first reported that both the morphology and molecular structure of Aβ40

fibrils are retained by self-propagation *in-vitro* when the fibrils are grown from their respective preformed seeds by adding them to the soluble Aβ40 substrate (Petkova et al. 2005). Aβ-fibrils are known to adopt multiple different fibril structures (Aβ polymorphism), the total number of fibril structures that Aβ can adopt has not yet been completely determined (Refer, Introduction, Section- 1.4). Hence, a seeding assay was developed by Paravastu et.al to determine the molecular structure of Aβ in the AD brain by seeding the soluble substrate Aβ40 with sonicated brain-extracted Aβ seeds (Roher & Kuo 1999) from the deceased AD patients. They subsequently obtained evidence that the fibrils seeded from the AD brain tissue from two AD patients have similar molecular structures (homogenous) but are different from the *de-novo* aggregated Aβ40 fibrils (heterogeneous) (Paravastu et al. 2009).

In a later investigation by Tycko and coworkers in the year 2013 they spiked soluble Aβ40 substrate with sonicated brain extracts from two deceased AD patients who had quite different clinical presentation. The result from this study indicated that fibrils grown from Aβ extracted from multiple brain regions of the same patient had identical structures whereas fibrils from the two patients varied markedly from each other and also differed from Aβ40 *de-novo* aggregated fibrils. This study indicated the first concrete evidence to presence of Aβ strains in AD patients (Lu et al. 2013). The fibril amplification assay developed by Tycko and co-workers however do have few limitations. Firstly, the fibril amplification protocol only utilized Aβ40 (not Aβ42) as the substrate peptide to capture the brain aggregated-Aβ fibril conformation. Furthermore, they have also acknowledged that their brain-seeded Aβ40 fibrils are most likely to be seeded from the Aβ40 fibrils (not Aβ42 fibrils) in the brain tissue of AD patients as polymorphic Aβ42 fibrils prepared *in-vitro* did not seed the growth of Aβ40 fibrils in their hands (Lu et al. 2013). Secondly, the denaturants and detergents used in the lengthy multistep amyloid extraction protocol to obtain pure Aβ fibrils from the AD brains can potentially select out an particular Aβ strain or the reagents used in extraction procedure can alter the seed structure and also potentially interfere with the Aβ substrate oligomerization in the amplification assay. Thirdly, it is well know that Aβ can adopt plethora of polymorphic conformations in the brain (different chain length and modifications), still after seeding the final Aβ40 fibril structure was found to

be more homogenous than the heterogeneous initial seed added in the amplification assay. This selective amplification of a particular fibril type could be due to arbitrary sonication performed on the brain extracted Aβ fibrils to generate seeds. Arbitrary sonication can lead in selective fragmentation or denaturation of the seed structure from polymorphic Aβ sample pool. Aβ40 polymorphic fibrils having significantly different rates of fragmentation in the presence of shear forces have been shown to favour growth of a particular type of Aβ40 fibril over the other in a study by same group (Qiang et al. 2013). Due to these limitations in the fibril amplification assay, the final brain Aβ seeded Aβ40 fibril structure cannot be trusted to faithfully represent the fibrillar heterogeneity found in AD brains.

Few seeding assays have partially addressed the limitations of fibril amplification assay. The kinetic aggregation assay developed by Jeffery Kelly and co-workers is one such assay. The kinetic aggregation assay is selective and sensitive method for quantifying Aβ fibrils in complex biological samples without having need to purify or extract the Aβ fibrils from the sample. However, this assay is also based on utilizing Aβ40 (not Aβ42) as the substrate peptide to capture the fibrillar seeds in the sample. The major limitation of this assay is that it does not claim structure amplification of *in-vivo* aggregated Aβ fibril but rather focuses more on quantification of amyloid load in the biological sample (Du et al. 2011).

Recently a new seeding assay, Aβ-PMCA (Protein Misfolding Cyclic Amplification) for detection and amplification of Aβ seeds was established by the Soto's lab, which originally developed the PMCA assay for prion amplification. It is the first seeding assay to utilize Aβ42 peptide as the substrate to detect oligomeric seeds from the CSF. Rather than applying sonication to multiply the seeds as used in the earlier protocols, Aβ-PMCA uses strong shaking (agitation) to fragment and improve the seeding in the assay. The major drawback of this assay is that it can only capture the Aβ oligomeric seeds from the CSF samples. The assay is incompatible to capture Aβ seeds from complex biological samples like brain homogenate tissues and hence no *in-vivo* AD specific Aβ seed structural amplification is possible (Salvadores et al. 2014).

We do not yet know whether there is a connection between variations in Aβ fibril structure and the development of AD, but this remains a promising and interesting hypothesis that we are pursuing. So in order to amplify and characterize the brain aggregated-Aβ conformation there persists a need for the development of a Aβ conformational seeding assay method that utilizes recombinant Aβ42 as the substrate combined with addition of whole brain homogenate as a seed without purifying the Aβ seeds.

5.2 Development of Aβ-Conformational Seeding Assay

Keeping in mind the needs and perspectives a seeding assay development was undertaken in our lab. The assay was developed using recombinant Aβ(1-42)M35L and Aβ(1-40)M35L as the substrate for initially detecting *de-novo* quiescently aggregated Aβ(1-42)M35L and Aβ(1-40)M35L fibrils as seeds in the assay. We initially concentrated on establishing an optimized method for detection of Aβ seed in the assay by assessing key parameters like substrate concentration, effect of Aβ substrate mixes, cross-seeding, seed detection limit, plate reading interval, buffer pH condition etc. that would influence either positive or negative effect to detect the *de-novo* aggregated Aβ seed added in the assay. Fibril seed detection by concentration and time dependent linearity was established for Aβ(1-42)M35L fibrils in the assay.

The substrate peptides that were used in the development of the assay are recombinant Aβ(1-40)M35L and Aβ(1-42)M35L, single mutants of the wild type Aβ that contains methionine instead of leucine at the 35th position. The M35L mutants were preferred as Aβ substrates in the assay as the wild-type Aβ42 peptide starts to aggregate within few seconds (Finder et al. 2010), making it difficult to maintain in a soluble state for seeding studies. Owing to the wild type peptide's higher aggregation propensity and difficulty in maintaining it in a monomeric state, single mutants Aβ(1-40)M35L and Aβ(1-42)M35L were preferred as substrates and were produced recombinantly in higher quantities and purity for the seeding in the assay. The Aβ

mutants (M35L) are known to aggregate slower compared the recombinant Aβ42 wild type peptide as the single mutation from methionine to leucine in 35th position greatly reduces the aggregation propensity of the peptide, which can be contributed to loss of methionine oxidation. Oxidation lowers the energy minima for peptide aggregation that results in increased aggregation propensity (Hou et al. 2004). Aβ M35L mutants are suitable for the assay as the Aβ(1-42)M35L fibril structural morphology, and its H/D-exchange pattern has been shown to be similar to that of Aβ(1–42) 35^{Mox} (Methionine Sulfoxide at 35th position) (Thorsten et al. 2005). The leucine amino acid substitution at the 35th position is known to occupy approximately the same molecular 3D space as compared to methionine in the Aβ-fibril packaging. Cysteine mutation studies have also indicated that, introduction of cysteine residues in the 35th methionine position did not abolish the hexamers and tetramer formation, that are known represent the right pathway intermediates of wild type Aβ42 oligomerization (Ngo & Guo 2011). Hence, the choice of Aβ(-42)M35L is suitable as an ideal read-out substrate peptide for capturing the brain aggregated- Aβ conformation in the assay.

The increase in fluorescence intensity in Aβ kinetic aggregation kinetics illustrates amyloid specific binding of thioflavin-t molecules to the β-sheets of Aβ(1-42)M35L and Aβ(1-40)M35L aggregates (Result, Fig.- 4.2 A&B). This result gives a clear indication, that thioflavin-t can be used a tracer-molecule in the assay to monitor the Aβ aggregation kinetics. There is substantial decrease in lagtimes (early lag-phase) of aggregation with the increase in Aβ substrate concentration and increase in lagtime (late lag-phase) of aggregation with the decrease in Aβ substrate concentration (Results, Fig.- 4.2C). The monomeric concentration dependent spontaneous Aβ aggregation data is very much in agreement with amyloid literature, where increase and decrease in amyloid monomeric concentration is known to influence the rate of Aβ peptide aggregation (Cohen et al. 2013). The Aβ substrate concentration in the assay was limited to 30μM, as higher substrate concentration would encourage spontaneous nucleation and lower substrate concentration would result in arbitrary nucleation among the replicates. As both the extremes can limit the seed resolutivity in the assay, the substrate concentration in the assay was maintained at 30μM.

Aβ is an amphipathic peptide with a theoretical pI of 5.31 and its aggregation kinetics is known to be pH dependent. Increase in pH of the aggregation buffer towards alkalinity results in impeded Aβ aggregation and pronounced increase in determined lagtimes. Decrease in pH nearing to pI, resulted in accelerated Aβ aggregation and decrease in lagtimes (Result, Fig. - 4.3B). This data is consistent with literature studies that have reported similar results of pH effect on Aβ aggregation have been reported (Burdick et al. 1992). Increase in thioflavin-t fluorescence intensity levels in the plateau phase is also observed with the increasing pH of Aβ aggregation (Results, Fig. – 4.3A, C&D). The fluorescence intensity changes can be attributed to the change in aggregate morphology, population of fibril structures and oligomeric aggregates formed because of changes in pH (Results, Fig.– 4.12, 4.13 and Table-4.1). From this experiment, it was decided to maintain the pH of the aggregation buffer at 8.1 as the lagphase was short and the pH condition did not influence change in Aβ fibril morphology.

In the Aβ ratios co-aggregation, seeding and cross-seeding assay, soluble Aβ(1-40)M35L and Aβ(1-42)M35L reciprocally delayed each other's spontaneous aggregation in a concentration dependent manner. It was also observed that the aggregation lagphase was arbitrary for the reactions where Aβ(1-40)M35L peptide was equal or more in ratio to the soluble Aβ(1-42)M35L peptide. The seeding activity of Aβ stoichiometric mixtures was found to be Aβ(1-42)M35L fibril seed dependent (Results, Fig.– 4.4A&B). The results of co-aggregation assay are consistent with literature data where Aβ40 is known to inhibit the fibrillation of Aβ42 peptide (Yan & Wang 2007; Jan et al. 2008; Pauwels et al. 2012). Aβ40 fibrils are known to seed soluble substrate Aβ40 (Petkova et al. 2005; Paravastu et al. 2009; Lu et al. 2013) and also Aβ42 substrate (Pauwels et al. 2012) in literature. However, in our assay, Aβ40 fibril seeding was trivial compared to the Aβ42 fibril seeding. This could be because we did not fragment the added Aβ(1-40)M35L fibrils by sonication or by mechanical agitation before adding them to the substrate Aβ in the assay (Results, Fig. – 4.7B). Aβ(1-42)M35L fibrils did not seed the soluble substrate Aβ(1-40)M35L in our hands (Results, Fig.- 4.4A). There are however contradictory seeding claims in

literature, where Aβ42 fibrils have been suggested to seed (Du et al. 2011) and also have been shown to not seed (Lu et al. 2013; Pauwels et al. 2012) the monomeric Aβ40 substrate. Hence utilizing Aβ(1-42)M35L as the substrate read-out peptide is meaningful as it can capture and amplify both the Aβ40 and Aβ42 fibril conformations in the assay.

An overall decrease in substrate spontaneous aggregation lagtime can be observed in this experiment (Result, Fig.- 4.4) compared to the earlier results (Result, Fig.- 4.3), this is because of the reduction in plate reading interval to 25 minutes compared to the earlier experiment with read interval of 40 minutes. The increased movement of the plate introduced due to frequency of reads has lead to a dual effect, primarily increasing the entropy of aggregation and secondarily generating mechanical forces that can fragment the aggregates to promote seeded nucleation in the assay. This is consistent with the results in literature where aggregation is promoted by agitation has been shown to decrease the aggregation lagtimes in Aβ (Cohen et al. 2013).

In conclusion, an *in-vitro* based aggregation and seeding assay was established for detecting *de-novo* aggregated Aβ(1-42)M35L fibrils with seed concentration dependent linearity. The assay was established with 30μM as the Aβ peptide substrate concentration and with aggregation buffer condition at pH 8.1. The assay could reproducibly resolute lagtime differences between spontaneous aggregation and logarithmically diluted *de-novo* Aβ(1-42)M35L seeded fibril from 5μM to 50pM (Results, Fig.- 4.4A). The next step was undertaken to detect and amplify the *in-vivo* aggregated-Aβ seed from the brain using the developed seeding assay.

5.3 Amplifying brain aggregated-Aβ in the assay

In a decade of research on Aβ conformations, it has been largely accepted by researchers that, Aβ material aggregated in the brain has a different conformation compared to the Aβ that aggregates *in-vitro* (Hatami et al. 2014; Aguzzi 2014; Cohen et al. 2015). Several studies have attempted to amplify the *in-vivo* brain aggregated-Aβ by developed seeding and conformational amplification assays (Paravastu et al.

2009; Du et al. 2011; Lu et al. 2013). So, far these assays have only succeeded in amplifying the Aβ40 conformations presented to them from the brain, as Aβ42 fibrils have been shown not seed the Aβ40 substrate (Lu et al. 2013), but Aβ40 fibrils have been shown to seed monomeric Aβ42 substrate (Pauwels et al. 2012). We have attempted to address these lacunas in our study by developing an Aβ-Conformational Seeding Assay (Aβ-CSA), that utilizes Aβ(1-42)M35L as the substrate peptide to amplify the brain aggregated-Aβ conformation.

Addition of brain aggregated-Aβ seed (as brain homogenate) in the assay resulted in considerable impediment in the aggregation lag phase and there was no observable seeding difference between the Aβ-laden APP/PS1(TG) brains and Aβ negative APP/PS1(WT) brains despite the high presence protease-inhibitor in the assay (Results, Fig.- 4.5). This is consistent with the data in literature, where addition of brain homogenate material is known to retard the Aβ aggregation in the assay (Du et al. 2011). Proteinase-K (PK) digestion of brain homogenate greatly reduced the impediment in Aβ aggregation induced by the brain homogenate, but still it could not aid in resoluting the seeding difference between the Aβ laden APP/PS1(TG) seed and the Aβ negative APP/PS1(WT) brain homogenate added reactions in the assay (Results, Fig.- 4.6). PK was however successful in mitigating the retardation effect of brain homogenate added as seed in the assay by reducing the overall aggregation lagtimes in the same regime ranges to that of spontaneous Aβ substrate aggregation (Results, Fig.- 4.6). PK and PI has been shown to distinguish between Aβ laden brains and controls in the Aβ40 kinetic aggregation assay developed by Jeffery Kelly's lab (Du et al. 2011). However, seeding did not occur in our developed seeding assay that utilized recombinant Aβ(1-42)M35L as the substrate.

The reason for the seeding failure of the Aβ-laden brain [APP/PS1(TG)] was deliberated and it was hypothesized that, the added brain aggregated-Aβ seed (brain homogenate) could be too negligible for seeding in the assay. At the same time, it has to be comprehended that spontaneous nucleation and formation of *de-novo* seeds is also concomitantly occurring in the substrate Aβ in the assay. Therefore, in a seeding assay, there is always competition between the spontaneous nucleation self-seeding and the introduced seed replication. In our case, due to the limited

availability of the brain aggregated-Aβ seed (0.1 % and 0.2% brain homogenate) added in the assay, the spontaneous *de-novo* seed formation becomes dominant when competing with the introduced brain aggregated Aβ-seeding in the assay. Therefore, the spontaneous aggregation process of the substrate could be suppressing the added brain aggregated Aβ-seed amplification in the assay.
A clever manipulation was introduced in the assay by modifying the *in-vitro* aggregation conditions to closely resemble the *in-vivo* brain milieu by introduction of phospholipids in the assay. It is known that Aβ aggregation in the brain environment occurs amidst the highest concentration of lipids. Phospholipid DHPC (1,2-dihexanoyl-*sn*-glycero-3-phosphocholine) as a lipid model system has been earlier used to study the amyloid aggregation processes in the case of Aβ40 and apoC-II (Apolipoprotein C-II) amyloid. DHPC is known to affect amyloid formation at micellar and sub-micellar concentrations playing a significant role in amyloid folding pathways *in-vivo* (Hatters et al. 2001; Dahse et al. 2010).

We decided to investigate the effect of phospholipid DHPC in our developed seeding assay. The spontaneous aggregation kinetics of Aβ(1-42)M35L in the presence of DHPC (Result, Fig.- 4.7) presents a similar trend in agreement to the aggregation behavior of Aβ(1-40) (Dahse et al. 2010). There are many papers in the literature that discuss the role of phospholipids in spontaneous Aβ aggregation, but none of them have investigated the influence of seeding activity in the presence of phospholipids. From our data, we can observe that, DHPC at 4mM overall delays both spontaneous and seeded aggregation in the assay. However, it impedes spontaneous Aβ aggregation relatively stronger than seeded aggregation. The overall increase in aggregation lagtimes accompanied by a preference to relatively impede the spontaneous aggregation has greatly boosted the seeding resolutivity in the assay at 4mM DHPC condition. Our data shows that DHPC at 4mM increases the seeding resolutivity upto 4 times compared to the standard spontaneous and seeded aggregation (Result, Fig.- 4.7B & C).

The rationale behind delay in amyloid aggregation can be hypothesized to be as follows: Phospholipid condition (in our case, DHPC at 4mM) delays spontaneous

primary nucleation by maintaining the Aβ in a non-β conformational state for a considerably long time indicated by an extended lagphase. Fibril nucleation is delayed due to slow formation of the seed in the mixed micellar condition (in our case, 4mM DHPC micelle condition) as compared to seed formation in the absence of lipid micelles (standard aggregation). Because of the number of peptides in the mixed micelles is smaller than the nucleus size or the seed size for fibril formation and due to the effect of micelles hindering the formation of homogenous seed within the mixed micelle condition the aggregation is substantially delayed. This hypothesis is so far the most accommodating hypothesis that we could obtain for our data from literature adapted from a simulation study of surfactants on amyloid aggregation kinetics (Friedman & Caflisch 2011).

Our study is the first study, to report a finding that, that in the presence of 4mM DHPC, the seeding resolutivity in a seeding system can be dramatically improved to detect and amplify low amounts of added seeds in the assay. The developed assay can reliably detect spiked seed upto 25pM both in the presence and absence of brain homogenate in the assay (Result, Fig.- 4.8). It is important to note here, that our assay was able to detect non-sonicated fibrillar seeds. The seed detection limit can be further improved by fragmenting the fibrillar seeds by sonication as done in the kinetic seeding assay (Du et al. 2011).

The increase in seeding resolutivity has enabled detection and amplification of brain aggregated-Aβ from the APP/PS1(TG) brain homogenate in the assay (Results, Fig.- 4.9 & 4.10). The APP/PS1(TG) seeded reactions display higher fluorescence intensity compared to the non-Aβ containing APP/PS1(WT) and BL6 controls. The seed detection and amplification in the assay was further improved by introducing a number of measures that reduced the time delay between the digestion of the brain homogenate and production of the recombinant soluble Aβ(1-42)M35L substrate (Result, Fig.- 4.11). The brain homogenate seeding experiment was repeated more than 6-7 times and in all the assays, the brain- aggregated-Aβ seeded reactions displayed earlier lagtime kinetics along with higher fluorescence compared to the non-Aβ seeded brain homogenates. The reason for this increase in relative fluorescence has not yet been completely understood and whether this increased

fluorescence corresponds to peculiarity of an Aβ conformation type is not known. However, higher intensity fluorescence from brain seeded samples have also been observed earlier in Aβ fibril amplification assays developed by Tycko's lab (Paravastu et al. 2009; Lu et al. 2013). The Aβ40 seed dominant APP23 transgenic mice brain homogenate did not seed the Aβ(1-42)M35L substrate in our assay (Fig.- 4.9D & 4.10B), that agrees with our earlier data, where Aβ40 fibrils poorly seeded the Aβ42 monomer in the assay (Results, Fig.- 4.4B).

In conclusion, the developed Aβ conformational seeding assay (Aβ-CSA) could detecting and amplify the *in-vivo* brain aggregated-Aβ from the 10% brain homogenate added in the assay. The unique feature of our assay as compared to other amplification assay is that, this assay can seed the native brain aggregated -Aβ directly from the brain homogenate, without having to extract or purify the aggregated Aβ from the brain. This was possible because, we were able to strike an appropriate balance between two competing aggregation processes in the assay (i) Spontaneous primary nucleation- seeding (ii) sensitized detection of added seed by increasing the seeding resolutivity in the system.

5.4 Brain homogenate seeded Aβ morphologies and its fragmentability

TEM micrographs of APP/PS1(TG) brain seeded sample showed distinct morphological differences when compared to APP/PS1(WT) and BL6 seeded reactions in the assay (Results, Fig.- 4.14, 4.15 and Table- 4.2). These differences distinctly point out the difference in morphology that arises from the conformational amplification of the brain aggregated-Aβ seeds from the APP/PS1(TG) brain homogenate added to the assay. The APP/PS1(WT) and BL6 seeded aggregates displayed similar fibrillar and oligomeric morphologies compared to APP/PS1(TG) seeded aggregates. The fibrillar heterogeneity was higher in non-Aβ brain homogenate seeded reactions compared to the distinct structures observed in APP/PS1(TG) seeded aggregates. Fibrillar Aβ was seldom found in the APP/PS1(TG) seeded reactions in sharp contrast to higher fibrillar content in

APP/PS1(WT) and BL6. In the APP/PS1 (TG) seeded samples large prefibrillar oligomeric structures were observed (~100-300nm) in large populations and fibrils found were thin and fragile appearance. These distinctive prefibrillar oligomeric structures were absent in the non-Aβ brain homogenate seeded reactions. Our seeding assay is the first one, where we have been able to show morphological differences between the brain aggregated-Aβ seeded material and non-Aβ brain seeded material utilizing Aβ42 as the substrate peptide. In the literature there are studies which shows difference in fibril structure and morphology but they are limited with respect to Aβ40 peptide as the substrate in the assays (Paravastu et al. 2009; Lu et al. 2013).

Fragmentation of amyloid fibrils by sonication energy to generate seeds is widely used technique in amyloid seeding and aggregation studies (Yamaguchi et al. 2005; Chatani et al. 2009). Fragmentation of Aβ40 fibrils by ultrasonication to produce seeds have been used extensively in literature albeit, the sonication based fragmentation technique has been poorly characterized or quantified in detail to understand effect of sonication induced fragmentation on Aβ fibrils due to current limitations in biophysical methods. This limitation was overcome in our lab by constructing a special ultrasonication device Acoustic-SSA (Selective Shear Amplification) specially focusing on prion amplification. The method is very well established for prion amplification and explained in detail in PhD thesis of Dr. Felix.

As a proof of the concept study, fragmentation of fibril by Acoustic-SSA was performed on aged *de-novo* Aβ(1-42)M35L fibrils that poorly seeded in the assay, but seeded robustly after fragmentation (Results, Fig.- 4.16 and 4.17). Using Acoustic-SSA coupled with the developed seeding assay, the optimal shear force to fragment the *de-novo* Aβ(1-42)M35L fibril into homogenous seeds was determined at 1.5mm of height in the Acoustic-SSA device. Acoustic-SSA method was able to generate seeds from non-Aβ brain homogenate seeded fibrils but not from the APP/PS(TG) brain aggregated-Aβ seeded reactions (Results, Fig.– 4.18). Increasing and the decreasing the processing times along with varying the intensity of shear force by adjusting the heights still did not result in seeding of the APP/PS1(TG) seeded

aggregates. Whereas the APP/PS1(WT) and BL6 seeded samples fragmented and seeded in the assay (Result, Fig.- 4.18). This result is the first indication that suggests amplification of a different Aβ conformation when seeded from brain aggregated-Aβ seed. This is in agreement with results shown by Tycko and co-workers in Aβ40 polymorphic fibrils, where two fibrils grown in different conditions were found to have different rates of fragmentation in the presence of shear forces applied to them (Qiang et al. 2013).

In summary, our experimentally developed conformational seeding assay can be used to detect and amplify brain aggregated-Aβ. Our study clearly indicates that the *in-vivo* brain aggregated-Aβ conformations in transgenic mice brains are different as compared to the *de-novo* spontaneous aggregated Aβ. Our indications are in agreement to a result where brain tissue from APP mice show the presence of different fibril structures in different plaque types when stained with luminescent conjugated polymers (Nilsson et al. 2007).

5.5 Future Perspectives

Aβ42 conformations and its structure elucidation continues to be a major bottleneck in the AD field. Many studies have only focused on the Aβ40 peptide aggregation and seeding, whereas it is clearly known that Aβ42 is the major culprit and amyloidogenic compared to Aβ40 (Bitan et al. 2003). Hence, there is an acute requirement to develop an assay that can amplify the brain aggregated-Aβ conformations of both the Aβ42 and Aβ40 variants. The Aβ42 fibril has been shown in several studies to not seed the Aβ40 monomer, whereas the Aβ40 fibril has been shown to seed the Aβ42 monomer (Pauwels et al. 2012; Kuperstein et al. 2010).

Our study, presents the first seeding and aggregation assay that detects brain aggregated-Aβ from AD transgenic mice using recombinant Aβ(1-42) as the substrate. Our method does not employ any amyloid extraction and purification protocols to isolate Aβ fibrils or oligomers from the brain cellular tissue. Using amyloid extraction protocol to isolate Aβ from the brains has lead to criticism,

where detergents and denaturants used in the protocol has been insinuated to affect, alter or select out an *in-vivo* aggregated Aβ conformation. Our assay shall enable researchers to detect and amplify brain aggregated-Aβ. There still exists a scope for improvement in the assay, where the brain-Aβ conformation could be serially propagated by many generations to dilute out the original added seed and perform structural studies by isotope labeling the substrate. But this step requires further intricate understanding of Aβ aggregation and nucleation processes and optimization of Aβ fibril fragmentation method to serially propagate over generations.

With this developed Aβ-conformational seeding assay, a basic platform has been created that can allow researchers to amplify the brain aggregated-Aβ conformations. There is a growing body of evidence that suggests Aβ curls into distinct Aβ strains that can propagate through the brain by templated protein misfolding (Stöhr et al. 2014; Watts et al. 2014). Recently, a new study has linked rapid clinical decline in AD to Aβ42 structural conformations that may play a role in pathogenesis of distinct AD phenotypes (Cohen et al. 2015). Since a decade, there has been a growing body of evidence indicating family of prion-like proteins involved in neurodegenerative diseases including AD (Jucker & Walker 2013; Morales et al. 2015). Applying our developed, Aβ conformational seeding assay framework from this study can immensely help in understanding the Aβ structure to its pathogenic progression in Alzheimer's disease.

6 References and Bibliography

Abelein, A. et al., 2014. The hairpin conformation of the amyloid β peptide is an important structural motif along the aggregation pathway. *Journal of biological inorganic chemistry : JBIC : a publication of the Society of Biological Inorganic Chemistry*. Available at: http://www.ncbi.nlm.nih.gov/pubmed/24737040 [Accessed April 29, 2014].

Agopian, A. & Guo, Z., 2012. Structural origin of polymorphism for Alzheimers amyloid beta fibrils. *The Biochemical journal*, 447(1), pp.43–50. Available at: http://www.ncbi.nlm.nih.gov/pubmed/22823461 [Accessed April 28, 2013].

Aguzzi, A., 2014. Neurodegeneration: Alzheimer's disease under strain. *Nature*, 512(7512), pp.32–4. Available at: http://www.ncbi.nlm.nih.gov/pubmed/25100477 [Accessed October 14, 2014].

Ahmed, M. et al., 2010. Structural conversion of neurotoxic amyloid-beta(1-42) oligomers to fibrils. *Nat Struct Mol Biol*, 17(5), pp.561–567. Available at: http://www.pubmedcentral.nih.gov/articlerender.fcgi?artid=2922021&tool=pmcentrez&rendertype=abstract [Accessed March 19, 2012].

Arce, F.T. et al., 2011. Polymorphism of amyloid β peptide in different environments: implications for membrane insertion and pore formation. *Soft matter*, 7(11), pp.5267–5273. Available at: http://www.pubmedcentral.nih.gov/articlerender.fcgi?artid=3170770&tool=pmcentrez&rendertype=abstract [Accessed May 25, 2014].

Arnold, K. et al., 2006. The SWISS-MODEL workspace: a web-based environment for protein structure homology modelling. *Bioinformatics (Oxford, England)*, 22(2), pp.195–201. Available at: http://www.ncbi.nlm.nih.gov/pubmed/16301204 [Accessed July 13, 2012].

Arosio, P. et al., 2014. Quantification of the concentration of Aβ42 propagons during the lag phase by an amyloid chain reaction assay. *Journal of the American Chemical Society*, 136(1), pp.219–25. Available at: http://www.ncbi.nlm.nih.gov/pubmed/24313551 [Accessed April 10, 2014].

Atarashi, R. et al., 2011. Real-time quaking-induced conversion: a highly sensitive assay for prion detection. *Prion*, 5(3), pp.150–3. Available at: http://www.pubmedcentral.nih.gov/articlerender.fcgi?artid=3226039&tool=pmcentrez&rendertype=abstract [Accessed July 23, 2012].

Auer, S. & Kashchiev, D., 2010. Insight into the correlation between lag time and aggregation rate in the kinetics of protein aggregation. *Proteins*, 78(11), pp.2412–6. Available at: http://www.ncbi.nlm.nih.gov/pubmed/20602358 [Accessed March 20, 2014].

Baker, H.F. et al., 1993. Experimental induction of beta-amyloid plaques and cerebral angiopathy in primates. *Annals of the New York Academy of Sciences*, 695, pp.228–31. Available at: http://www.ncbi.nlm.nih.gov/pubmed/8239287.

Baker, H.F. et al., 1994. Induction of beta (A4)-amyloid in primates by injection of Alzheimer's disease brain homogenate. Comparison with transmission of spongiform encephalopathy. *Molecular neurobiology*, 8(1), pp.25–39. Available at: http://www.ncbi.nlm.nih.gov/pubmed/8086126 [Accessed July 18, 2012].

Balbach, J.J. et al., 2002. Supramolecular structure in full-length Alzheimer's beta-amyloid fibrils: evidence for a parallel beta-sheet organization from solid-state nuclear magnetic resonance. *Biophysical journal*, 83(2), pp.1205–16. Available at: http://www.pubmedcentral.nih.gov/articlerender.fcgi?artid=1302222&tool=pmcentrez&rendertype=abstract [Accessed April 3, 2012].

Benilova, I., Karran, E. & De Strooper, B., 2012. The toxic Aβ oligomer and Alzheimer's disease: an emperor in need of clothes. *Nature neuroscience*, 15(3), pp.349–57. Available at: http://www.ncbi.nlm.nih.gov/pubmed/22286176 [Accessed March 9, 2012].

Bertini, I. et al., 2011. A new structural model of Aβ40 fibrils. *Journal of the American Chemical Society*, 133(40), pp.16013–22. Available at: http://dx.doi.org/10.1021/ja2035859 [Accessed May 10, 2014].

Bitan, G. et al., 2003. Amyloid β-protein (A β) assembly : A β 40 and A β 42 oligomerize through distinct pathways. *PNAS*, 100(1), pp.330–335.

Brookmeyer, R. et al., 2007. Forecasting the global burden of Alzheimer's disease. *Alzheimers Dement*, 3(3), pp.186–191. Available at: http://www.ncbi.nlm.nih.gov/pubmed/19595937.

Brown, P. et al., 1982. Alzheimer's disease and transmissible virus dementia (Creutzfeldt-Jakob disease). *Annals of the New York Academy of Sciences*, 396, pp.131–43. Available at: http://www.ncbi.nlm.nih.gov/pubmed/6758661 [Accessed September 16, 2012].

Buchhave, P. et al., 2012. Cerebrospinal fluid levels of β-amyloid 1-42, but not of tau, are fully changed already 5 to 10 years before the onset of Alzheimer dementia. *Archives of general psychiatry*, 69(1), pp.98–106. Available at: http://www.ncbi.nlm.nih.gov/pubmed/22213792.

Burdick, D. et al., 1992. Assembly and aggregation properties of synthetic Alzheimer's A4/beta amyloid peptide analogs. *The Journal of biological chemistry*, 267(1), pp.546–54. Available at: http://www.ncbi.nlm.nih.gov/pubmed/1730616 [Accessed July 17, 2012].

Chatani, E. et al., 2009. Ultrasonication-dependent production and breakdown lead to minimum-sized amyloid fibrils. *Proceedings of the National Academy of Sciences of the United States of America*, 106(27), pp.11119–24. Available at:

http://www.pubmedcentral.nih.gov/articlerender.fcgi?artid=2708754&tool=pmcentrez&rendertype=abstract.

Chiti, F. et al., 2003. Rationalization of the effects of mutations on peptide and protein aggregation rates. *Nature*, 424(6950), pp.805–8. Available at: http://www.ncbi.nlm.nih.gov/pubmed/12917692 [Accessed July 20, 2012].

Choi, S.H. et al., 2014. A three-dimensional human neural cell culture model of Alzheimer's disease. *Nature*. Available at: http://www.nature.com/doifinder/10.1038/nature13800 [Accessed October 12, 2014].

Cohen, M.B., 1995. Robbins' pathologic basis of disease,5th Edition Authors: Ramzi S. Cotran, Vinay Kumar, and Stanley L. Robbins W.B. Saunders, Philadelphia, 1994. *Diagnostic Cytopathology*, 12(4), pp.377–377. Available at: http://doi.wiley.com/10.1002/dc.2840120422 [Accessed September 16, 2012].

Cohen, M.L. et al., 2015. Rapidly progressive Alzheimer's disease features distinct structures of amyloid-. *Brain*. Available at: http://www.brain.oxfordjournals.org/cgi/doi/10.1093/brain/awv006.

Cohen, S.I. a, Vendruscolo, M., Welland, M.E., et al., 2011. Nucleated polymerization with secondary pathways. I. Time evolution of the principal moments. *The Journal of chemical physics*, 135(6), p.065105. Available at: http://www.ncbi.nlm.nih.gov/pubmed/21842954 [Accessed March 2, 2012].

Cohen, S.I. a, Vendruscolo, M., Dobson, C.M., et al., 2011. Nucleated polymerization with secondary pathways. II. Determination of self-consistent solutions to growth processes described by non-linear master equations. *The Journal of chemical physics*, 135(6), p.065106. Available at: http://www.ncbi.nlm.nih.gov/pubmed/21842955 [Accessed March 27, 2012].

Cohen, S.I.A. et al., 2013. Proliferation of amyloid-β42 aggregates occurs through a secondary nucleation mechanism. *Proceedings of the National Academy of Sciences of the United States of America*, 110(24), pp.9758–63. Available at: http://www.pubmedcentral.nih.gov/articlerender.fcgi?artid=3683769&tool=pmcentrez&rendertype=abstract [Accessed April 7, 2014].

Colby, D.W. et al., 2007. Prion detection by an amyloid seeding assay. *Proceedings of the National Academy of Sciences of the United States of America*, 104(52), pp.20914–9. Available at: http://www.pubmedcentral.nih.gov/articlerender.fcgi?artid=2409241&tool=pmcentrez&rendertype=abstract.

Colletier, J. et al., 2011. Molecular basis for amyloid-β polymorphism.

Cushman, M. et al., 2010. Prion-like disorders: blurring the divide between transmissibility and infectivity. *Journal of cell science*, 123(Pt 8), pp.1191–201. Available at: http://www.pubmedcentral.nih.gov/articlerender.fcgi?artid=2848109&tool=pmcen

trez&rendertype=abstract [Accessed July 22, 2012].

Dahse, K. et al., 2010. DHPC strongly affects the structure and oligomerization propensity of Alzheimer's Abeta(1-40) peptide. *J Mol Biol*, 403(4), pp.643–659. Available at: http://www.ncbi.nlm.nih.gov/pubmed/20851128.

Döbeli, H. et al., 1995. A biotechnological method provides access to aggregation competent monomeric Alzheimer's 1-42 residue amyloid peptide. *Bio/technology (Nature Publishing Company)*, 13(9), pp.988–93. Available at: http://www.ncbi.nlm.nih.gov/pubmed/9636276 [Accessed October 11, 2012].

Du, D. et al., 2011. A kinetic aggregation assay allowing selective and sensitive amyloid-beta quantification in cells and tissues. *Biochemistry*, 50(10), pp.1607–1617. Available at: http://www.ncbi.nlm.nih.gov/pubmed/21268584.

DuBay, K.F. et al., 2004. Prediction of the absolute aggregation rates of amyloidogenic polypeptide chains. *Journal of molecular biology*, 341(5), pp.1317–26. Available at: http://www.ncbi.nlm.nih.gov/pubmed/15302561 [Accessed July 24, 2012].

Eanes, E.D. & Glenner, G.G., 1968. X-ray diffraction studies on amyloid filaments. *The journal of histochemistry and cytochemistry : official journal of the Histochemistry Society*, 16(11), pp.673–7. Available at: http://www.ncbi.nlm.nih.gov/pubmed/5723775 [Accessed September 1, 2012].

Eisele, Y.S. et al., 2009. Induction of cerebral beta-amyloidosis: intracerebral versus systemic Abeta inoculation. *Proceedings of the National Academy of Sciences of the United States of America*, 106(31), pp.12926–31. Available at: http://www.pubmedcentral.nih.gov/articlerender.fcgi?artid=2722323&tool=pmcentrez&rendertype=abstract.

Eisele, Y.S. et al., 2010. Peripherally applied Abeta-containing inoculates induce cerebral beta-amyloidosis. *Science (New York, N.Y.)*, 330(6006), pp.980–2. Available at: http://www.pubmedcentral.nih.gov/articlerender.fcgi?artid=3233904&tool=pmcentrez&rendertype=abstract [Accessed March 10, 2012].

Eisenberg, D. & Jucker, M., 2012. The amyloid state of proteins in human diseases. *Cell*, 148(6), pp.1188–203. Available at: http://www.ncbi.nlm.nih.gov/pubmed/22424229 [Accessed July 19, 2012].

Esch, F.S. et al., 1990. Cleavage of amyloid beta peptide during constitutive processing of its precursor. *Science (New York, N.Y.)*, 248(4959), pp.1122–4. Available at: http://www.ncbi.nlm.nih.gov/pubmed/2111583 [Accessed September 11, 2012].

Finder, V.H. et al., 2010. The recombinant amyloid-beta peptide Abeta1-42 aggregates faster and is more neurotoxic than synthetic Abeta1-42. *Journal of molecular biology*, 396(1), pp.9–18. Available at:

http://www.ncbi.nlm.nih.gov/pubmed/20026079 [Accessed March 14, 2012].

Finder, V.H. & Glockshuber, R., 2007. Amyloid-beta aggregation. *Neuro-degenerative diseases*, 4(1), pp.13–27. Available at: http://www.ncbi.nlm.nih.gov/pubmed/17429215 [Accessed March 5, 2012].

Forny-Germano, L. et al., 2014. Alzheimer's Disease-Like Pathology Induced by Amyloid-β Oligomers in Nonhuman Primates. *The Journal of neuroscience : the official journal of the Society for Neuroscience*, 34(41), pp.13629–43. Available at: http://www.jneurosci.org/cgi/doi/10.1523/JNEUROSCI.1353-14.2014 [Accessed October 12, 2014].

Fraser, P.E. et al., 1991. pH-dependent structural transitions of Alzheimer amyloid peptides. *Biophysical journal*, 60(5), pp.1190–201. Available at: http://www.pubmedcentral.nih.gov/articlerender.fcgi?artid=1260174&tool=pmcentrez&rendertype=abstract [Accessed October 21, 2013].

Friedman, R. & Caflisch, A., 2011. Surfactant effects on amyloid aggregation kinetics. *Journal of molecular biology*, 414(2), pp.303–12. Available at: http://www.ncbi.nlm.nih.gov/pubmed/22019473 [Accessed June 19, 2013].

Fritschi, S.K. et al., 2014. Highly potent soluble amyloid-β seeds in human Alzheimer brain but not cerebrospinal fluid. *Brain : a journal of neurology*, pp.1–7. Available at: http://www.ncbi.nlm.nih.gov/pubmed/25212850 [Accessed September 16, 2014].

Glabe, C.G., 2006. Common mechanisms of amyloid oligomer pathogenesis in degenerative disease. *Neurobiology of aging*, 27(4), pp.570–5. Available at: http://www.ncbi.nlm.nih.gov/pubmed/16481071 [Accessed May 28, 2013].

Glenner, G.G. & Bladen, H.A., 1966. Purification and reconstitution of the periodic fibril and unit structure of human amyloid. *Science (New York, N.Y.)*, 154(3746), pp.271–2. Available at: http://www.ncbi.nlm.nih.gov/pubmed/5914761 [Accessed September 1, 2012].

Glenner, G.G. & Wong, C.W., 1984. Alzheimer's disease and Down's syndrome: sharing of a unique cerebrovascular amyloid fibril protein. *Biochemical and biophysical research communications*, 122(3), pp.1131–5. Available at: http://www.ncbi.nlm.nih.gov/pubmed/6236805 [Accessed September 1, 2012].

Glenner, G.G. & Wong, C.W., 1984. Alzheimer's disease: Initial report of the purification and characterization of a novel cerebrovascular amyloid protein. *Biochemical and Biophysical Research Communications*, 120(3), pp.885–890. Available at: http://dx.doi.org/10.1016/S0006-291X(84)80190-4 [Accessed July 13, 2012].

Godec, M.S. et al., 1991. Evidence against the transmissibility of Alzheimer's disease. *Neurology*, 41(8), p.1320. Available at: http://www.ncbi.nlm.nih.gov/pubmed/1866028 [Accessed May 23, 2014].

Goldgaber, D. et al., 1987. Characterization and chromosomal localization of a cDNA encoding brain amyloid of Alzheimer's disease. *Science (New York, N.Y.)*, 235(4791), pp.877–80. Available at: http://www.ncbi.nlm.nih.gov/pubmed/3810169 [Accessed September 11, 2012].

Goldsbury, C. et al., 2005. Multiple assembly pathways underlie amyloid-beta fibril polymorphisms. *Journal of molecular biology*, 352(2), pp.282–98. Available at: http://www.ncbi.nlm.nih.gov/pubmed/16095615 [Accessed July 30, 2012].

Goudsmit, J. et al., 1980. Evidence for and against the transmissibility of Alzheimer disease. *Neurology*, 30(9), pp.945–50. Available at: http://www.ncbi.nlm.nih.gov/pubmed/6775247 [Accessed May 23, 2014].

Goudsmit, J., 1982. Transmissibility of Alzheimer's disease. *The American journal of psychiatry*, 139(10), pp.1380–1. Available at: http://www.ncbi.nlm.nih.gov/pubmed/6751101 [Accessed September 16, 2012].

Hamaguchi, T. et al., 2012. The presence of Aβ seeds, and not age per se, is critical to the initiation of Aβ deposition in the brain. *Acta neuropathologica*, 123(1), pp.31–7. Available at: http://www.pubmedcentral.nih.gov/articlerender.fcgi?artid=3297471&tool=pmcentrez&rendertype=abstract [Accessed April 2, 2012].

Hardy, J., 2006. Alzheimer's disease: the amyloid cascade hypothesis: an update and reappraisal. *J Alzheimers Dis*, 9(3 Suppl), pp.151–153. Available at: http://www.ncbi.nlm.nih.gov/pubmed/16914853.

Hardy, J. & Higgins, G., 1992. Alzheimer's disease: the amyloid cascade hypothesis. *Science*, 256(5054), pp.184–185. Available at: http://www.sciencemag.org/cgi/doi/10.1126/science.1566067 [Accessed July 17, 2012].

Hardy, J. & Selkoe, D.J., 2002. The amyloid hypothesis of Alzheimer's disease: progress and problems on the road to therapeutics. *Science (New York, N.Y.)*, 297(5580), pp.353–6. Available at: http://www.ncbi.nlm.nih.gov/pubmed/12130773 [Accessed February 29, 2012].

Hardy, J.A. et al., 1986. An integrative hypothesis concerning the pathogenesis and progression of Alzheimer's disease. *Neurobiology of aging*, 7(6), pp.489–502. Available at: http://www.ncbi.nlm.nih.gov/pubmed/2882432 [Accessed September 10, 2012].

Harper, J.D. & Lansbury, P.T., 1997. Models of amyloid seeding in Alzheimer's disease and scrapie: mechanistic truths and physiological consequences of the time-dependent solubility of amyloid proteins. *Annual review of biochemistry*, 66, pp.385–407. Available at: http://www.ncbi.nlm.nih.gov/pubmed/9242912 [Accessed July 13, 2012].

Hatami, A. et al., 2014. Monoclonal Antibodies Against Aβ42 Fibrils Distinguish Multiple Aggregation State Polymorphisms in vitro and in Alzheimer's Disease

Brain. *The Journal of biological chemistry*. Available at: http://www.ncbi.nlm.nih.gov/pubmed/25281743 [Accessed October 6, 2014].

Hatters, D.M., Lawrence, L.J. & Howlett, G.J., 2001. Sub-micellar phospholipid accelerates amyloid formation by apolipoprotein C-II. *FEBS letters*, 494(3), pp.220–4. Available at: http://www.ncbi.nlm.nih.gov/pubmed/11311244.

Heilbronner, G. et al., 2013. Seeded strain-like transmission of β-amyloid morphotypes in APP transgenic mice. *EMBO reports*, (August). Available at: http://www.ncbi.nlm.nih.gov/pubmed/23999102 [Accessed September 23, 2013].

Hong-Qi, Y., Zhi-Kun, S. & Sheng-Di, C., 2012. Current advances in the treatment of Alzheimer's disease: focused on considerations targeting Aβ and tau. *Translational neurodegeneration*, 1(1), p.21. Available at: http://www.pubmedcentral.nih.gov/articlerender.fcgi?artid=3514124&tool=pmcentrez&rendertype=abstract [Accessed April 28, 2014].

Hou, L. et al., 2004. Solution NMR studies of the A beta(1-40) and A beta(1-42) peptides establish that the Met35 oxidation state affects the mechanism of amyloid formation. *Journal of the American Chemical Society*, 126(7), pp.1992–2005. Available at: http://www.ncbi.nlm.nih.gov/pubmed/14971932 [Accessed June 20, 2013].

Irie, K. et al., 2005. Structure of beta-amyloid fibrils and its relevance to their neurotoxicity: implications for the pathogenesis of Alzheimer's disease. *Journal of bioscience and bioengineering*, 99(5), pp.437–47. Available at: http://www.ncbi.nlm.nih.gov/pubmed/16233815 [Accessed March 20, 2014].

Jan, A. et al., 2008. The ratio of monomeric to aggregated forms of Abeta40 and Abeta42 is an important determinant of amyloid-beta aggregation, fibrillogenesis, and toxicity. *J Biol Chem*, 283(42), pp.28176–28189. Available at: http://www.ncbi.nlm.nih.gov/pubmed/18694930.

Jarrett, J.T. & Lansbury, P.T., 1993. Seeding "one-dimensional crystallization" of amyloid: a pathogenic mechanism in Alzheimer's disease and scrapie? *Cell*, 73(6), pp.1055–8. Available at: http://www.ncbi.nlm.nih.gov/pubmed/8513491 [Accessed June 4, 2014].

Jeong, J.S. et al., 2013. Novel Mechanistic Insight into the Molecular Basis of Amyloid Polymorphism and Secondary Nucleation during Amyloid Formation. *Journal of Molecular Biology*, 425(10), pp.1765–1781. Available at: http://dx.doi.org/10.1016/j.jmb.2013.02.005.

Jucker, M. & Walker, L.C., 2013. Self-propagation of pathogenic protein aggregates in neurodegenerative diseases. *Nature*, 501(7465), pp.45–51. Available at: http://www.ncbi.nlm.nih.gov/pubmed/24005412 [Accessed September 19, 2013].

Kane, M.D. et al., 2000. Evidence for seeding of beta -amyloid by intracerebral infusion of Alzheimer brain extracts in beta -amyloid precursor protein-transgenic mice. *The Journal of neuroscience : the official journal of the Society for*

Neuroscience, 20(10), pp.3606–11. Available at: http://www.ncbi.nlm.nih.gov/pubmed/10804202.

Karran, E., Mercken, M. & De Strooper, B., 2011. The amyloid cascade hypothesis for Alzheimer's disease: an appraisal for the development of therapeutics. *Nat Rev Drug Discov*, 10(9), pp.698–712. Available at: http://www.ncbi.nlm.nih.gov/pubmed/21852788.

Kayed, R. et al., 2010. Conformation dependent monoclonal antibodies distinguish different replicating strains or conformers of prefibrillar Abeta oligomers. *Mol Neurodegener*, 5, p.57. Available at: http://www.ncbi.nlm.nih.gov/pubmed/21144050.

Kirschner, D.A., Abraham, C. & Selkoe, D.J., 1986. X-ray diffraction from intraneuronal paired helical filaments and extraneuronal amyloid fibers in Alzheimer disease indicates cross-beta conformation. *Proceedings of the National Academy of Sciences of the United States of America*, 83(2), pp.503–7. Available at: http://www.pubmedcentral.nih.gov/articlerender.fcgi?artid=322888&tool=pmcentrez&rendertype=abstract [Accessed September 10, 2012].

Klein, A.M., Kowall, N.W. & Ferrante, R.J., 1999. Neurotoxicity and oxidative damage of beta amyloid 1-42 versus beta amyloid 1-40 in the mouse cerebral cortex. *Annals of the New York Academy of Sciences*, 893, pp.314–20. Available at: http://www.ncbi.nlm.nih.gov/pubmed/10672257 [Accessed June 12, 2014].

Knowles, T.P.J. et al., 2009. An analytical solution to the kinetics of breakable filament assembly. *Science (New York, N.Y.)*, 326(5959), pp.1533–7. Available at: http://www.ncbi.nlm.nih.gov/pubmed/20007899 [Accessed April 30, 2014].

Kodali, R. et al., 2010. Abeta(1-40) forms five distinct amyloid structures whose beta-sheet contents and fibril stabilities are correlated. *Journal of molecular biology*, 401(3), pp.503–17. Available at: http://www.pubmedcentral.nih.gov/articlerender.fcgi?artid=2919579&tool=pmcentrez&rendertype=abstract [Accessed March 1, 2012].

Kuperstein, I. et al., 2010. Neurotoxicity of Alzheimer's disease Aβ peptides is induced by small changes in the Aβ42 to Aβ40 ratio. *The EMBO journal*, 29(19), pp.3408–20. Available at: http://www.pubmedcentral.nih.gov/articlerender.fcgi?artid=2957213&tool=pmcentrez&rendertype=abstract [Accessed March 1, 2012].

Langer, F. et al., 2011. Soluble A{beta} Seeds Are Potent Inducers of Cerebral {beta}-Amyloid Deposition. *J Neurosci*, 31(41), pp.14488–14495. Available at: http://www.ncbi.nlm.nih.gov/pubmed/21994365.

Lee, J. et al., 2011. Amyloid-β forms fibrils by nucleated conformational conversion of oligomers. *Nature chemical biology*, 7(9), pp.602–9. Available at: http://www.pubmedcentral.nih.gov/articlerender.fcgi?artid=3158298&tool=pmcen

trez&rendertype=abstract [Accessed June 4, 2014].

Lesné, S. et al., 2006. A specific amyloid-beta protein assembly in the brain impairs memory. *Nature*, 440(7082), pp.352–357. Available at: http://www.ncbi.nlm.nih.gov/pubmed/16541076 [Accessed March 4, 2012].

LeVine, H., 1999. Quantification of beta-sheet amyloid fibril structures with thioflavin T. *Methods in enzymology*, 309, pp.274–84. Available at: http://www.ncbi.nlm.nih.gov/pubmed/10507030 [Accessed July 13, 2012].

LeVine, H., 1993. Thioflavine T interaction with synthetic Alzheimer's disease beta-amyloid peptides: detection of amyloid aggregation in solution. *Protein science : a publication of the Protein Society*, 2(3), pp.404–10. Available at: http://www.pubmedcentral.nih.gov/articlerender.fcgi?artid=2142377&tool=pmcentrez&rendertype=abstract [Accessed July 20, 2012].

Levine, H., Walker, L.C. & Levine 3rd, H., 2010. Molecular polymorphism of Abeta in Alzheimer's disease. *Neurobiol Aging*, 31(4), pp.542–548. Available at: http://www.ncbi.nlm.nih.gov/pubmed/18619711 [Accessed April 18, 2012].

Lim, K.H., 2013. Molecular Basis of Amyloid Polymorphism : Multiple Misfolding Pathways. *Physical Chemistry & Biophysics*, 3(2), pp.2–3.

Lomakintt, A. et al., 1996. On the nucleation and growth of amyloid beta -protein fibrils: Detection of nuclei and quantitation of rate constants. *Proceedings of the National Academy of Sciences*, 93(3), pp.1125–1129. Available at: http://www.pnas.org/content/93/3/1125.abstract [Accessed October 28, 2012].

Lu, J.-X. et al., 2013. Molecular structure of β-amyloid fibrils in Alzheimer's disease brain tissue. *Cell*, 154(6), pp.1257–68. Available at: http://linkinghub.elsevier.com/retrieve/pii/S0092867413010295 [Accessed May 26, 2014].

Maclean, C.J. et al., 2000. Naturally occurring and experimentally induced beta-amyloid deposits in the brains of marmosets (Callithrix jacchus). *Journal of neural transmission (Vienna, Austria :*, 107(7), pp.799–814. Available at: http://www.ncbi.nlm.nih.gov/pubmed/11005545.

Manuelidis, E.E. et al., 1988. Transmission studies from blood of Alzheimer disease patients and healthy relatives. *Proceedings of the National Academy of Sciences of the United States of America*, 85(13), pp.4898–901. Available at: http://www.pubmedcentral.nih.gov/articlerender.fcgi?artid=280544&tool=pmcentrez&rendertype=abstract [Accessed May 23, 2014].

Marshall, K.E. & Serpell, L.C., 2009. Insights into the Structure of Amyloid Fibrils. , pp.185–192.

Masters, C.L. et al., 1985. Amyloid plaque core protein in Alzheimer disease and Down syndrome. *Proc Natl Acad Sci U S A*, 82(12), pp.4245–4249. Available at:

http://www.ncbi.nlm.nih.gov/pubmed/3159021.

Meyer-luehmann, M., 2006. Exogenous Induction of Cerebral b-Amyloidogenesis Is Governed by Agent and Host. , 1781(2006).

Moore, B.D. et al., 2012. Overlapping profiles of Aβ peptides in the Alzheimer's disease and pathological aging brains. *Alzheimer's research & therapy*, 4(3), p.18. Available at: http://www.pubmedcentral.nih.gov/articlerender.fcgi?artid=3506932&tool=pmcentrez&rendertype=abstract [Accessed May 24, 2014].

Morales, R. et al., 2011. De novo induction of amyloid-β deposition in vivo. *Molecular psychiatry*, pp.1–7. Available at: http://www.ncbi.nlm.nih.gov/pubmed/21968933 [Accessed March 17, 2012].

Morales, R. et al., 2012. Protein misfolding cyclic amplification of infectious prions. *Nature Protocols*, 7(7), pp.1397–1409. Available at: http://www.nature.com/doifinder/10.1038/nprot.2012.067 [Accessed June 29, 2012].

Morales, R., Callegari, K. & Soto, C., 2015. Prion-like features of misfolded Aβ and tau aggregates. *Virus Research*. Available at: http://dx.doi.org/10.1016/j.virusres.2014.12.031.

Mullan, M. et al., 1992. A pathogenic mutation for probable Alzheimer's disease in the APP gene at the N-terminus of beta-amyloid. *Nature genetics*, 1(5), pp.345–7. Available at: http://www.ncbi.nlm.nih.gov/pubmed/1302033 [Accessed August 3, 2012].

Naiki, H. et al., 1989. Fluorometric determination of amyloid fibrils in vitro using the fluorescent dye, thioflavin T1. *Analytical biochemistry*, 177(2), pp.244–9. Available at: http://www.ncbi.nlm.nih.gov/pubmed/2729542 [Accessed September 9, 2012].

Ngo, S. & Guo, Z., 2011. Key residues for the oligomerization of Aβ42 protein in Alzheimer's disease. *Biochemical and biophysical research communications*, 414(3), pp.512–6. Available at: http://www.ncbi.nlm.nih.gov/pubmed/21986527 [Accessed July 5, 2012].

Nilsson, P. et al., 2007. Imaging distinct conformational states of amyloid-beta fibrils in Alzheimer's disease using novel luminescent probes. *ACS chemical biology*, 2(8), pp.553–60. Available at: http://www.ncbi.nlm.nih.gov/pubmed/17672509 [Accessed September 12, 2012].

O'Brien, R.J. & Wong, P.C., 2011. Amyloid precursor protein processing and Alzheimer's disease. *Annual review of neuroscience*, 34, pp.185–204. Available at: http://www.pubmedcentral.nih.gov/articlerender.fcgi?artid=3174086&tool=pmcentrez&rendertype=abstract [Accessed July 13, 2012].

Palmert, M.R. et al., 1988. Antisera to an amino-terminal peptide detect the amyloid protein precursor of Alzheimer's disease and recognize senile plaques. *Biochemical and biophysical research communications*, 156(1), pp.432–7. Available at: http://www.ncbi.nlm.nih.gov/pubmed/3140814 [Accessed September 11, 2012].

Paravastu, A.K. et al., 2008a. Molecular structural basis for polymorphism in Alzheimer ' s □ -amyloid fibrils. , 105(47).

Paravastu, A.K. et al., 2008b. Molecular structural basis for polymorphism in Alzheimer's beta-amyloid fibrils. *Proceedings of the National Academy of Sciences of the United States of America*, 105(47), pp.18349–54. Available at: http://www.pubmedcentral.nih.gov/articlerender.fcgi?artid=2587602&tool=pmcentrez&rendertype=abstract [Accessed April 29, 2014].

Paravastu, A.K. et al., 2009. Seeded growth of beta-amyloid fibrils from Alzheimer's brain-derived fibrils produces a distinct fibril structure. *Proc Natl Acad Sci U S A*, 106(18), pp.7443–7448. Available at: http://www.ncbi.nlm.nih.gov/pubmed/19376973.

Pauwels, K. et al., 2012. Structural basis for increased toxicity of pathological aβ42:aβ40 ratios in Alzheimer disease. *The Journal of biological chemistry*, 287(8), pp.5650–60. Available at: http://www.pubmedcentral.nih.gov/articlerender.fcgi?artid=3285338&tool=pmcentrez&rendertype=abstract [Accessed May 31, 2013].

Petkova, A.T. et al., 2005. Self-propagating, molecular-level polymorphism in Alzheimer's beta-amyloid fibrils. *Science*, 307(5707), pp.262–265. Available at: http://www.ncbi.nlm.nih.gov/pubmed/15653506 [Accessed March 18, 2012].

Petkova, A.T. et al., 2004. Solid state NMR reveals a pH-dependent antiparallel beta-sheet registry in fibrils formed by a beta-amyloid peptide. *Journal of molecular biology*, 335(1), pp.247–60. Available at: http://www.ncbi.nlm.nih.gov/pubmed/14659754 [Accessed May 18, 2014].

Petkova, A.T., Yau, W.-M. & Tycko, R., 2006. Experimental constraints on quaternary structure in Alzheimer's beta-amyloid fibrils. *Biochemistry*, 45(2), pp.498–512. Available at: http://www.pubmedcentral.nih.gov/articlerender.fcgi?artid=1435828&tool=pmcentrez&rendertype=abstract [Accessed May 22, 2014].

Piccini, A. et al., 2005. beta-amyloid is different in normal aging and in Alzheimer disease. *The Journal of biological chemistry*, 280(40), pp.34186–92. Available at: http://www.ncbi.nlm.nih.gov/pubmed/16103127 [Accessed July 24, 2012].

Ponte, P. et al., 1988. A new A4 amyloid mRNA contains a domain homologous to serine proteinase inhibitors. *Nature*, 331(6156), pp.525–7. Available at: http://www.ncbi.nlm.nih.gov/pubmed/2893289 [Accessed September 11, 2012].

Powers, E.T. & Powers, D.L., 2006. The kinetics of nucleated polymerizations at high

concentrations: amyloid fibril formation near and above the “supercritical concentration”. *Biophysical journal*, 91(1), pp.122–32. Available at: http://www.pubmedcentral.nih.gov/articlerender.fcgi?artid=1479066&tool=pmcentrez&rendertype=abstract [Accessed June 4, 2014].

Price, J.L. et al., 2009. Neuropathology of nondemented aging: presumptive evidence for preclinical Alzheimer disease. *Neurobiology of aging*, 30(7), pp.1026–36. Available at: http://www.pubmedcentral.nih.gov/articlerender.fcgi?artid=2737680&tool=pmcentrez&rendertype=abstract [Accessed May 5, 2014].

Prusiner, S.B. et al., 1984. Purification and structural studies of a major scrapie prion protein. *Cell*, 38(1), pp.127–34. Available at: http://www.ncbi.nlm.nih.gov/pubmed/6432339 [Accessed April 19, 2014].

Prusiner, S.B., 1984. Some speculations about prions, amyloid, and Alzheimer’s disease. *The New England journal of medicine*, 310(10), pp.661–3. Available at: http://www.ncbi.nlm.nih.gov/pubmed/6363926 [Accessed September 17, 2012].

Prusiner, S.B. & Kingsbury, D.T., 1985. Prions--infectious pathogens causing the spongiform encephalopathies. *CRC critical reviews in clinical neurobiology*, 1(3), pp.181–200. Available at: http://www.ncbi.nlm.nih.gov/pubmed/3915974 [Accessed September 16, 2012].

Qiang, W., Kelley, K. & Tycko, R., 2013. Polymorph-specific kinetics and thermodynamics of β-amyloid fibril growth. *Journal of the American Chemical Society*, 135(18), pp.6860–71. Available at: http://www.ncbi.nlm.nih.gov/pubmed/23627695.

Qiang, W., Yau, W.-M. & Tycko, R., 2011. Structural evolution of Iowa mutant β-amyloid fibrils from polymorphic to homogeneous states under repeated seeded growth. *Journal of the American Chemical Society*, 133(11), pp.4018–29. Available at: http://www.pubmedcentral.nih.gov/articlerender.fcgi?artid=3060308&tool=pmcentrez&rendertype=abstract.

Rangachari, V. et al., 2006. Secondary structure and interfacial aggregation of amyloid-beta(1-40) on sodium dodecyl sulfate micelles. *Biochemistry*, 45(28), pp.8639–48. Available at: http://www.ncbi.nlm.nih.gov/pubmed/16834338 [Accessed June 8, 2014].

Ridley, R.M. et al., 2006. Very long term studies of the seeding of beta-amyloidosis in primates. *J Neural Transm*, 113(9), pp.1243–1251. Available at: http://www.ncbi.nlm.nih.gov/pubmed/16362635.

Roher, A.E. & Kuo, Y.M., 1999. Isolation of amyloid deposits from brain. *Methods in enzymology*, 309, pp.58–67. Available at: http://www.sciencedirect.com/science/article/pii/S0076687999090060 [Accessed June 11, 2014].

Rosen, R.F. et al., 2011. Exogenous seeding of cerebral beta-amyloid deposition in betaAPP-transgenic rats. *J Neurochem*. Available at: http://www.ncbi.nlm.nih.gov/pubmed/22017494.

Rosen, R.F. et al., 2012. Exogenous seeding of cerebral β-amyloid deposition in βAPP-transgenic rats. *Journal of neurochemistry*, 120(5), pp.660–666. Available at: http://www.ncbi.nlm.nih.gov/pubmed/22017494 [Accessed March 5, 2012].

Salvadores, N. et al., 2014. Detection of Misfolded Aβ Oligomers for Sensitive Biochemical Diagnosis of Alzheimer's Disease. *Cell Reports*, pp.1–8. Available at: http://linkinghub.elsevier.com/retrieve/pii/S2211124714001454 [Accessed March 23, 2014].

Sato, T., Kienlen-Campard, P., Ahmed, M., Liu, W., Li, H., Elliott, J.I., Aimoto, S., Constantinescu, S.N., Octave, J.-N., et al., 2006. Inhibitors of amyloid toxicity based on beta-sheet packing of Abeta40 and Abeta42. *Biochemistry*, 45(17), pp.5503–16. Available at: http://www.pubmedcentral.nih.gov/articlerender.fcgi?artid=2593882&tool=pmcentrez&rendertype=abstract.

Sato, T., Kienlen-Campard, P., Ahmed, M., Liu, W., Li, H., Elliott, J.I., Aimoto, S., Constantinescu, S.N., Octave, J., et al., 2006. Inhibitors of amyloid toxicity based on beta-sheet packing of Abeta40 and Abeta42. *Biochemistry*, 45(17), pp.5503–16. Available at: http://www.pubmedcentral.nih.gov/articlerender.fcgi?artid=2593882&tool=pmcentrez&rendertype=abstract [Accessed May 11, 2014].

Schmit, J.D., Ghosh, K. & Dill, K., 2011. What drives amyloid molecules to assemble into oligomers and fibrils? *Biophysical journal*, 100(2), pp.450–8. Available at: http://www.pubmedcentral.nih.gov/articlerender.fcgi?artid=3021675&tool=pmcentrez&rendertype=abstract [Accessed May 28, 2014].

Schreck, J.S. & Yuan, J.-M., 2013. A kinetic study of amyloid formation: fibril growth and length distributions. *The journal of physical chemistry. B*, 117(21), pp.6574–83. Available at: http://www.ncbi.nlm.nih.gov/pubmed/23638987.

Schubert, D. et al., 1989. The regulation of amyloid beta protein precursor secretion and its modulatory role in cell adhesion. *Neuron*, 3(6), pp.689–94. Available at: http://www.ncbi.nlm.nih.gov/pubmed/2518372 [Accessed September 11, 2012].

Selkoe, D., Mandelkow, E. & Holtzman, D., 2012. Deciphering Alzheimer disease. *Cold Spring Harbor perspectives in medicine*, 2(1), p.a011460. Available at: http://www.pubmedcentral.nih.gov/articlerender.fcgi?artid=3253026&tool=pmcentrez&rendertype=abstract [Accessed July 24, 2012].

Serio, T.R., 2000. Nucleated Conformational Conversion and the Replication of Conformational Information by a Prion Determinant. *Science*, 289(5483), pp.1317–1321. Available at: http://www.sciencemag.org/cgi/doi/10.1126/science.289.5483.1317 [Accessed

March 22, 2012].

Seubert, P. et al., 1992. Isolation and quantification of soluble Alzheimer's beta-peptide from biological fluids. *Nature*, 359(6393), pp.325–7. Available at: http://www.ncbi.nlm.nih.gov/pubmed/1406936 [Accessed August 9, 2012].

Shankar, G.M. et al., 2007. Natural oligomers of the Alzheimer amyloid-beta protein induce reversible synapse loss by modulating an NMDA-type glutamate receptor-dependent signaling pathway. *The Journal of neuroscience : the official journal of the Society for Neuroscience*, 27(11), pp.2866–75. Available at: http://www.ncbi.nlm.nih.gov/pubmed/17360908 [Accessed March 12, 2012].

Shi, J.-Q. et al., 2011. Anti-TNF-α reduces amyloid plaques and tau phosphorylation and induces CD11c-positive dendritic-like cell in the APP/PS1 transgenic mouse brains. *Brain research*, 1368(null), pp.239–47. Available at: http://dx.doi.org/10.1016/j.brainres.2010.10.053 [Accessed September 21, 2012].

Sievers, S.A. et al., 2011. Structure-based design of non-natural amino-acid inhibitors of amyloid fibril formation. *Nature*, 475(7354), pp.96–100. Available at: http://www.ncbi.nlm.nih.gov/pubmed/21677644 [Accessed May 2, 2014].

Singh, P.K. et al., 2010. Ultrafast bond twisting dynamics in amyloid fibril sensor. *The journal of physical chemistry. B*, 114(7), pp.2541–6. Available at: http://www.ncbi.nlm.nih.gov/pubmed/20095597 [Accessed September 11, 2012].

Sipe, J.D. & Cohen, A.S., 2000. Review: history of the amyloid fibril. *Journal of structural biology*, 130(2-3), pp.88–98. Available at: http://www.ncbi.nlm.nih.gov/pubmed/10940217 [Accessed July 12, 2012].

Sisodia, S.S., 1992. Beta-amyloid precursor protein cleavage by a membrane-bound protease. *Proceedings of the National Academy of Sciences of the United States of America*, 89(13), pp.6075–9. Available at: http://www.pubmedcentral.nih.gov/articlerender.fcgi?artid=49440&tool=pmcentrez&rendertype=abstract [Accessed September 11, 2012].

Sisodia, S.S. et al., 1990. Evidence that beta-amyloid protein in Alzheimer's disease is not derived by normal processing. *Science (New York, N.Y.)*, 248(4954), pp.492–5. Available at: http://www.ncbi.nlm.nih.gov/pubmed/1691865 [Accessed September 11, 2012].

Spirig, T. et al., 2014. Direct Evidence for Self-Propagation of Different Amyloid-β Fibril Conformations. *Neuro-degenerative diseases*. Available at: http://www.ncbi.nlm.nih.gov/pubmed/25300967 [Accessed October 12, 2014].

Srivastava, A. et al., 2010. Identifying the bond responsible for the fluorescence modulation in an amyloid fibril sensor. *Chemistry (Weinheim an der Bergstrasse, Germany)*, 16(30), pp.9257–63. Available at: http://www.ncbi.nlm.nih.gov/pubmed/20583044 [Accessed September 11, 2012].

Stohr, J. et al., 2012. Purified and synthetic Alzheimer's amyloid beta (Abeta) prions. *Proc Natl Acad Sci U S A*. Available at: http://www.pnas.org/cgi/doi/10.1073/pnas.1206555109 [Accessed June 19, 2012].

Stöhr, J. et al., 2014. Distinct synthetic Aβ prion strains producing different amyloid deposits in bigenic mice. *Proceedings of the National Academy of Sciences of the United States of America*. Available at: http://www.ncbi.nlm.nih.gov/pubmed/24982137 [Accessed July 10, 2014].

De Strooper, B. et al., 1993. Study of the synthesis and secretion of normal and artificial mutants of murine amyloid precursor protein (APP): cleavage of APP occurs in a late compartment of the default secretion pathway. *The Journal of cell biology*, 121(2), pp.295–304. Available at: http://www.pubmedcentral.nih.gov/articlerender.fcgi?artid=2200101&tool=pmcentrez&rendertype=abstract [Accessed September 11, 2012].

Studier, F.W., 2005. Protein production by auto-induction in high density shaking cultures. *Protein expression and purification*, 41(1), pp.207–34. Available at: http://www.ncbi.nlm.nih.gov/pubmed/15915565 [Accessed October 11, 2012].

Tanzi, R.E. et al., 1987. Amyloid beta protein gene: cDNA, mRNA distribution, and genetic linkage near the Alzheimer locus. *Science (New York, N.Y.)*, 235(4791), pp.880–4. Available at: http://www.ncbi.nlm.nih.gov/pubmed/2949367 [Accessed September 11, 2012].

Thorsten et al., 2005. 3D structure of Alzheimer's amyloid-beta(1-42) fibrils. *Proc Natl Acad Sci U S A*, 102(48), pp.17342–17347. Available at: http://www.ncbi.nlm.nih.gov/pubmed/16293696.

Tischer, E. & Cordell, B., 1996. Beta-Amyloid precursor protein. Location of transmembrane domain and specificity of gamma-secretase cleavage. *The Journal of biological chemistry*, 271(36), pp.21914–9. Available at: http://www.ncbi.nlm.nih.gov/pubmed/8702994 [Accessed September 11, 2012].

Toyama, B.H. & Weissman, J.S., 2011. Amyloid structure: conformational diversity and consequences. *Annual review of biochemistry*, 80, pp.557–85. Available at: http://www.ncbi.nlm.nih.gov/pubmed/21456964 [Accessed July 23, 2012].

Tycko, R. et al., 2009. Evidence for novel beta-sheet structures in Iowa mutant beta-amyloid fibrils. *Biochemistry*, 48(26), pp.6072–84. Available at: http://www.pubmedcentral.nih.gov/articlerender.fcgi?artid=2910621&tool=pmcentrez&rendertype=abstract [Accessed May 18, 2014].

Tycko, R., 2006. Molecular structure of amyloid fibrils: insights from solid-state NMR. *Quarterly reviews of biophysics*, 39(1), pp.1–55. Available at: http://www.ncbi.nlm.nih.gov/pubmed/16772049 [Accessed May 10, 2014].

Tycko, R., 2011. Solid-state NMR studies of amyloid fibril structure. *Annual review of physical chemistry*, 62, pp.279–99. Available at:

http://www.pubmedcentral.nih.gov/articlerender.fcgi?artid=3191906&tool=pmcentrez&rendertype=abstract [Accessed April 30, 2014].

VASSAR, P.S. & CULLING, C.F., 1959. Fluorescent stains, with special reference to amyloid and connective tissues. *Archives of pathology*, 68, pp.487–98. Available at: http://www.ncbi.nlm.nih.gov/pubmed/13841452 [Accessed April 21, 2014].

Walker, J.M., 2005. *The Proteomics Protocols Handbook*, Humana Press. Available at: http://www.springer.com/life+sciences/biochemistry+&+biophysics/book/978-1-58829-343-5.

Walker, L.C. et al., 2008. Diversity of Abeta deposits in the aged brain: a window on molecular heterogeneity? *Rom J Morphol Embryol*, 49(1), pp.5–11. Available at: http://www.ncbi.nlm.nih.gov/pubmed/18273496.

Walker, L.C. et al., 2002. Exogenous induction of cerebral beta-amyloidosis in betaAPP-transgenic mice. *Peptides*, 23(7), pp.1241–1247. Available at: http://www.ncbi.nlm.nih.gov/pubmed/12128081.

Wang, Y.-Q. et al., 2011. Relationship between prion propensity and the rates of individual molecular steps of fibril assembly. *The Journal of biological chemistry*, 286(14), pp.12101–7. Available at: http://www.pubmedcentral.nih.gov/articlerender.fcgi?artid=3069414&tool=pmcentrez&rendertype=abstract [Accessed April 5, 2012].

Watts, J.C. et al., 2014. Serial propagation of distinct strains of Aβ prions from Alzheimer's disease patients. *Proceedings of the National Academy of Sciences of the United States of America*, (26). Available at: http://www.ncbi.nlm.nih.gov/pubmed/24982139 [Accessed July 10, 2014].

Wiltzius, J.J.W. et al., 2009. Molecular mechanisms for protein-encoded inheritance. *Nature structural & molecular biology*, 16(9), pp.973–8. Available at: http://www.ncbi.nlm.nih.gov/pubmed/19684598 [Accessed July 24, 2012].

Wong, C.W., Quaranta, V. & Glenner, G.G., 1985. Neuritic plaques and cerebrovascular amyloid in Alzheimer disease are antigenically related. *Proceedings of the National Academy of Sciences of the United States of America*, 82(24), pp.8729–32. Available at: http://www.pubmedcentral.nih.gov/articlerender.fcgi?artid=391510&tool=pmcentrez&rendertype=abstract [Accessed September 1, 2012].

Wu, C., Bowers, M.T. & Shea, J.-E., 2010. Molecular structures of quiescently grown and brain-derived polymorphic fibrils of the Alzheimer amyloid abeta9-40 peptide: a comparison to agitated fibrils. *PLoS computational biology*, 6(3), p.e1000693. Available at: http://www.pubmedcentral.nih.gov/articlerender.fcgi?artid=2832665&tool=pmcentrez&rendertype=abstract [Accessed May 27, 2013].

Yamaguchi, K.-I. et al., 2005. Seeding-dependent propagation and maturation of amyloid fibril conformation. *Journal of molecular biology*, 352(4), pp.952–60.

Available at: http://www.ncbi.nlm.nih.gov/pubmed/16126222 [Accessed May 14, 2012].

Yan, Y. & Wang, C., 2007. Abeta40 protects non-toxic Abeta42 monomer from aggregation. *Journal of molecular biology*, 369(4), pp.909–16. Available at: http://www.ncbi.nlm.nih.gov/pubmed/17481654 [Accessed June 24, 2013].

Yan, Y. & Wang, C., 2006. Abeta42 is more rigid than Abeta40 at the C terminus: implications for Abeta aggregation and toxicity. *Journal of molecular biology*, 364(5), pp.853–62. Available at: http://www.ncbi.nlm.nih.gov/pubmed/17046788 [Accessed June 6, 2014].

Zhong, Z. et al., 1994. Secretion of beta-amyloid precursor protein involves multiple cleavage sites. *The Journal of biological chemistry*, 269(1), pp.627–32. Available at: http://www.ncbi.nlm.nih.gov/pubmed/8276862 [Accessed September 11, 2012].

7 Supplementary Data

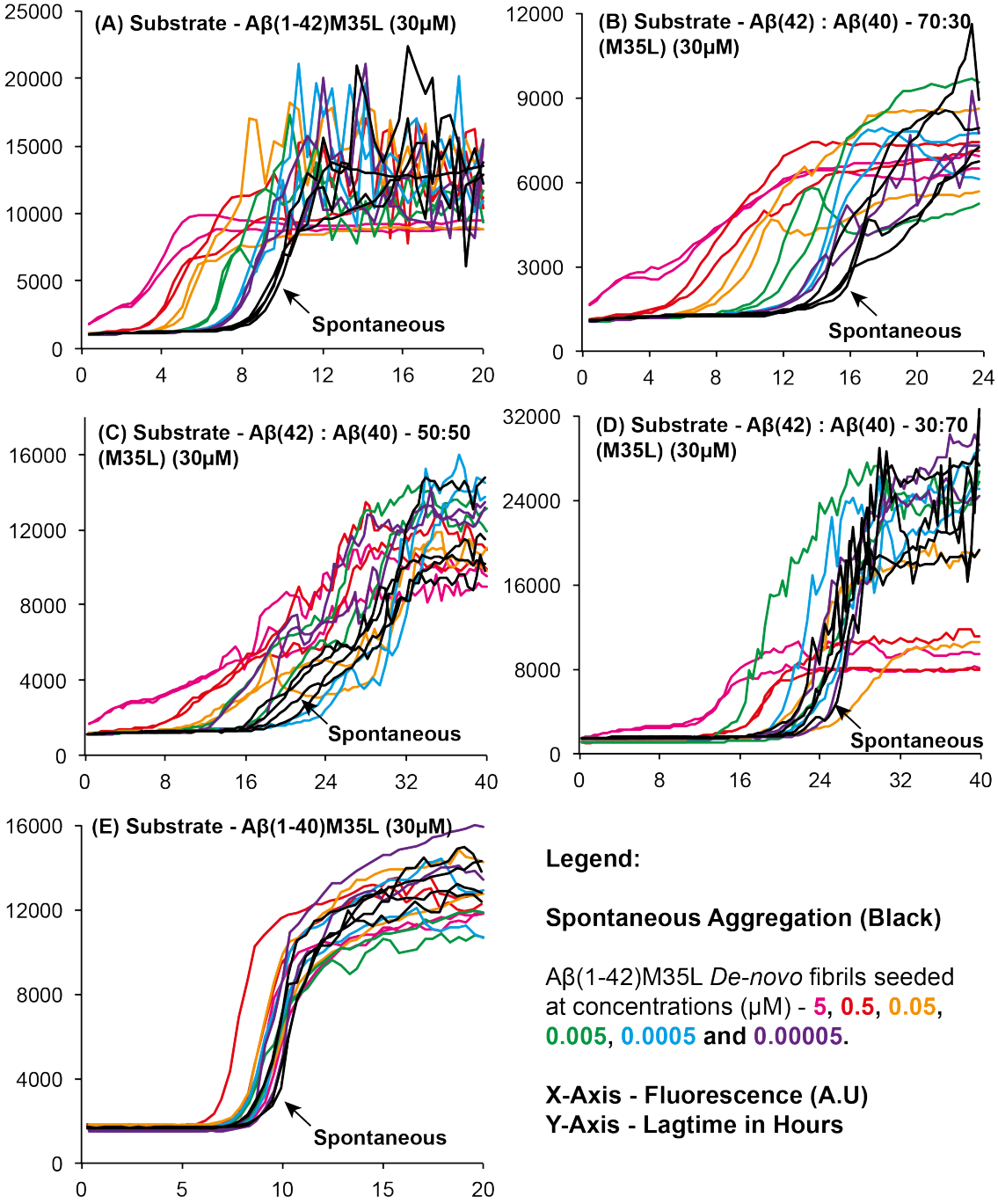

Fig.- 7.1 – Aβ substrates in stoichiometric ratios [Aβ(1-42)M35L : Aβ(1-42)M35L], both spontaneous and seeded by *de-novo* aggregated Aβ(1-42) fibrillar seeds in the assay (Refer Legend). (**A**) Only Aβ(1-42)M35L (**B-D**) Aβ(1-42)M35L : Aβ(1-40)M35L in ratios 70:30, 50:50 and 30:70 respectively (**E**) Only Aβ(1-40)M35L

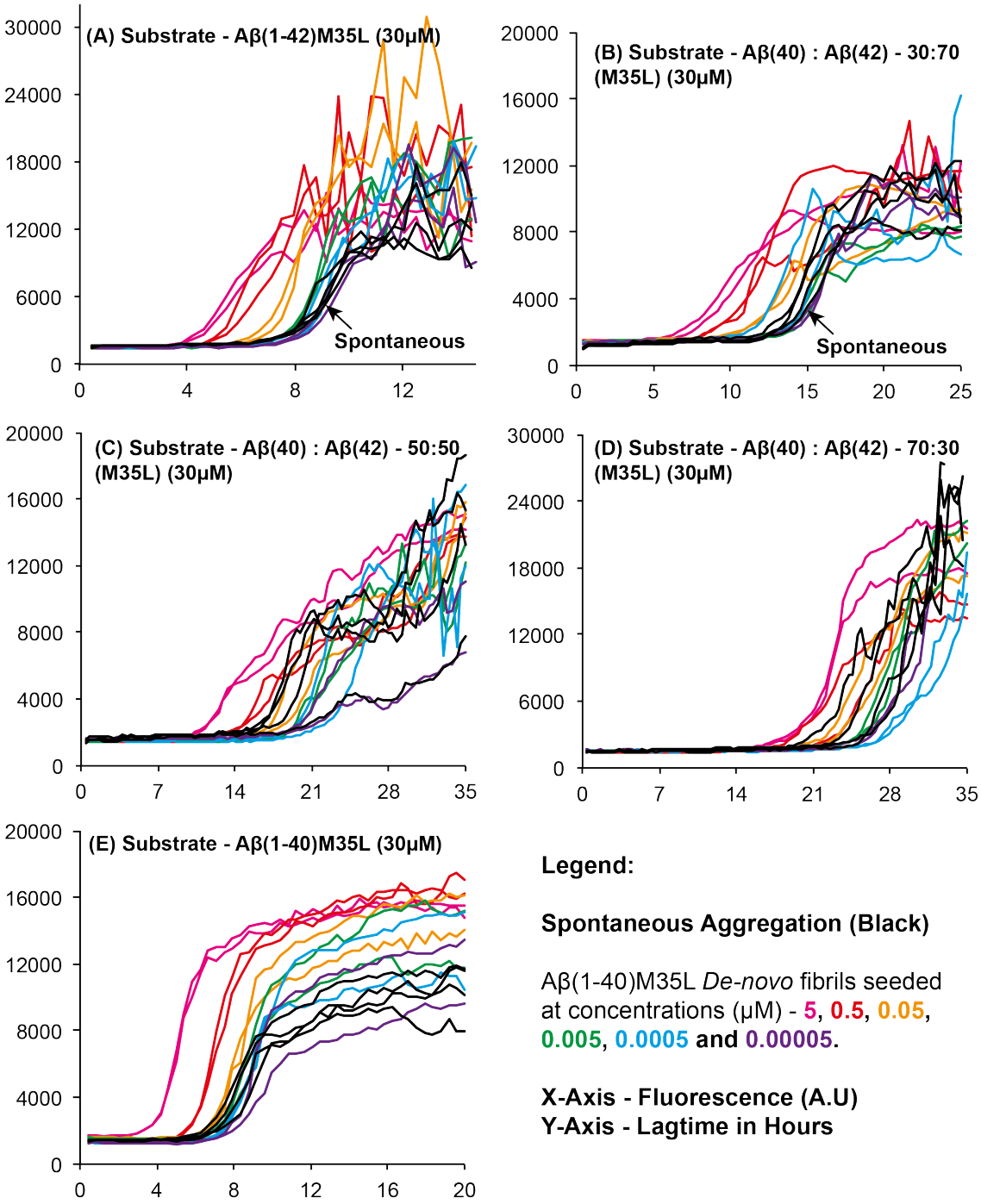

Fig.- 7.2 - Aβ substrates in stoichiometric ratios [Aβ(1-42)M35L : Aβ(1-42)M35L], both spontaneous and seeded by de-novo aggregated Aβ(1-40) fibrillar seeds in the assay (Refer Legend). (**A**) Only Aβ(1-42)M35L (**B-D**) Aβ(1-42)M35L : Aβ(1-40)M35L in ratios 70:30, 50:50 and 30:70 respectively (**E**) Only Aβ(1-40)M35L

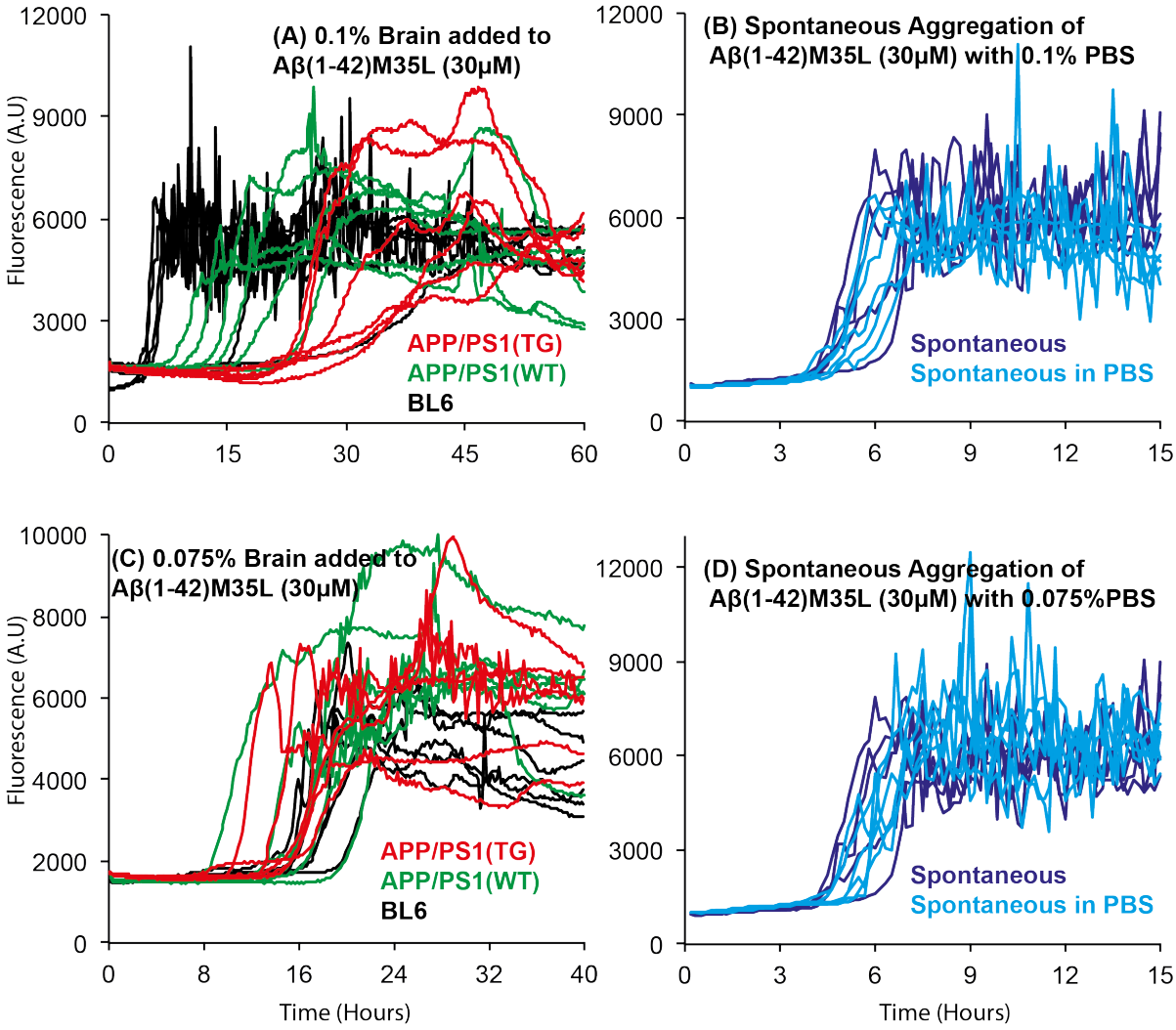

Fig.- 7.3 - **Brain homogenate seeding with 2X Protease inhibitor in the assay**. (**A**) APP/PS1(TG/WT) and BL6 added to assay at 0.1% BH concentration. (**B**) Spontaneous aggregation in the absence of brain homogenate but with 0.1% PBS. (**C**) APP/PS1(TG/WT) and BL6 added to assay at 0.075% BH concentration. (**D**) Spontaneous aggregation in the absence of brain homogenate but with 0.075% PBS.

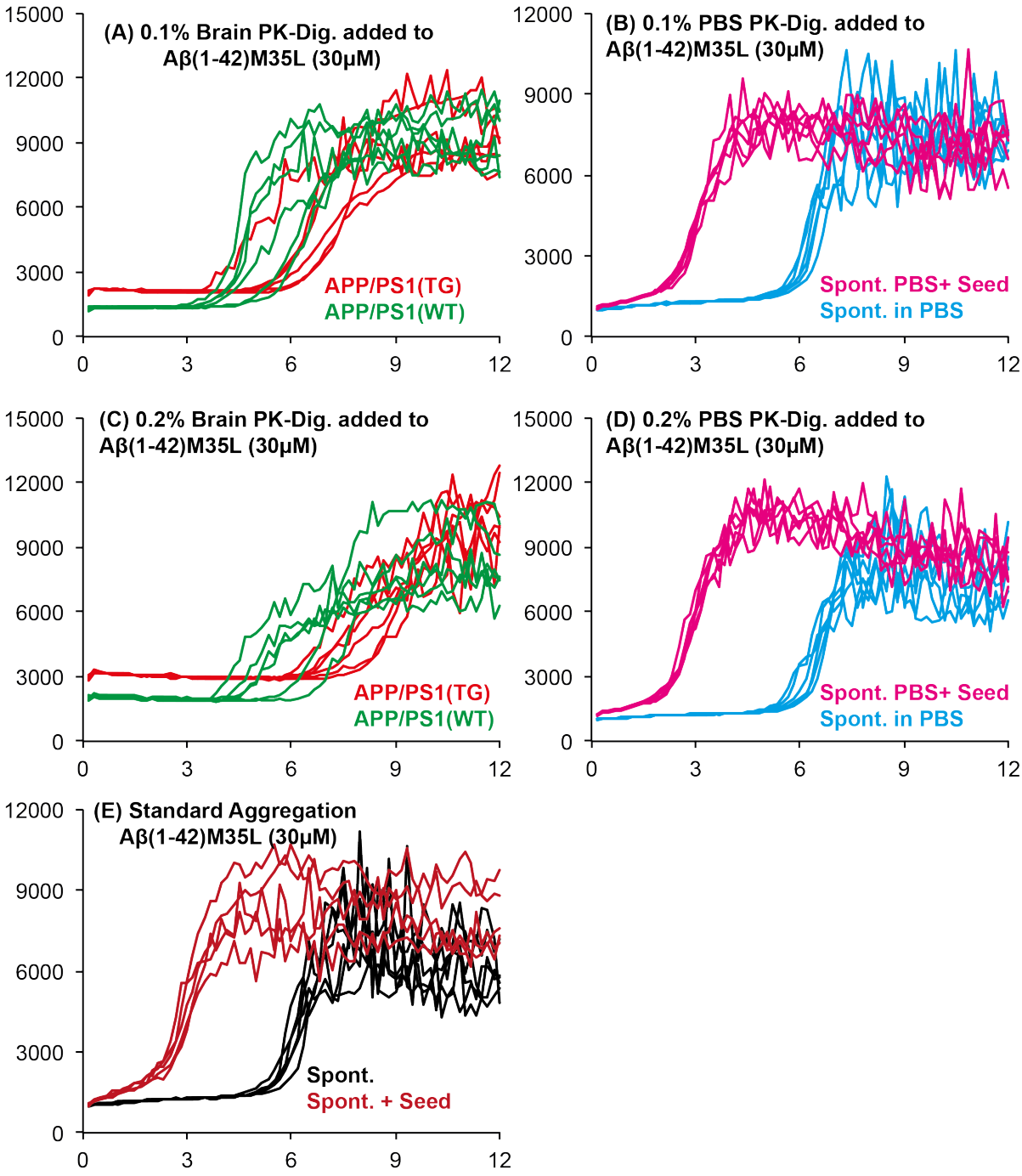

Fig.- 7.4 - **Brain homogenate seeding with PK digestion** (1:500) in the assay. (**A**) APP/PS1(TG/WT) and BL6 added to assay at 0.2% BH concentration. (**B**) Spontaneous aggregation in the absence of brain homogenate but with 0.2% PBS. (**C**) APP/PS1(TG/WT) and BL6 added to assay at 0.1% BH concentration. (**D**) Spontaneous aggregation in the absence of brain homogenate but with 0.1% PBS. (**E**) Standard spontaneous aggregation and seeded aggregation reaction.

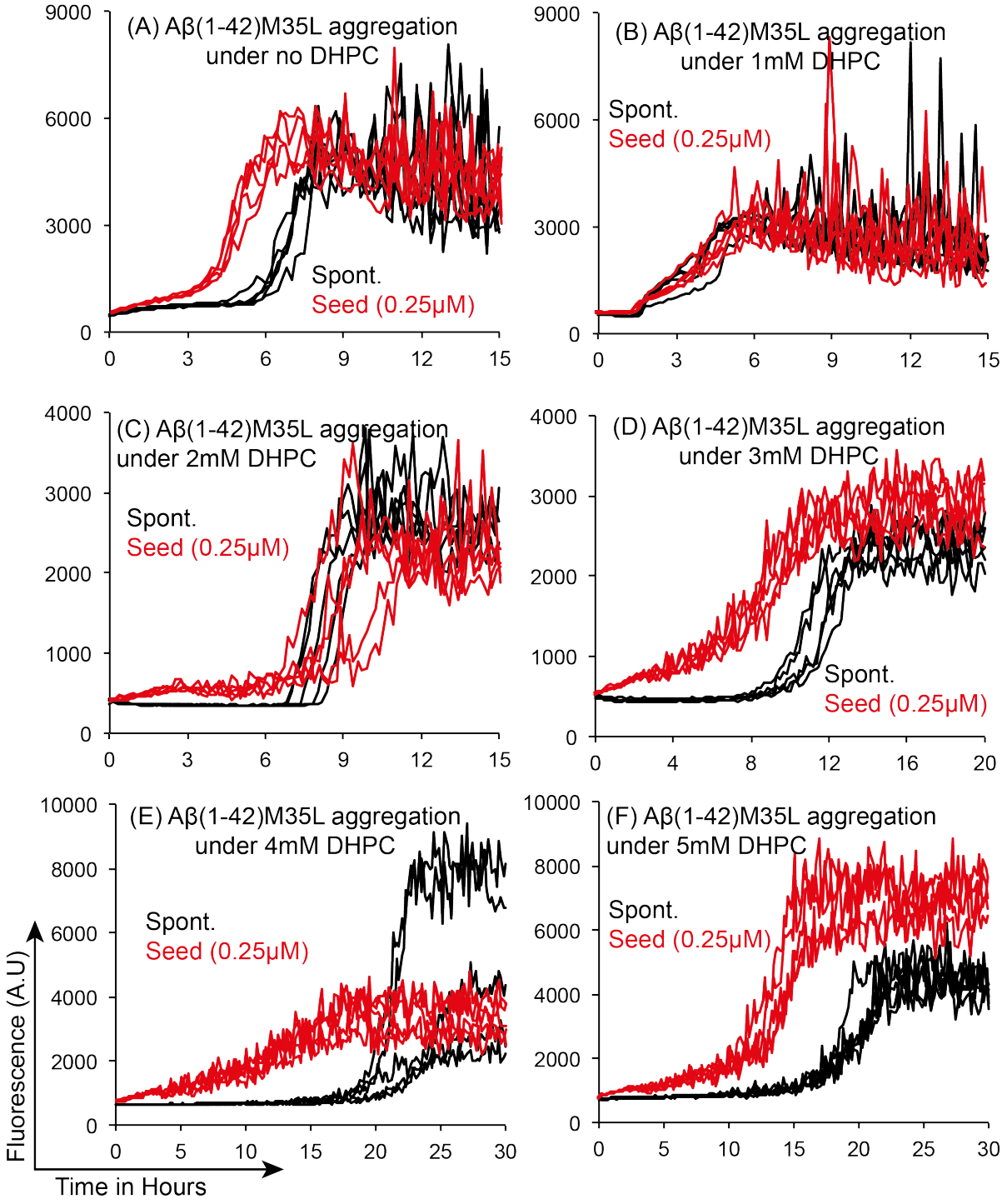

Fig.- 7.5 – Spontaneous and seeded aggregation of Aβ(1-42)M35L substrate in varying concentration of DHPC (0 - 6mM) (A-G). (**A**) Standard spontaneous aggregation and seeding reaction. (**B**) Spontaneous and seeded aggregation at 1mM DHPC. (**C**) Spontaneous and seeded aggregation at 2mM DHPC. (**D**) Spontaneous and seeded aggregation at 3mM DHPC. (**E**) Spontaneous and seeded aggregation at 4mM DHPC. (**F**) Spontaneous and seeded aggregation at 5mM DHPC. (Refer, next

page)

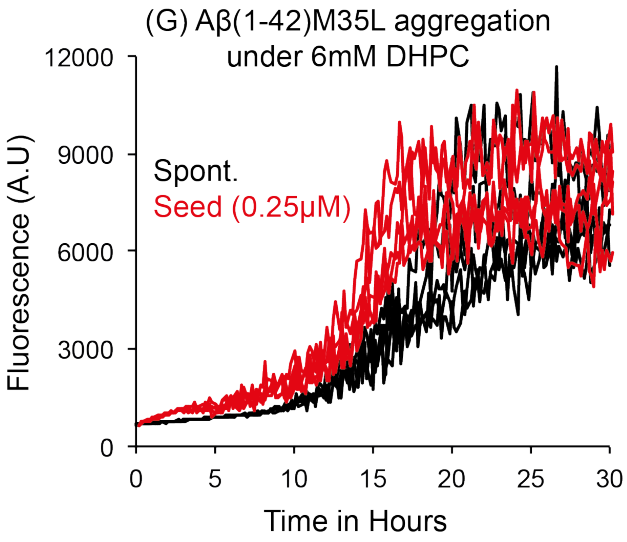

Fig.- 7.5 – (**G**) Spontaneous and seeded aggregation at 6mM DHPC.

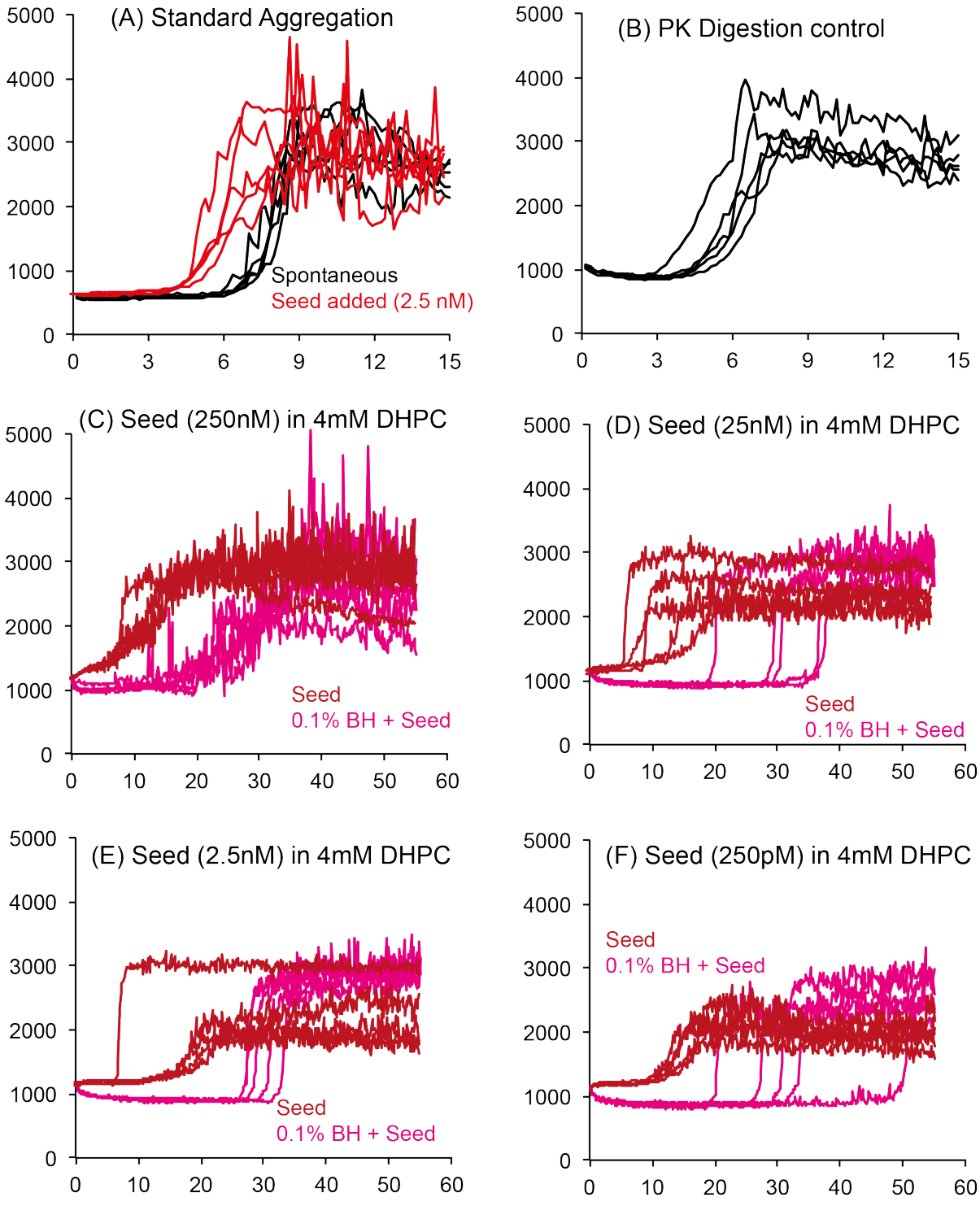

Fig.- 7.6 – Detection of *de-novo* Aβ(1-42)M35L spiked fibrillar seeds in logarithmically diluted concentrations in the assay under 4mM DHPC condition. (**A**) Standard spontaneous and seeded aggregation with no DHPC. (**B**) PK digestion control Spontaneous aggregation with 0.1%BH, no DHPC. (**C-H**) aggregation in the presence specified seed in the presence of 0.1%BH, 4mM DHPC. (Refer, next page)

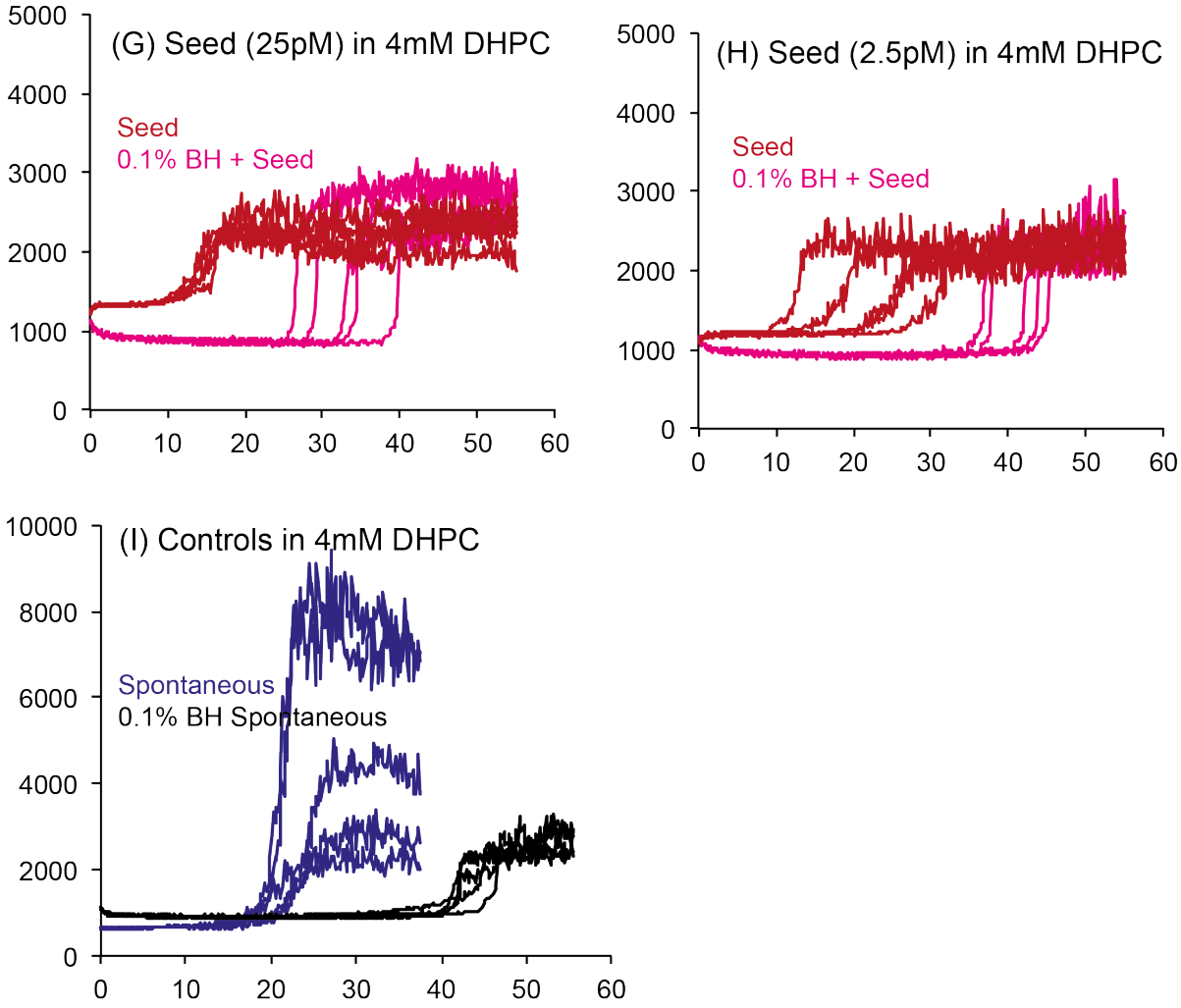

Fig.- 7.6 - (**I**) Comparison of DHPC spontaneous aggregation controls in the presence and absence of 0.1%BH.

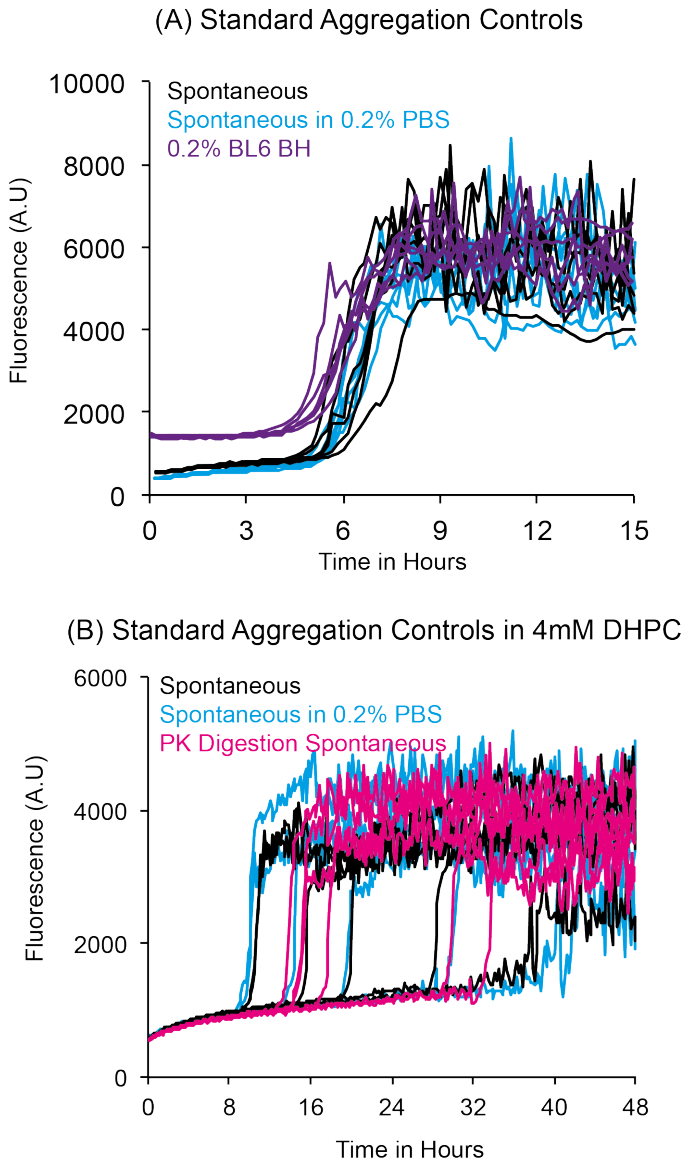

Fig.- 7.7 – Controls for brain aggregated-Aβ seeding assay. (**A**) Aβ(1-42)M35L spontaneous aggregation in the presence of 0.2% PBS and PK digested 0.2% BL6 brain homogenate. (**B**) Spontaneous Aβ(1-42)M35L aggregation in the presence of 4mM DHPC in the presence of 0.2% PBS and PK digested aggregation buffer.

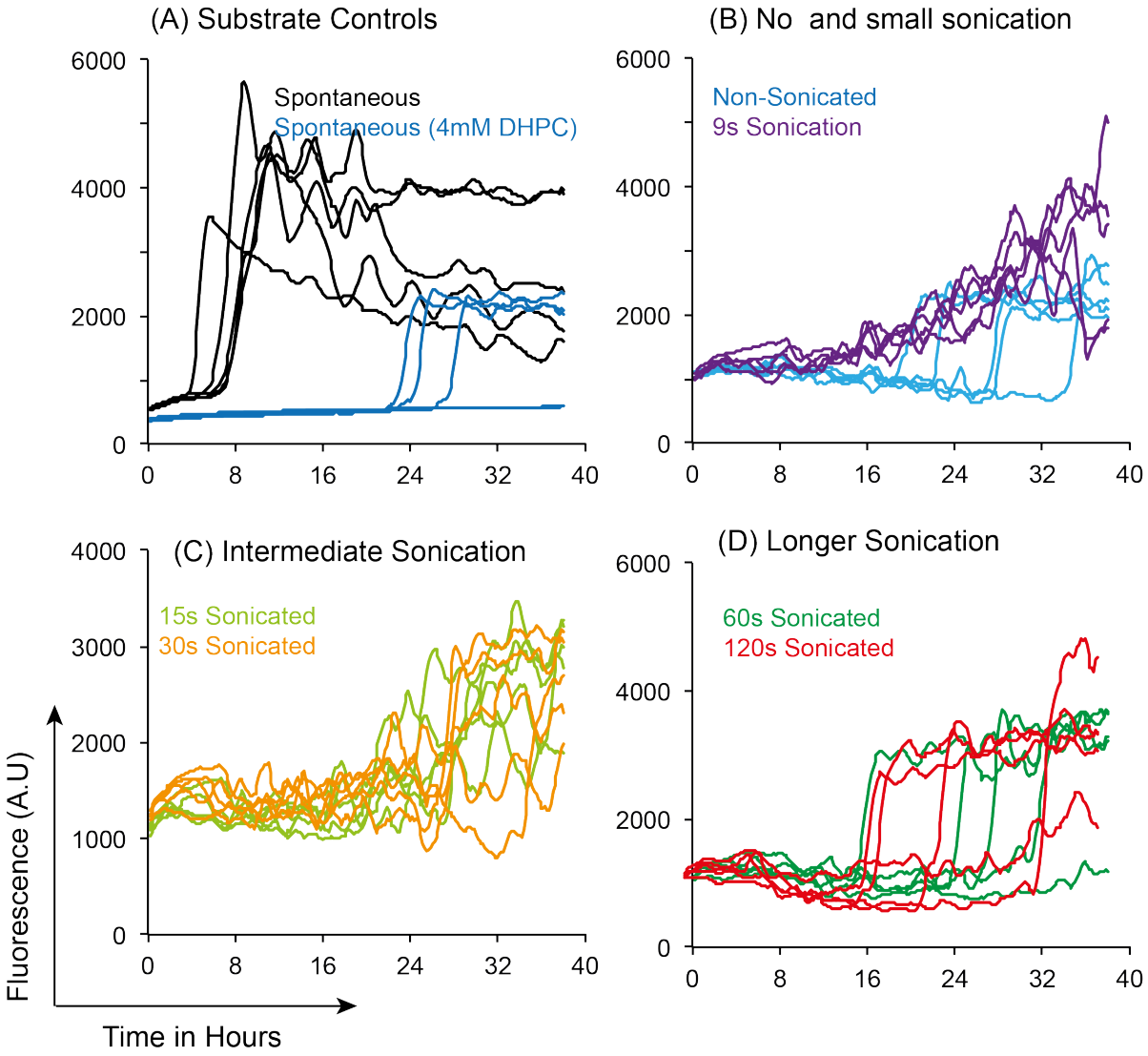

Fig.- 7.8 – Processing times of APP/PS1(TG)-1G aggregates by acoustic-ssa and later seeding in the assay. (**A**) Standard spontaneous aggregation in the presence and absence of 4mM DHPC. (**B**) APP/PS1(TG)-1G material sonicated (9 seconds) and not sonicated. (**C**) APP/PS1(TG)-1G material sonicated for 15 and 30 seconds. (**D**) APP/PS1(TG)-1G material sonicated for 60 and 120 seconds.

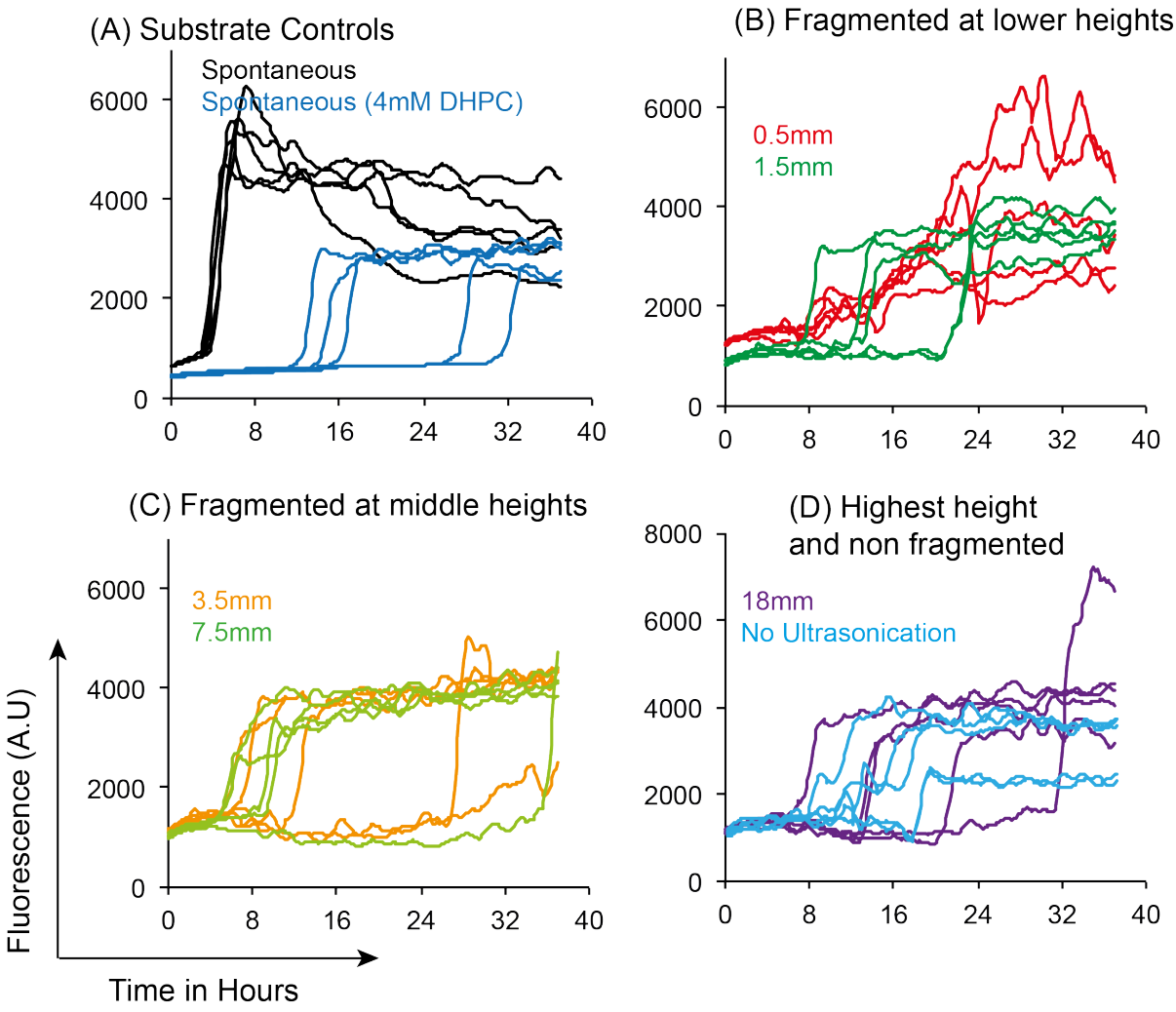

Fig.- 7.9 – Change in sonication shear forces applied for fragmenting APP/PS1(TG)-1G material by adjusting the sample holder height in the acoustic-ssa and seeding the fragmented material in the assay. (**A**) Standard spontaneous aggregation in the presence and absence of 4mM DHPC. (**B-D**) APP/PS1(TG)-1G material fragmentation at 0.5mm, 1.5mm, 3.5mm, 7.5mm and 18mm heights. (**D**) APP/PS1(TG)-1G material not fragmented and added in the assay.

8 List of Figures and Tables

List of Tables